KWAME NKRUMAH UNIVERSITY OF SCIENCE AND TECHNOLOGY, KUMASI, GHANA

MODELLING SOIL CARBON DIOXIDE EMISSIONS FROM DIFFERENT LAND-USE TYPES IN A SEMI-DECIDUOUS FOREST IN GHANA

BY

FAMOUSSA DEMBELE

(B.Sc. Agricultural Economics, M.Phil. Climate Change and Integrated Natural Resource Management)

A Thesis Submitted to The Department of Civil Engineering,

College of Engineering

In Partial Fulfilment of the Requirements of the Degree of

DOCTOR OF PHILOSOPHY

in

Climate Change and Land Use

February 2025

CERTIFICATION

I hereby declare that this submission is my work towards the PhD in Climate Change and Land-use and that, to the best of my knowledge and belief, it contains no material previously published or written by another person nor material that has been accepted for the award of any other degree or diploma at Kwame Nkrumah University of Science and Technology, Kumasi or any other educational institution, except where due acknowledgement is made in the thesis.

Famoussa Dembélé	…….....	21\03\2025
ID. PG6993021	Signature	Date

Certified by:

Prof. Stephen Adu-Bredu	…….....	24\03\2025
(Main Supervisor)	Signature	Date
Prof. Atinuke Adebanji	…….....	21/03/2025
(Co-Supervisor)	Signature	Date
Prof. Samuel Kingsley Oppong	…….....	10\04\2025
(Co-Supervisor)	Signature	Date
Prof. Dr. Rüdiger Schaldach	…….....	24\03\2025
(Co-Supervisor)	Signature	Date
Dr. Sie Sylvester Da	…….....	25\03\2025
(Co-Supervisor)	Signature	Date
Prof. Richard Akwasi Buamah	…….....	12\04\2025
Head of Department, Civil Engineering	Signature	Date

DEDICATION

This work is dedicated to the Almighty GOD, the ultimate source of my life, and inspiration, to whom all credit and glory belong.

To my father, Prof. Filifing DEMBELE and my mother, Kadia Bakary SAMAKE for their unwavering love, and support, and my brothers, sisters, and cousins for their guidance throughout my journey. Only GOD knows your contribution to this work and my life.

To my wife, Fatoumata TRAORE, for her steadfast encouragement and understanding.

Finally, a sincere thank you to everyone who has guided my path to success.

May the Almighty bless you all abundantly.

ABSTRACT

This study provides baseline data and analyses of the evolution of carbon dioxide emissions in the Agriculture, Forestry and Other Land Use (AFOLU) sector in Ghana, focusing on the Bobiri Forest Reserve and fringe areas. The first objective was to analyse land-use/land cover (LULC) changes from 1986 to 2022 in a semi-deciduous forest zone using intensity analysis. The results showed significant land transformations, with Croplands and mixed vegetation and non-vegetated having substantial gains, while closed forest areas decreased by over 36%. These changes were primarily driven by the increasing demand for food and population growth, highlighting the pressure on forested landscapes. The second objective assessed the impact of LULC changes and seasonal variability on soil respiration rate (SRR) across three dominant land categories; forest, fallow (open forest) and cropland (maize and rice). Seasonal variability significantly influenced SRR, with higher emissions observed during the wet season. Forests recorded the lowest SRR due to minimal disturbance and lower sunlight reaching the soil surface. In contrast, fallow and cropland areas showed higher emissions, driven by increased soil disturbance and organic matter decomposition. The model results indicated that SRR was strongly influenced by organic matter (OM), pH, soil moisture (SM) and silt content, as captured in the predictive equation: $SR = (3.77\ x10^{-4} exp^{(0.0771OM)})(55.94 \log(pH) - 36.30)(6.36 \log(Silt) + 36.94)(3.23 \log(SM) + 24.48)$ explaining up to 58% of the variability in SRR. The results highlight the role of land-use changes in altering soil carbon dynamics and SRR. The third objective projected the future evolution of soil CO_2 emissions from 2022 to 2050 under a Business-as-Usual (BAU) scenario using DINAMICA EGO modelling software and a forest-based regression model in ArcGIS Pro. The projections indicated a significant increase in emissions from open forests (55 kg CO_2 ha^{-1} d^{-1}) compared to closed forests (50 kg CO_2 ha^{-1} d^{-1}) and cropland and mixed vegetation (52 kg CO_2 ha^{-1} d^{-1}), driven by continued deforestation and land-use conversion. The findings highlight the critical need for effective land management strategies to mitigate GHG emissions, conserve forest cover, and promote sustainable agricultural practices. Future studies should expand the scope to include methane (CH_4) and nitrous oxide (N_2O) emissions using advanced tools like gas chromatographs, to provide a more comprehensive assessment of emissions dynamics. Furthermore, integrating alternative land-use scenarios, alongside the BAU scenario, and comparing IPCC Tier 1 with Tier 2/3 emissions factors, will improve the accuracy of SRR projections and support more effective policy development.

TABLE OF CONTENTS

LIST OF TABLES

LIST OF FIGURES

LIST OF ABBREVIATIONS AND ACRONYMS

ABM	Agent-Based Modelling
AFOLU	Agriculture, Forestry, and Other Land-use
AIC	Akaike Information Criterion
BAU	Business as usual
BFR	Bobiri Forest Reserve
CBD	Convention on Biological Diversity
CH_4	Methane
CILSS	Comité Inter-États de Lutte contre la Sécheresse au Sahel (Inter-State Committee for Drought Control in the Sahel)
CLUE-S	Conversion of Land-use and its Effects at Small Scales
CMV	Cropland and Mixed Vegetation
CO_2	Carbon Dioxide
CSIR	Council for Scientific and Industrial Research
DEM	Digital Elevation Model
DN	Digital Number
EGM	Environmental Gas Monitor
EGO	Environmental Geoprocessing Object
EOS	Earth Observing System
ESRI	Environmental Systems Research Institute
ETM	Enhanced Thematic Mapper
FORIG	Forestry Research Institute of Ghana
FSI	Fussy Similarity Index
GCF	Green Climate Fund
GCIC	Ghana Climate Innovation Centre
GIS	Geographic Information System
GPS	Global Positioning System
GSS	Geodetic Surveying System
HSD	Highest Significant Difference
IMAGE	Integrated Model to Assess the Global Environment

IPCC	Intergovernmental Panel on Climate Change
IPPU	Industrial Processes and Product Use
ITPS	Intergovernmental Technical Panel on Soils
LCM	Land Change Modeller
LUCF	Land-use Change and Forestry
LULC	Land-use / Land Cover
LULCC	Land-use / Land Cover Change
LUM	Land-use/land Cover Map
MMU	Minimum Mapping Unit
MODIS	Moderate Resolution Imaging Spectroradiometer
N_2O	Nitrous Oxide
NASA	National Aeronautics and Space Administration
NDVI	Normalized Difference Vegetation Index.
NFPDP	National Forest Planning and Development Project
NIR	Near Infrared
NPK	Nitrogen, Phosphorus, and Potassium
NVA	Non-Vegetated Area
OLI	Operational Land Imager
PCA	Principal Component Analysis
PRSE	Predictive Residual Standard Error
PVC	Polyvinyl Chloride
QGIS	Quantum Geographic Information System
REDD	Reducing Emissions from Deforestation and Forest Degradation
RF	Random Forest
SLEUTH	Slope, Land-use, Exclusion, Urban, Transportation, and Hillshade
SOM	Soil Organic Matter
SRR	Soil Respiration Rate
SRTM	Shuttle Radar Topography Mission
TIRS	Thermal Infrared Sensor
TN	Total Nitrogen
TSP	Total Soil Porosity

UNDP	United Nations Development Program
UNEP	United Nations Environment Program
UNFCCC	United Nations Framework Convention on Climate Change
UP	Upland
USAID	United States Agency for International Development
USDA	United States Department of Agriculture
USGS	United States Geological Survey
UTM	Universal Transverse Mercator
WFPS	Water-Filled Pore Space
WGS	World Geodetic System
WRI	World Resources Institute
WRS	Worldwide Reference System
μS	Microsiemens

ACKNOWLEDGEMENT

My utmost appreciation goes to the Almighty God for the strength given throughout these challenging, but insightful times of research.

I am extremely grateful to my supervisors, Prof. Stephen Adu-Bredu of CSIR – FORIG (Kumasi, Ghana), Prof Atinuke Adebanji, Department of Statistics and Actuarial Science and Prof Samuel Kingsley Oppong Department of the Department of Wildlife and Range Management of Kwame Nkrumah University of Science and Technology (KNUST), Kumasi, Ghana, respectively, Prof Dr Rüdiger Schaldach of Centre for Environmental Systems Research (University Kassel, CESR, Germany) and Dr Sie Sylvester Da of the (WASCAL Competence Centre, Ouagadougou, Burkina Faso) for their guidance, suggestions, comments, objective criticism, encouragement and motivation. They shaped this whole work and shaped me as an individual.

I would like to express my heartfelt gratitude to my scientific advisor, Dr Reginald Tang Guuroh (CSIR FORIG, Kumasi, Ghana), for his mentorship throughout this thesis work and for providing valuable insights and guidance. Additionally, my sincere appreciation goes to Dr Amanuel Gebremichael (GFZ German Research Centre for Geosciences, Germany) for his technical support and expert advice during the greenhouse gas (GHG) measurement data collection process.

My sincere thanks go to Prof Dr Ing. René Burghardt (Department of Environmental Meteorology, University of Kassel, Kassel, Germany), Mr. Da-Costa Boakye Mensah Asare (Department of Geomatic Engineering, College of Engineering, KNUST, Kumasi, Ghana) for their support and the facilitation of activities related to geospatial analysis using ArcGIS Pro and QGIS software.

I extend my sincere appreciation to the Federal Ministry of Education and Research of Germany (BMBF) and the West African Science Centre on Climate Change and Adapted Land Use (WASCAL) in Ghana, Accra, for providing the scholarship and financial support that made this research possible. I would like to acknowledge the support from the Greenhouse Gas Determination in West African Landscape (GreeGaDe) WASCAL WRAP 2 project, which provided the necessary equipment and advice to enable the GHG

data collection in Ghana. I am also grateful to the team at the "University of Kassel, Institute for Sustainability, Centre for Environmental Systems Research (CESR)", under whose auspices I was hosted and supervised during my time in Germany.

I am deeply grateful to Prof Wilson Agyei Agyare, the Director of the Doctorate Research Program (DRP – CCLU / KNUST) in Kumasi and Prof Eric Kwabena Forkuo, the Deputy Director of the same programme, for their guidance and support. I would also like to express my appreciation to the entire staff of the Climate Change and Land Use (CCLU) programme, as well as the management of the KNUST for their assistance, dedication and unwavering support throughout the completion of this thesis.

I extend my thanks to Mr Padmore Boateng Ansah, Eunice Okyere-Agyapong, Bismark Owusu, and Ms. Dzigbordi Solomon-Ayeh, for their support during the GHG data collection process and data analysis. My gratitude also extends to those who contributed to my work in various ways, including my colleagues from WASCAL CCLU, Batch 5.

CHAPTER 1 : GENERAL INTRODUCTION

1.1 Background

Climate change has been a worldwide and ongoing concern over the years, as a result of increasing atmospheric concentrations of greenhouse gases (GHGs), of which carbon dioxide (CO_2) is the most dominant (IPCC, 2021). Land management practices that sequester carbon or reduce CO_2 emissions play a key role in climate change mitigation strategies (Anokye et al., 2021; Zomer et al., 2008). National and international programmes and institutions have been created to study climate change and land-use, forecast the probable transitions and their effects, and propose adaptation and mitigation strategies (FAO, 2016; Garnaut, 2008). Such programmes include but not limited to:

- The Ghana Climate Innovation Centre (GCIC), established in 2016, provides support to small and medium enterprises and start-ups in developing business concepts that are profitable and can help solve climate change mitigation and adaptation in Ghana (GCIC, 2016);
- The Green Climate Fund (GCF), a global initiative under the United Nations Framework Convention on Climate Change (UNFCCC), focuses on helping developing countries reduce their GHG emissions while adapting to the effects of climate change (GCF, 2010);
- The United Nations Collaborative Programme on Reducing Emissions from Deforestation and Forest Degradation (UN-REDD), a collaboration between the Food and Agriculture Organization (FAO), the United Nations Development Program (UNDP) and the United Nations Environment Program (UNEP). This program supports national REDD+ efforts by providing financial and technical assistance to help countries reduce emissions from deforestation and forest degradation, and enhance carbon sequestration through sustainable forest management (UN-REDD, 2008).

These institutions provide financial support to promote carbon sequestration and reduce greenhouse gas emissions from land-use and land cover changes. However, the limited availability of data on soil carbon stocks and land-use-related CO_2 emissions hinders the

implementation of these mechanisms in developing countries (FAO, 2017; Smith et al., 2014; Zomer et al., 2017).

The world's population is projected to reach nine billion by 2050, and the increasing demand for food, fibre and fuel has increased the pressure on agricultural land and other natural resources (Haile-Mariam et al., 2008). This growing demand contributes to CO_2 emissions in diverse manners. The conversion of forests, grasslands and wetlands to agricultural land is a major driver of CO_2 emissions. Clearing these natural ecosystems release carbon stored in vegetation and soil into the atmosphere, exacerbating climate change. Deforestation in particular has a significant impact on CO_2 levels as it removes critical carbon sinks that absorb CO_2 from the atmosphere. It also significantly impacts CO_2 levels as it removes vital carbon sinks that absorb CO_2 from the atmosphere, thus reducing future carbon sequestration potential (Houghton et al., 2012; IPCC, 2019). Additionally, the use of synthetic fertilizers and pesticides, which are commonly applied to increase crop yields, leads to the oxidation of soil organic matter (SOM) and the emission of CO_2 (Khan et al., 2007). The application of fertilizers in particular can stimulate microbial activity in the soil, leading to further decomposition of organic matter and subsequent release of CO_2 (Smith et al., 2014; Stavi and Lal, 2013).

Soil is among the world's most vulnerable resources threatened by climate change, land degradation and biodiversity loss (FAO and ITPS, 2015). It has an essential function in combating climate change through the regulation of the global carbon cycle. As the largest long-term reservoir of organic carbon in terrestrial ecosystems, it acts as both a source and a sink for atmospheric CO_2 (Lal, 2004). Globally, soil contains approximately twice as much carbon (about 1500 Pg C) as the atmosphere (about 800 Pg C), and almost three times more than plant biomass (500 Pg C) (Anokye et al., 2021; IPCC, 2007; Lal, 2004; Schimel, 2014). However, this large soil carbon reservoir is dynamic, balancing organic and inorganic matter inputs and outputs within the system. Therefore, small changes in the soil carbon pool can have a significant impact on atmospheric CO_2 concentrations, either increasing or decreasing them (Anokye et al., 2021; FAO, 2017; Lal, 2004). The exchange of CO_2 between the land and the atmosphere is largely mediated by soil respiration (SR), also known as soil CO_2 flux (Schlesinger and Andrews, 2000). Land-use change (LUC) plays a critical role in influencing soil respiration, thereby contributing

to variations in soil carbon storage and atmospheric CO_2 levels (Schlesinger and Andrews, 2000).

Land-use change (LUC) represents a major anthropogenic source of greenhouse gas emissions. From 1990 to 2005, net CO_2 emissions from LUC was estimated at 1.5 ± 0.7 Pg C per year, accounting for 8 – 12% of total CO_2 fluxes to the atmosphere (Le Quéré et al., 2009), mainly driven by deforestation in tropical and subtropical regions (Don et al., 2011).

Land-use change is related to changes in vegetation type and management practices. These changes can affect above-ground biomass, soil organic matter content, soil microbial communities and the microenvironment for plant growth, thereby affecting SR and temperature changes (Han et al., 2014). Monitoring soil respiration and temperature is therefore critical to understanding the terrestrial carbon balance (Han et al., 2014). Factors such as soil moisture and nutrient content can alter soil organic matter and soil organic carbon content, both of which are crucial for soil carbon storage and respiration (Cheng-Fang et al., 2012; Xiaojun et al., 2013).

Therefore, understanding the effects of different LUCs on soil respiration (SR) provides critical insights for ecosystem management practices (Liu et al., 2016). These include practices that maintain soil health and increase soil organic matter content through organic farming and agroforestry. Furthermore, with the increasing global population and growing demand for food and fibre, understanding how future land development and LUCs may affect SR remains highly relevant for predicting and mitigating potential impacts on the global carbon cycle.

1.2 Problem Statement and Justification

The accumulation of greenhouse gases (GHGs) in the atmosphere, particularly carbon dioxide (CO_2), methane (CH_4) and nitrous oxide (N_2O), contributes significantly to global warming. These gases absorb shortwave solar radiation and re-emit it as longwave radiation, increasing atmospheric temperature and ultimately driving changes in the Earth's climate (IPCC, 2021; Montzka et al., 2011). The primary sources of these emissions are energy production, agriculture, LUC and industrial processes (WRI, 2017). Globally, CO_2 accounts for approximately 65% of GHG emissions, mainly from fossil

fuel combustion, cement production and land conversion, followed by CH_4 at 16% (largely from agriculture) and N_2O at 6% (primarily from industry and agriculture) (IPCC, 2014).

Land-use and land cover (LULC) change represents a major human impact on the Earth's surface (Foley et al., 2005). Activities including cultivation, tree plantations, vegetation removal, slash-and-burn practices and other forms of degradation or restoration, can function as either GHG sinks or sources, influencing the global carbon cycle (Lal, 2004).

In West Africa, the major sources of GHG emissions are land-use change and forestry (LUCF), accounting for 31.5% of emissions, followed by energy at 27.1% and agriculture at 22.7% (USAID, 2019). In Ghana, however, the total GHG emissions are estimated at 51.78 million tonnes of CO_2 equivalent ($MtCO_2e$), primarily from the energy sector, agriculture, forestry and other land-uses (AFOLU), waste and industrial processes and product use (IPPU) (EPA, 2024). In 2021, the emissions breakdown by sector was 51.2% from energy, 38.3% from AFOLU, 7.3% from waste and 3.2% from IPPU (EPA, 2024).

The AFOLU sector is the second largest source of GHG emissions in Ghana (Owusu and Asumadu-Sarkodie, 2017; EPA, 2024). Agriculture and climate change are closely intertwined. As mentioned in the IPCC (2019) report, agriculture contributes about 13.5% of annual GHG emissions, with forestry adding another 19%. However, both agriculture and forestry also present significant mitigation opportunities, including carbon sequestration, improved soil and land-use management and biomass production (IPCC, 2019; Smith et al., 2020). Soil CO_2 release through respiration is a major source of carbon emissions to the atmosphere, driven by interactions between climate and the biological, chemical and physical properties of the soil (Kirschbaum, 2000; Lal, 2004; Oorts et al., 2007).

In recent years, much research has focused on soil respiration due to its role in increasing global warming. In Ghana for example, Quansah et al. (2015) estimated CO_2 fluxes from three contrasting ecosystems, made up of grassland, a mixture of fallow and cropland and a nature reserve in the Sudanian Savanna using the Eddy Covariance (EC) method.

Similarly, Anokye et al. (2021) and Maccarthy et al. (2018) estimated CO_2 emissions from three land-use systems (arable land, oil palm plantation and forestland) in the semi-deciduous forest zone of Ghana using a gas entrapment method and back titration with 1.0M HCl and phenolphthalein indicator to measure soil CO_2 emissions. Internationally, studies by Fan et al. (2015), Lima et al. (2020) and Díaz et al. (2017) used CO_2 sensors (infrared analysers) to directly measure soil respiration in the field.

Research on soil respiration in West Africa has largely focused on short-term measurements, typically ranging from 10 days to a maximum of six months. As a result, full-year soil respiration data across different land-use types are limited, despite their importance in capturing seasonal variations in CO_2 fluxes and providing reliable emission factors for different LULC types. Only a few studies have explored the seasonal dynamics of soil respiration. Brümmer et al. (2009), for instance, measured soil-atmosphere CH_4 fluxes in southwestern Burkina Faso over a 10-month period, covering June to September 2005 and April to September 2006, across four land-use types: sorghum, cotton, peanut, and savanna woodland. Similarly, Owusu et al. (2024) investigated soil respiration dynamics in the Vea catchment, a sparsely gauged semi-arid savanna ecosystem in northeastern Ghana, focusing on savanna woodland, cropland, and grazeland. However, these studies were conducted in semi-arid regions, which have distinct climatic conditions compared to the moist semi-deciduous forest. Furthermore, research aimed at projecting future CO_2 emissions remains scarce, with most existing studies originating from Western countries.

It is worth noting that most developing countries, including Ghana rely on default estimated values when reporting their nationally determined contributions (NDCs). These estimates are often derived from satellite imagery, the Intergovernmental Panel on Climate Change (IPCC) Tier 1 dataset and other secondary data sources (Federici et al., 2015; Grassi et al., 2017; IPCC, 2006, 2019). Utilizing Tier 1 dataset involves applying default emission factors provided by the IPCC and activity data, which can be used by regions or countries with limited resources, data or technical expertise. This approach requires minimal country-specific data, making it a feasible option for many developing countries, including Ghana that lack comprehensive dataset (IPCC, 2006, 2019).

However, there are more advanced tiers, such as Tier 2 and Tier 3, that provide higher accuracy but require greater resources and data specificity. The Tier 2 approach uses country-specific emission factors and more detailed activity data, improving the accuracy of the estimates over Tier 1. It includes data that reflects local conditions and management practices, enabling a better approximation of actual emissions (IPCC, 2006, 2019). However, this approach requires more investment in data collection, research and analysis, making it more resource-intensive than Tier 1. On the other hand, Tier 3 delivers the highest level of detail and accuracy by using sophisticated models and comprehensive, often site-specific, measurements. It involves direct measurements and repeated inventories over time, which requires significant technical, financial and data resources. This tier is particularly valuable for countries aiming for high-accuracy reporting in AFOLU sectors (IPCC, 2006; 2019).

Therefore, there is an urgent need to adopt a Tier 2 or Tier 3 approaches for more accurate quantification of GHG emissions from different land-uses. This would provide accurate and reliable baseline data for more appropriate estimates of Ghana's national GHG inventory (IPCC, 2006; 2019). This transition is important because Ghana currently relies on the Tier 1 method to estimate GHG emissions from several land-use types (EPA, 2024). In light of the Paris Climate Agreement (The Paris Agreement/UNFCCC), many countries have committed not only to accurately report their GHG emissions at the national level using either a Tier 2 or Tier 3 approach, but also to begin mitigating anthropogenic GHG emissions in the coming decades, as outlined in their Nationally Determined Contributions (NDCs). To achieve these goals, accurate locally derived data is needed.

1.3 Aim and Objectives

1.3.1 Aim

This study aims to provide baseline data and to analyse the evolution of soil carbon dioxide emissions in the AFOLU sector in Ghana.

1.3.2 Specific Objectives

i. Determine land-use and land cover (LULC) change and intensity analysis of land transformation from 1986 to 2022 of a semi-deciduous forest (Bobiri Forest Reserve) and its environs in Ghana.
ii. Determine the effect of LULC change and seasonal variability on soil respiration rate from three dominant land categories (Forest, Fallow and Cropland) in a semi-deciduous forest enclave in Ghana.
iii. Project the evolution of CO_2 emissions from soil and possible emission pathways in a semi-deciduous forest enclave in Ghana from 2022 to 2050.

1.4 Research Questions

i. How did land-use and land cover (LULC) change in the Bobiri Forest Reserve (BFR) and its environs from 1986 to 2022?
ii. How do LULC changes and seasonal variability influence soil respiration rate across three dominant land categories in BFR and its environs?
iii. What are the projected trends and potential emission pathways of soil CO_2 emissions in a semi-deciduous forest enclave in Ghana from 2022 to 2050?

1.5 Structure of the Thesis

The thesis is structured based on manuscript format. It contains six (6) chapters. **Chapter One** provides an overview of the study. This includes the background, problem statement and justification, aim, objectives, research questions, and scope and limitations of the study.

Chapter Two presents a conceptual and theoretical review of the literature on the topic. The conceptual review contains a definition of terms and concepts used in the study, a brief overview of land-use land cover, remote sensing (RS) and geographic information system (GIS) techniques. The review consists of RS and land-use studies, the impact of agriculture, forestry and other land-use (AFOLU), factors affecting soil respiration in the AFOLU sector and spatial models used for projecting future emissions.

Chapter Three addresses specific objective one, which deals with the determination of land cover change and intensity analysis of land transformation from 1986 to 2022 of a semi-deciduous forest (Bobiri forest reserve) and its environs in Ghana.

Chapter Four reports on specific objective two. This deals with determining the effect of LULC change and seasonal variability on soil respiration rate from three dominant land categories (Forest, Fallow, cropland) in a semi-deciduous forest in Ghana.

Chapter Five addresses specific objective three. This looks at projecting future land-use change using business as usual (BAU) scenario and soil CO_2 evolution in a semi-deciduous Forest in Ghana. **Chapter Six** presents the general discussion. **Chapter Seven** presents the summary, conclusions and recommendations of the research.

1.6 Research Scope and Limitation

The study is limited to the BFR, a semi-deciduous forest type, and its environs approximately, within 10 km from the BFR, located in the Ashanti Region of Ghana. Additionally, the study only measured soil respiration, i.e. CO_2 efflux from the dominant land-use in the study area, namely: Forest, Fallow land and Cropland (maize and rice). Variation of CO_2 efflux in these land-use were monitored for a period of 13 months starting in June 2023 to June 2024 to capture the seasonal variation across the various land-use types.

The limitations of the study are:

i. The LULC change and intensity analyses were done in this study, where remote sensing (RS) and GIS techniques were applied and was limited to a maximum distance of 10 km from the Forest Reserve (BFR). Expanding beyond this area was not feasible due to the constraints of measuring CO_2 efflux, which was also conducted within the designated area. Consequently, this study did not explore land-use and land cover changes beyond the reserve environs, such as within 20 to 30 km away, to determine whether the rate of deforestation would differ as you move further away from the forest reserve.
ii. The assessment of Greenhouse gas (GHG) efflux across different land-use types was limited to only soil CO_2. This was due to the fact that even though gas samples

of methane (CH_4) and nitrous oxide (N_2O) were collected, there was lack of adequate equipment for the analyses of CH_4 and N_2O. As a result, these two gases could not be included in the study. In addition, plant carbon dioxide exchange could not be measured, which would have allowed the determination of net carbon balance and quantification of the amount of carbon sequestered in these ecosystems. Furthermore, due to budget constraints, soil microbial biomass carbon and nitrogen analyses could not be performed for the selected plots and to relate these results with the CO_2 emissions.

iii. In terms of future projection of land-use change and the associated evolution of soil CO_2 emission, the analysis was limited by the lack of data, particularly regarding the specific quantification of future plantations, afforestation and agroforestry projects or activities in the study area. This limitation prevented simulating future LULC maps under alternative scenarios, such as an integrated or sustainable land management scenario aimed at reducing deforestation and restoring forest cover, or a land degradation scenario representing the worst situation with increased deforestation and cropland expansion. These scenarios could have offered a more comprehensive perspective on the potential future of land-use change in the study area. As a result, the simulation was restricted to the business as usual (BAU) scenario, based on the observed trends from 1986 to 2022, and projecting these trends to 2050.

CHAPTER 2 : LITERATURE REVIEW

2.1 Conceptual Review

2.1.1 Definition of Key Concepts

Soil greenhouse gas emissions: Soil greenhouse gases (GHGs) are gases released from soils that contribute to the greenhouse effect, trapping heat in the Earth's atmosphere. The primary soil GHGs are carbon dioxide (CO_2), methane (CH_4) and nitrous oxide (N_2O) (EPA, 2024; IPCC, 2019). However, this study focuses on soil CO_2 emission also known as soil respiration, which refers to the process through which CO_2 is emitted from the soil into the atmosphere. It occurs due to the combined activities of soil organisms, plant roots, and microorganisms breaking down organic matter (Lal, 2004). The soil respiration was measured using a sensor equipped with an infrared gas analyser (Vaisala, 2024).

Modelling soil CO_2 emission: Modelling is the process of creating a simplified representation or simulation of a real-world system, process or phenomenon to better understand, analyse, or predict its behaviour. Models are valuable tools used across various fields to study complex systems by breaking them down into manageable and comprehensible components (Grimm and Railsback, 2005; Sterman, 2002). In the context of this study, two modelling approaches will be employed. One involves using site-specific CO_2 data collected from different fields to develop a model that estimates soil CO_2 emissions without directly measuring the CO_2 on the field. By using a few key soil parameters, the model will allow the estimation of the amount of GHG emissions from the land-use under investigation with relatively good accuracy (Sileshi, 2014). The second is stochastic modelling, which allows the simulation of future LULC development in the study area using the Dinamica Environmental Geoprocessing Object (EGO) (Soares-Filho et al., 2002).

2.2 Empirical Review

2.2.1 Land-use and Land-cover Change (LULCC)

Land-use is defined as the human utilization of land for several purposes including agriculture, urban development, forestry and recreation, while land cover refers to the physical material on the Earth's surface, which includes vegetation, water and man-made structures (Bufebo and Elias, 2021; Lambin et al., 2006; Turner et al., 2007). Understanding the interactions between land-use and land cover is essential to assess human impacts on the environment and to develop sustainable land management strategies.

Land-use and land cover (LULC) change is one of the most significant human activities affecting the Earth's surface, with implications for global environmental systems (Foley al., 2005). In recent decades, extensive agricultural expansion, urbanization, deforestation and infrastructure development have drastically changed natural landscapes. These transformations have led to habitat loss, biodiversity decline and significant disruptions to ecosystem services, such as carbon sequestration, water regulation and soil fertility (Foley et al., 2005; Vitousek et al., 1997). For example, the conversion of forests to agricultural land, especially in tropical regions, has been a major driver of changes in the global carbon cycle by reducing carbon sequestration capacity and increasing greenhouse gas (GHG) emissions (Lambin and Meyfroidt, 2011).

Globally, land-use and land cover (LULC) change contributes about 10 – 12% of anthropogenic carbon dioxide (CO_2) emissions, mainly due to deforestation and land degradation (Smith et al., 2014). These land-use changes are driven by a complex mix of socio-economic, political and technological factors, including population growth, agricultural intensification and economic development (Meyfroidt et al., 2013).

In Ghana, LULC change has been of particular interest. It is largely driven by agricultural expansion and deforestation to meet the demands of a rapidly increasing population for staple food and cash crops such as maize and rice, and cocoa and oil palm, respectively (Acheampong et al., 2016).

Between 1990 and 2010, the country lost about 33.7% of its forest cover, corresponding to about 2.5 million hectares, mainly due to agricultural activities and illegal logging (Damnyag et al., 2013; Hansen et al., 2013). This deforestation has led to increased greenhouse gas emissions, loss of biodiversity and changes in local climate patterns (Asante and Ayee, 2019). In addition, the conversion of natural forests to agricultural land has altered carbon dynamics, reducing carbon sequestration and exacerbating soil degradation (Ansari et al., 2022). In Ghana, like many other developing countries, the challenge is how to balance economic development with the need to protect natural ecosystems and mitigate the impacts of climate change (UNDP, 2022). Addressing LULC change in Ghana will require integrated land management strategies that promote sustainable agriculture, protect forests and restore degraded lands (Asubonteng et al., 2018).

2.2.2 Remote Sensing and Land-use Land-cover Studies

Land-use and land cover change studies are widely used to monitor human-induced environmental changes. Numerous studies worldwide recognize that LULCC results from complex interactions between human activities and environmental factors (Goswami et al., 2019; Issa, 2018; Qader, 2016). Consequently, information on LULCC at various spatial and temporal scales is crucial for assessing trends in the abiotic and biotic components of ecosystems (Nguyen and Hens, 2019; Prabhu and Kulkarni, 2012). For optimal planning, management, regulation and utilization of the Earth's resources, it is essential for resource managers and users to understand the nature and rate of LULCC (Deka et al., 2019; Gashu and Gebre-Egziabher, 2018). Therefore, remote sensing (RS) combined with geographic information systems (GIS) provides a vital tool for analysing LULC history from the past to the present and projecting future land cover changes using satellite imagery. This helps in understanding the dynamics and direction of change. In addition, it provides the basis for systematic land-use planning, management and ecological restoration, contributing to socio-economic development (Liping et al., 2018). Remote Sensing (RS) and Geographic Information Systems(GIS) are fundamental tools for acquiring accurate spatial data on LULC and analysing changes within a study area (Pervez et al., 2016; Srivastava et al., 2013). Satellite images effectively capture LULC

states, providing real-time data for analysing, simulated and monitoring land systems at various spatial and temporal resolutions using RS applications (Rai et al., 2017; Singh et al., 2017). It also provides valuable information on the nature and intensity of land change, including the shape and pattern of forest loss, and it can monitor forest disturbance and dynamics using time series data (Hansen et al., 2009; Kennedy et al., 2010). Meanwhile, GIS offers a flexible environment for collecting, storing, analysing and displaying digital data necessary for change detection (Panwar and Malik, 2017).

There are numerous satellite data sources with varying image properties, such as MODIS, Landsat series, Ikonos, QuickBird and Sentinel (Lillesand et al., 2015). The Landsat satellite series is a primary source of environmental data and is widely used at local and regional levels for various research purposes with a spatial resolution of 30m x 30m. These include but are not limited to, LULC change (Ampim et al., 2021; CILSS, 2016; Kleemann et al., 2017; Koranteng et al., 2017; Panwar and Malik, 2017), soil erosion (Bessah et al., 2019; Moriaque et al., 2020), land degradation (Ayele et al., 2018; Gebrehiwet, 2004), and biodiversity assessment (Baan et al., 2013; Gary et al., 2017). Landsat products can be easily downloaded for free from Earth Explorer with historical data available from 1982 to the present (https://earthexplorer.usgs.gov/).

Similarly, Sentinel satellite data is another excellent source, offering a higher spatial resolution of 10 x 10m. It is also available to download free of charge from the Copernicus Open Access Hub (https://sentinels.copernicus.eu/web/sentinel/sentinel-data-access/sentinel-products). However, the availability of historical imagery is limited as Sentinel data only started in 2013. Since then, researchers have used it to determine forest loss and other land-uses (Koranteng, 2021; Koranteng et al., 2018; 2020), monitor land cover and crop production (Qader, 2016), and linked patterns to processes using intensity analysis of land change dynamics (Aldwaik and Pontius, 2012; Manzoor et al., 2022).

2.2.3 Remote Sensing and Satellite Image Classification

Satellite image has significantly advanced over the years and coupled with RS techniques has led to the development of numerous techniques and datasets for classifying and mapping LULC changes. Among the various satellite datasets available, the Landsat

series stands out due to its ability to classify different landscape components on a large scale using historical images from the 1990s (Foody and hill, 1996; Lu et al., 2004).

Satellite image analysis involves several steps, including pre-processing, image classification or segmentation, post-processing and evaluation (Jensen, 2015). Common pre-processing methods in remote sensing include radiometric and geometric correction, radiometric, spatial, and spectral enhancements and Fourier analysis (Jensen, 2015; Lillesand et al., 2015). Radiometric correction specifically resolves inconsistencies in pixel intensities that are unrelated to the scene being scanned, reducing variations caused by factors, such as changing sun angles and incident solar radiation. Various algorithms have been developed to perform radiometric correction (Jensen, 2015). Geometric correction is another crucial step in pre-processing, which helps to avoid geometric errors caused by distorted images. It is essential for accurate LULC mapping and quantitative change detection, particularly when aligning multiple images from different times (Lillesand et al., 2015).

Image classification, a key process in remote sensing, involves categorizing pixels in an image into specific classes based on spectral patterns and radiance measurements obtained in various bands (Lillesand et al., 2015). The two main classification techniques are unsupervised and supervised classification (Ampim et al., 2021; Hackman et al., 2017; Jensen, 2015; Koranteng, Adu-Poku, et al., 2017; Neya et al., 2020; Nyamekye et al., 2020).

Unsupervised classification does not rely heavily on the analyst's knowledge of the study area. Instead, it uses clustering algorithms to partition image data using the numerical information (DN values) within the image. However, the analyst must determine the number of classes in the dataset and may need to adjust the output by merging or splitting groups. The primary goal is to generate spectral categories on the basis of spectral similarities, although the process is not entirely free from human inference (Mohd Hasmadi et al., 2009).

Supervised classification, on the other hand, relies on pre-existing knowledge of the study site. The analyst defines the classes by selecting training areas, which are specific cover

types known from ground data (Tempfli et al., 2009). This method generally provides more accurate class definitions and higher classification accuracy than unsupervised classification (Hassan and Elhag, 2013; Mohd Hasmadi et al., 2009; Prasetyo et al., 2009). After the algorithm is trained with these sample areas, it is applied to the entire image to produce the final classification. This method heavily relies on the analyst's expertise in defining the spectral characteristics of the classes (Hassan and Elhag, 2013; Mohd Hasmadi et al., 2009; Prasetyo et al., 2009).

Both classification methods utilise different types of algorithms, notably fuzzy logic (Venkateswaran et al., 2013), principal component analysis (PCA)) (Aziz et al., 2013; Mishra et al., 2017), minimum distance to mean, maximum likelihood, nearest-neighbour, artificial neural networks, support vector machines, decision trees, random forests and convolutional neural networks (Al-doski et al., 2013; Crisci et al., 2012; OpenGenus, 2022). Among these, the maximum likelihood classifier is the widely used method, considering not only cluster centres but also their shape, size and orientation by computing statistical distances using mean values and covariance matrices (Tempfli et al., 2009). This method typically achieves the highest classification accuracy (Mohd Hasmadi et al., 2009; Perumal and Bhaskaran, 2010).

The final step in image processing is accuracy assessment, crucial for estimating changes accurately in LULC change detection studies. This step ensures the reliability of the resulting data for decision-making processes (Congalton, 1991; Lillesand et al., 2015). The most used statistics in accuracy assessment are producer's and user's accuracies, errors of commission and omission, overall accuracy and the kappa coefficient (Lillesand et al., 2015). To be considered reliable, the producer and user's accuracies should be above 85 %, these accuracies are essential for assessing the quality of LULC classification (Congalton and Green, 2019; Lillesand et al., 2015).

Foody (2002) highlighted that errors of commission and omission should be kept below 10 – 15% to ensure a robust classification result (Pontius and Millones, 2011). Landis and Koch (1977) introduced the kappa coefficient and provided guidelines for interpreting its values: a kappa of 0.81 – 1.00 shows "nearly perfect" agreement; 0.61 – 8.00 shows "high"

agreement; and values below 0.60 indicate moderate to poor agreement. However, Lillesand et al. (2015) and Monserud and Leemans (1992) reported that a kappa coefficient above 0.80 is considered excellent for remote sensing image classification. They also emphasized that values between 0.60 and 0.80 are good to very good, while values below 0.60 indicate moderate or poor classification reliability in the classification results.

2.2.3.1 *Change Detection*

Change detection involves the spatial representation of two points in time by controlling all variances caused by unrelated factors and measuring changes caused by the variables of interest (Green et al., 1994). The primary reason for using remotely sensed data in change detection is that changes in the objects of interest will cause distinguishable changes in reflectance values or local textures (Deer, 1995). Despite spatial, spectral, thematic and temporal restrictions in digital change detection, numerous strategies are available, and choosing the most suitable method or algorithm is crucial for any research topic (Lu et al., 2004).

Change detection uses multi-temporal remote sensing data to quantitatively analyse the historical effects of events, thereby helping detect changes in LULC attributes (Ayele et al., 2018; Tempfli et al., 2009). The aim is to identify areas that show differences between two or more imaging dates and to quantify the temporal effects in a multi-temporal dataset (Théau, 2008). This method has been widely used in studies to monitor LULC changes such as, deforestation, regeneration, wetland change, urban expansion and cropland change (Ampim et al., 2021; CILSS, 2016; Firdaus, 2014; Gary et al., 2017; Hassan and Elhag, 2013; Koranteng et al., 2020; Lu et al., 2004; Mohd Hasmadi et al., 2009; Panwar and Malik, 2017; Peters, 2019; Prasetyo et al., 2009; Rai et al., 2017).

2.2.3.2 *Land Intensity Analyses*

Land intensity analysis refers to assessing the extent and intensity of human activity or use on a specific area of land over a given period. It examines how land is utilized, the degree of transformation or exploitation it undergoes, and its impact on ecosystems (Aldwaik and Pontius, 2012; Turner et al., 2007; Verburg et al., 2013). Understanding the patterns and processes of LULC change has become a central focus of research exploring

the complex relationships between humans and the environment, from local to global scales (Turner et al., 2007; Verburg et al., 2013). Tracking LULC change trends and characteristics is essential for monitoring land transformations, projecting future changes, analysing their consequences and managing natural resources. Therefore, initial characterizations of land changes must be presented in a manner that is accessible to a wide audience (Agarwal et al., 2002).

Land intensity involves creating maps of the same set of land classes over multiple periods. Overlaying these maps for any two points in time produces a cross-tabulation matrix. In this matrix, rows represent the classes at an initial time, columns represent the classes at a subsequent time, and the entries show the area that transitioned from one class to another during the time interval. Entries on the diagonal indicate land stability, while off-diagonal entries indicate land change. These matrices serve as the basis for a wide range of LULCC studies (Aldwaik and Pontius, 2012; Anwar, 2002; Bessah et al., 2019; Bufebo and Elias, 2021; Deka et al., 2019; Koranteng et al., 2020; Manzoor et al., 2022; Neya et al., 2020; Singh et al., 2015).

Examination of these matrices helps to identify important patterns of LULC. However, simply comparing elements in the matrices does not reveal whether the observed patterns are due to systematically more or less intensive processes than random or uniform processes. To address this, Pontius et al. (2004) developed a technique to analyse land change relative to class size to identify systematic transitions between two points in time. For example, in the US, Pontius et al. (2004) found that residential or built-up areas tend to expand at the expense of forest rather than bare land. In Ghana, Alo and Pontius (2008) developed this technique to compare two regions with different land category distributions and found different land change processes in protected and unprotected areas. Other studies have refined these techniques to analyse transitions from multiple land categories simultaneously (Versace et al., 2008) and to detect systematic transitions such as those between pasture/scrubland and vineyard (Manandhar et al., 2010). However, most of these methods only address changes between two or multiple points in time, answering questions on Which transitions are intensively avoided or targeted by a given land category, and is this pattern stable across time intervals?

Aldwaik and Pontius (2012), addressed these questions using three levels of analyses: (i) Identifying time intervals with slow versus fast annual rates of overall change; (ii) Determining which land categories are relatively dormant or active during specific intervals and whether this pattern remains stable; (iii) Examining which transitions are intensively avoided or targeted by specific categories and assessing their stability. The analyses involve examining all time points concurrently to understand land change processes. The interval level analyses, the total change in each interval, the category level examines gross gains and losses across space, and the transition level assesses how transition sizes and intensities vary among categories. This comprehensive approach provides detailed insights into land-use dynamics and land-cover changes.

2.2.4 Impact of Agriculture, Forestry and Other Land-use on Soil Greenhouse Gas Emissions

Globally, soil respiration is crucial for both sequestering and or emitting greenhouse gases, serving as a key element of the carbon cycle, particularly in the AFOLU sector. Soil respiration, which refers to the release of CO_2 from the soil resulting from microbial decomposition of organic matter and root respiration, is influenced by land-use practices and changing land cover (Luo and Zhou, 2006; Raich and Schlesinger, 1992). In Ghana, the AFOLU sector is the second largest source of national greenhouse gas emissions after the energy sector and contributes significantly to the country's overall emissions profile. The Environmental Protection Agency (EPA) of Ghana reported that in 2022, the AFOLU sector accounted for approximately 38.3% of the country's total GHG emissions (EPA, 2024). Land-use change, deforestation and soil management practices were the main contributors (EPA, 2019, 2022, 2024). Agricultural expansion, specifically for cash crops, such as cocoa and oil palm, has caused significant deforestation and soil disturbance, which has increased soil respiration rates and consequently CO_2 emissions (Lawrence and Vandecar, 2015; Nasser et al., 2020; Paustian et al., 2016). Traditional agricultural practices, such as slash-and-burn, exacerbate this problem by accelerating soil degradation and increasing CO_2 release through increased soil respiration (Acheampong et al., 2021).

2.2.4.1 *Estimation of Soil Respiration from AFOLU*

The accurate estimation of CO_2 emissions from soil respiration is a major constraint, particularly for developing countries where data availability and resources are limited. Soil respiration, a key process in the global carbon cycle, includes the release of CO_2 through microbial decomposition of organic matter and root respiration (Schlesinger and Andrews, 2000).

Globally, various techniques and technologies are available for monitoring soil respiration, including the static alkali absorption chamber method for trapping CO_2 flux, chamber-based methods using infrared gas analyser and the use of Gas chromatography, eddy covariance systems and soil flux models (Baldocchi, 2003; Chae et al., 2003; Ibrahim, 2020; Parkin et al., 1997; Pumpanen et al., 2004). Chamber-based methods, such as closed dynamic chambers or static chambers, are widely used for field measurements. These chambers capture the gas emitted from the soil, which can then be analysed using gas chromatography or infrared gas analysers (Chae et al., 2003; Pumpanen et al., 2004). More advanced techniques, like the eddy covariance system, measure CO_2 fluxes over larger spatial scales by analysing fluctuations in atmospheric CO_2 concentration and wind speed. This method is useful for continuous monitoring but requires substantial expertise and financial investment. Remote sensing technologies, including satellite-based tools, have also been employed for large-scale assessments of land-use changes and their impact on soil respiration, though these methods are often complemented by ground-truthing through on-site measurements (Li et al., 2021).

In many developing countries, including Ghana, the Tier 1 approach is commonly used to estimate GHG emissions as part of the country's Nationally Determined Contributions (NDCs). This is primarily due to limited access to localized data, advanced equipment and the technical expertise required for the more sophisticated Tier 2 and Tier 3 methods (EPA, 2022). In Ghana, efforts to monitor soil respiration are often hindered by the lack of continuous in situ measurement infrastructure. However, some projects have introduced handheld soil gas analysers using simple static chamber methods and gas entrapment methods (Anokye et al., 2021; GreenGaDe, 2024; Koomson, 2013;

Maccarthy et al., 2018). While these are less precise than more advanced systems, they provide an important starting point for collecting localized and site-specific data.

2.2.4.2 *Factors Regulating Soil Respiration from the AFOLU Sector*

In this study, soil respiration is monitored from cropland (maize and rice fields), forest land and fallow land (open forest).

Soil respiration is driven by a complex interplay of biological, chemical and physical factors (Davidson and Janssens, 2006; Raich and Schlesinger, 1992). In agricultural systems, such as maize and rice cultivation, soil respiration is regulated by management practices like fertilizer application and irrigation. Studies have shown that the application of nitrogen fertilizers can enhance microbial activity, leading to increased CO_2 flux from soils. For example, Song et al. (2014) observed that fertilizer application in maize fields increased soil organic carbon decomposition, driving higher CO_2 emissions. Additionally, tillage practices that disturb the soil structure can lead to increased aeration and the mineralization of organic matter, further contributing to elevated CO_2 flux (Baker et al., 2007). Conversely, no-till practices can reduce CO_2 emissions by preserving soil organic matter and maintaining more stable micro-environments for soil microbes (Almaraz et al., 2018). In rice fields, water management practices play a critical role.

Flooded conditions in paddy fields typically reduce aerobic microbial activity, resulting in lower CO_2 emissions compared to dryland crops such as maize (Zou et al., 2007). However, in rainfed rice systems or non-flooded lowland areas, CO_2 emissions tend to be higher than in continuously flooded fields that are more susceptible to CH_4 emission due to the dominance of aerobic conditions (Ma and Lu, 2011). Without consistent waterlogging, the soil remains aerobic, promoting greater microbial activity, which accelerates the decomposition of organic matter and increases CO_2 release. This effect is particularly pronounced in soils with higher organic matter content (Davidson and Janssens, 2006; Kuzyakov, 2006; Lal, 2004).

In natural forests, soil CO_2 emissions are regulated by factors such as temperature, moisture and root respiration. Forest soils are often rich in organic matter, and microbial decomposition is a primary driver of CO_2 flux. Temperature plays a critical role, with

warmer conditions generally increasing microbial metabolic rates, leading to higher soil respiration (Davidson and Janssens, 2006). Soil moisture is another key factor, for moderate levels enhance microbial activity and root respiration, but excessively wet or dry conditions can inhibit these processes (Liu et al., 2009). In tropical forests, the dense root systems contribute significantly to soil CO_2 emissions. Studies by Wang et al. (2019) have shown that root respiration can account for up to 50% of the total soil CO_2 flux in forest ecosystems.

In the fallow lands emissions are influenced by age of the land under fallow conditions which dictate the stage of ecological succession and the accumulation of organic matter (Humanas et al., 2013; Lal, 2004; Offiong and Iwara, 2012). On young fallow land, CO_2 emissions may be relatively low due to reduced vegetation cover and lower root biomass. As the fallow system matures or becomes older, plant growth and organic matter inputs increase, stimulating microbial activity and soil respiration (Ramesh et al., 2019). Research by Ramesh et al. (2019) demonstrated that older fallow plots tend to have higher CO_2 fluxes compared to younger plots, as a result of increased root biomass and organic carbon inputs from decaying plant material. Additionally, the recovery of soil structure and moisture retention capacity during the fallow period can also improve conditions for microbial activity, leading to higher emissions. However, the specific land-use history and prior agricultural practices can leave a lasting impact on soil respiration, with degraded soils potentially showing slower recovery of CO_2 emissions (Humanas et al., 2013).

2.2.5 Projection of Soil CO_2 Evolution using Spatial Land-use Models

Soil CO_2 emissions are critical to the global carbon cycle and influenced by different land-use practices including deforestation, agriculture and urban expansion. Spatial land-use models have become important tools for projecting future soil CO_2 evolution based on land-use changes. The commonly used models include but not limited to:

i. CA-Markov is the combination of cellular automata with Markov chains to simulate future land-use scenarios based on historical land-use changes (LUCs) (Pontius and Malanson, 2005);

ii. Agent-Based Model (ABM) is a multiscale integrated model of ecosystem services, which integrates human decision-making with ecosystem services, to simulate land-use changes (Boumans et al., 2015);

iii. Land change modeller (LCM) is the combination of logistic regression with remote sensing data to model and predict land-use transitions (Eastman and Toledano, 2018);

iv. Land Simulation to Harmonize and Integrate Freshwater Availability and the Terrestrial Environment (LandSHIFT) is a spatially explicit LUC model which simulates the impact of socioeconomic drivers, biophysical constraints and environmental policies on land-use dynamics. It is part of the Integrated Model to Assess the Global Environment (IMAGE) framework and was developed to model large-scale LUCs, particularly in the context of global change scenarios, such as climate change, population growth and agricultural expansion (Schaldach et al., 2011);

v. Conversion of Land-use and its Effects (CLUE-S) model is a spatially explicit LUC model that links socioeconomic, biophysical and policy drivers to simulate land-use transitions. It can operate at multiple scales and is highly suited for projecting LUC at both regional and local levels (Verburg et al., 2002),

vi. Dinamica-EGO, where EGO stands for Environment for Geoprocessing Objects, is a versatile software designed for building environmental models. It is a hybrid spatially explicit that combines cellular automata and probabilistic models to simulate land-use changes. It is widely used for simulating deforestation, urban sprawl and other LUCs, often using high-resolution data (Soares-Filho et al., 2010; Soares-Filho et al., 2002).

The above models are used for projecting future land-use change at various scales, i.e. Global/Regional and local scales, with each having its strengths and limitations. While CA-Markov, Dinamica-EGO and LCM provide a detailed spatial resolution suitable for local studies, models such as LandSHIFT, CLUE-S and Agent-Based models provide a more comprehensive integration of socioeconomic drivers, but with greater data and computational requirements. For studies using very fine spatial resolution, such as in this

study (30 m x 30 m), Dinamica-EGO is particularly useful. This is because it combines a cellular automata framework with probabilistic models (e.g., weights of evidence) and advanced geospatial analysis tools to simulate fine-scale land-use change and spatial dependencies. Its modular design allows for the adjustment of the transition rules to incorporate specific drivers, enabling precise modelling of spatial heterogeneity and region-specific dynamics. Furthermore, iterative simulations refine the model outputs to capture small-scale changes and cumulative effects over time. Additionally, its ability to integrate geospatial data ensures high-resolution representations of land-use transitions, enhancing the accuracy of the results (Mas et al., 2014; Rodrigues and Soares-Filho, 2018).

2.2.5.1 *Applications of Spatial Land-use Models for Soil CO_2 Emission Projections*

Globally models, such as Dinamica-EGO, have been widely used for the simulation of land-use change and its impact on soil carbon emissions. For example Soares-Filho et al. (2010) and Soares-Filho et al. (2002), have used it to project the effects of deforestation in the Amazon, highlighting the significant loss of soil carbon stocks due to the conversion of forests to agricultural land. Similarly, Fuchs et al. (2013) used CLUE-S in Europe to simulate agricultural expansion and its impact on soil CO_2 emissions and found that changing land-use was a major contributor to carbon loss. These studies highlight the importance of spatial land-use models in understanding how human activities, such as deforestation and agriculture, drive the dynamics of soil carbon and the emissions of CO_2. In Asia, CA-Markov models have been used to simulate urbanisation and agricultural expansion and have shown significant impacts on soil carbon stocks and future CO_2 emissions (Pontius and Malanson, 2005).

However, in Africa, where deforestation and agricultural expansion pose significant land-use challenges, the use of spatial land-use models is gaining momentum. Dinamica-EGO and CLUE-S have been applied in parts of sub-Saharan Africa to simulate land-use transitions and their effects on soil carbon dynamics. Luedeling et al. (2014) used a spatial model to assess the impacts of deforestation and agricultural expansion in East Africa on soil CO_2 emissions, demonstrating the rapid depletion of soil carbon as natural landscapes were converted into farmland. Grace et al. (2006) applied similar models to tropical

savannas. They found that fire management and deforestation significantly affected soil carbon storage and CO_2 emissions. These studies show that spatial land-use models can be a valuable tool for understanding the effect of different land management practices on soil CO_2 emissions.

Despite global advances in the use of spatial land-use models to project soil CO_2 emissions, there are significant gaps in their application in the African context, particularly in West Africa. While some studies have examined the immediate impacts of LUC on soil carbon (Amponsah et al., 2018; Iais et al., 2011; Luedeling et al., 2014; Yiran et al., 2012), few have developed spatially explicit models to project future emission pathways. Most of the existing research is observational and provides limited insight into the long-term effects of LUC on soil CO_2 emissions (Anokye et al., 2021; Maccarthy et al., 2018; Wanyama et al., 2019). There is a clear need for more comprehensive spatial modelling studies in Ghana and the wider African region to accurately predict future CO_2 emissions pathways and inform sustainable land management practices.

2.3 Identified research gaps

i. Studies on monitoring and modelling soil respiration in the AFOLU sector are grossly limited in developing countries.
ii. Previous studies in the region have predominantly relied on the gas entrapment method for measuring soil respiration, which is more suited to small-scale applications, such as laboratory experiments, due to the high risk of gas loss before sample analysis. However, large-scale field measurements and intensive monitoring of soil respiration using high-accuracy sensors, which provide significant advantages over the gas entrapment method, remain significantly limited.
iii. Overall, studies on soil respiration across different land-use types primarily focus on establishing linear relationships between CO_2 emissions and soil moisture or temperature. However, research that incorporates multiple soil parameters such as pH, nutrient levels, or soil texture, that are also critical to soil respiration is relatively limited.

CHAPTER 3 : LAND-USE LAND COVER CHANGE AND INTENSITY ANALYSIS OF LAND TRANSFORMATION IN AND AROUND A MOIST SEMI-DECIDUOUS FOREST IN GHANA

https://doi.org/10.1016/j.tfp.2024.100507

Abstract

Land-use land cover change, particularly deforestation has significant implications for global climate and socio-ecological systems as well as resulting ecosystem services from natural systems. In Ghana, the demand for fuel, food and fibre is projected to be the driver of significant expansion of Croplands and mixed vegetation, resulting in degradation and deforestation of natural ecosystems. This research presents a spatiotemporal analysis of land-use/cover change in the Bobiri Forest Reserve (BFR), a moist semi-deciduous forest, and its environs in Ghana. The study aims to investigate the specific changes in dominant land-use land cover (LULC) types in the area using land intensity analyses and to analyse the prevalence of deforestation leakage across the BFR (a protected) and its environs from 1986 and 2022. The study used measured land-cover changes at different levels, including intervals, categories and transitions. The analysis revealed significant changes in land-use intensity across different land classes in the area. The overall rate of land-use and land cover change exhibited acceleration, indicating extensive land development throughout the studied periods. Notably, croplands and mixed vegetation and non-vegetated areas experienced the most gains, while the closed forest class consistently declined. Transitions from forests to croplands and mixed vegetation were observed, highlighting the conversion of natural vegetation for agricultural purposes. Additionally, the results reveal ongoing leakages in the surrounding area of the BFR as compared to the forest reserve with an annual deforestation rate of 0.64% and 0.06% respectively, from 1986 to 2022, with non-vegetated areas and croplands and mixed vegetation dominating the periphery of protected forest areas. Implementing policy measures to define a legal boundary as a buffer zone for the protected area (PA) and restore the forest cover from the designated buffer area is highly recommended. This is particularly important to the entire surrounding of the PA, which is facing deforestation leakage, posing a substantial threat to conservation efforts by exposing the PA to various climatic threats.

Keywords: Bobiri forest reserve (BFR), Remote sensing, Land-use/cover, Intensity analysis, land conversion, leakage, Ghana.

3.1 Introduction

Land cover change is defined in literature as transformations of the biophysical state of the earth's surface, prompted by the interaction of anthropogenic activities and the natural environment impacting the local environment, accumulating into global environmental changes (Frimpong et al., 2023). Land cover change has received major research attention due to its effects on global climate and socio-ecological systems (Asubonteng, 2007; Frimpong et al., 2023; Turner et al., 1995). Land cover change effects on global climate occur through changes in the carbon cycle, considering that the terrestrial ecosystem is a major source and sink of carbon. Land transformation also alters the land's ecosystem services, resulting in the vulnerability or otherwise of places and people to climate and economic events (Lambin et al., 2003). There are two types of land cover changes identified in literature, total conversions and cover modifications. Total conversions occur when one land cover type is completely replaced by another, and cover modifications happen when the attributes of a particular land cover type are changed. An example of conversion is a shift of forest cover to agricultural land, whereas cover modifications include declines in tree density and species richness. The key driver of land cover change is human management (i.e., land-use) but also changes in biophysical factors (Kleemann et al., 2017). Although land cover changes may be monitored at a regional or national scale, the key processes of change occur at local hotspots and deforestation appears to be the most prominent change process in tropical countries, including Ghana, with significant global interest (Addo-Fordjour and Ankomah, 2017).

The process of deforestation commences with a gradual decline of healthy forests due to factors such as excessive (and often illegal) logging, slash-and-burn farming, fuelwood collection, and mining. This eventually results in forest fires, illegal land occupation, or conversion of forests to other land-uses/cover types (Asubonteng, 2007). Previous studies conducted in the tropics, specifically in Ghana, have documented the transformation of portions of many protected areas (PA), including the Bobiri Forest Reserve (BFR) to other land-use/cover (LULC) types, such as agricultural lands, rangelands and logging sites.

However, habitat loss due to deforestation and LUC is a major destructive force in the tropical regions (Asner et al., 2005; Sanfilippo et al., 2017) threatening essential forest ecosystem services, such as carbon storage and biodiversity conservation among others. Aimed to mitigate habitat loss and related decreases in biodiversity, protected areas are widely regarded as the cornerstones of contemporary efforts in the context of rapid human-induced change (Adams et al., 2023; Afriyie et al., 2021).

It is worth noting that PAs in Ghana have largely succeeded in halting or at least reducing deforestation activities and land clearing within their designated boundaries (Ajayi et al., 2023). Nevertheless, declaring a PA "successful" solely based on lower deforestation rates within its boundaries can be misleading if deforestation is simply shifted to surrounding areas of the PA. This phenomenon known as leakage, occurs when land-uses that are detrimental to conservation efforts (for example, deforestation) are transferred to areas outside of the PA's administrative limits (Ewers and Rodrigues, 2008). When this shift occurs in the environs of a PA, it has the potential to alter the composition and structure of vegetation in the PA's environs, potentially restricting the ranges and dispersal capabilities of organisms living within the PA and disrupting other ecological functions (DeFries et al., 2010).

In addition, the effectiveness assessments of PAs can be compromised by leakage patterns, as success is often gauged through a comparison of ecosystem health indicators between the PA and its enclave (Ewers and Rodrigues, 2008). The importance of PA environs has been emphasized in Article 8 of the Convention on Biological Diversity (CBD), which calls on its 196 member countries to “promote sustainable and environmentally sound development near the protected areas to enhance their conservation” (CBD, 1992). Similarly, Aichi Target 11, highlights the need to integrate conservation efforts within PAs into the larger landscape for effective biodiversity protection (CBD, 2010).

Despite acknowledging the impact of PA environs on the success of PA conservation efforts, understanding of the extent of leakages remains limited, with many studies attempting to quantify it globally and examining isolated cases in America, Asia Pacific

and Africa, which found no widespread evidence of deforestation leakage (Fuller et al., 2019; Lui and Coomes, 2016). However, there is only one study conducted in tropical and subtropical regions, encompassing 55 protected areas including one in Ghana (Assin-Attandanso Game Production Reserve), which observed deforestation leakage (Ford et al., 2020). These studies offer some insight into the LULC types that exist around the PA and the various transitions that took place within and around the PA.

Therefore, this research examined LUC in the BFR and its surrounding areas (10 km radius around the BFR) within Ghana's semi-deciduous forest zone from 1986 to 2022. Remote Sensing (RS) and Geographic Information Systems (GIS) were used to analyse patterns and changes in the land cover within the study area. The study aims to investigate the specific changes in dominant LULC types in the area using land intensity analyses developed by (Aldwaik and Pontius, 2012; Lambin and Geist, 1997) and analyse the prevalence of deforestation leakage within the environs of the PA between 1986 and 2022. Understanding the dynamic relationship between land-use and forest changes is of critical importance for the sustainable use and management of forest landscapes and plays a significant role in achieving Goal 15 of the United Nations' Sustainable Development Goals, i.e. “protect, restore, and sustainably utilize terrestrial ecosystems, manage forests sustainably, combat desertification and halt biodiversity loss by 2030”.

3.2 Materials and Methods

3.2.1 Description of the Study Area

The research was conducted in the Ashanti region located within Ghana’s moist semi-deciduous forest zone. With a total area of 853 km^2, the study area includes the BFR and its surrounding areas (Figure 3.1). The BFR covers over 54 km^2 (Hall and Swaime, 1981; Hawthorne and Abu-Juam, 1995) and is surrounded by communities in the Ejisu Municipal of Ashanti region, namely Kubease, Akuokrom, Bomfa, Duampopo, Hwereso, Konongo, New Koforidua, Nobewam, Odumasi, Lowcost, Besease, Donaso, Boankra and Edwenase. The reserve has been subdivided into management units consisting of a butterfly sanctuary, a research and strict nature reserve (protected), and a production area, which together serve production, tourism, research and conservation functions (Djagbletey et al., 2018). Located between latitudes 6° 33' 15" and 6° 48' 85" N and

longitudes 1° 25' 95" and 1° 11' 35" W with a land area of approximately 853.42 km^2, the study area concentrated on the LULC types and their evolutions over time to capture the different land transformations undertaken from 1986 to 2022.

The rainfall pattern in this area is bimodal with a wet semi-equatorial climate. The two rainy seasons occur from March to July and September to late November, with a long dry season starting from December to March and a short one in August. The average annual precipitation varies between 1200 and 1750 mm, with yearly temperatures ranging from 20°C in August to 32°C in March (Baffour-Ata et al., 2021; Benefoh et al., 2008). The BFR unveils a multifaceted vegetation composition highlighted by dominant species like Mahogany (*Khaya anthotheca*), Sapele (*Entandrophragma cylindricum*) and Wawa (*Triplochiton scleroxylon*), alongside a rich understory including Ofram (*Terminalia superba*) and Wawa trees. The coexistence of these trees suggests a complex and interconnected ecological association, potentially characterized by varying roles in the forest ecosystem, such as canopy structure, habitat provision, nutrient cycling, and support of diverse flora and fauna (Djagbletey et al., 2018).

Farming is the leading occupation in the area employing over 68% of the residents in the fringe communities, whereas the industry sector employs just 8% in the study area (Benefoh et al., 2008).

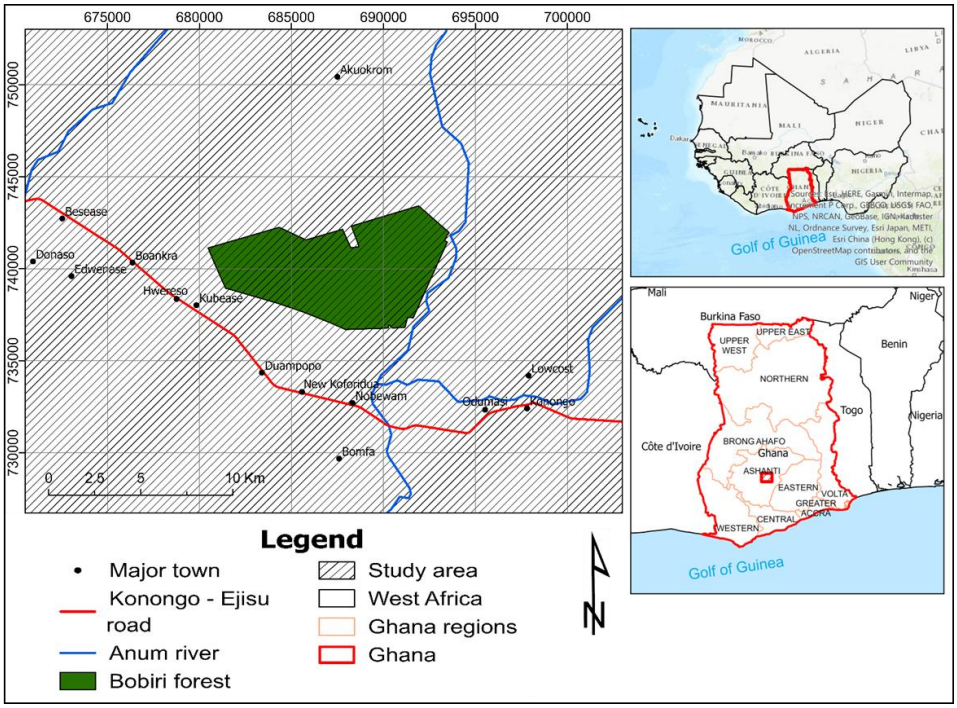

Figure 3.1: Map of the study area (Data source: Environmental Systems Research Institute (ESRI) base map, Google Maps and the Resource Management Support Centre of the Forestry Commission of Ghana)

3.2.2 Data Acquisition

The study utilized Landsat images, with a spatial resolution of 30 m x 30 m, obtained from the United States Geological Survey (USGS) in December 1986, January 2007 and January 2022 (Table 3.1.). The study area experiences significant cloud cover due to prolonged rainy seasons, which presents a challenge in obtaining cloud-free land cover data for change detection between the three different time steps as mentioned by Marshall et al. (1994) and Oduro Appiah et al. (2021). Consequently, Landsat images captured in the mid-dry season of southern Ghana (i.e., December and January) were specifically chosen to ensure minimal or no cloud coverage. In addition, the two months were selected to minimize variations resulting from phenological changes in the vegetation. The objective was to ensure spectral stability for accurately detecting land cover changes around the forest reserve. Change detection analysis focused on two intervals: 1986 – 2007 and 2007 – 2022. Images from Landsat Thematic Mapper (TM) 5, Landsat Enhanced Thematic Mapper Plus (ETM+) 7 and Landsat 9 Landsat Operational Land

Imager/Thermal Infrared (OLI/TIR) for the years 1986, 2007 and 2022 respectively, were used. For the 2007 image (Landsat 7), a gap-filling method using the "Fill no data" tool in QGIS was applied, and the maximum distance (pixels) of 20 was used to search out for values to interpolate, as the study area was affected by the scan-line-corrector error.

Training samples were collected for individual images using different techniques, such as normalized difference vegetation index (NDVI), unsupervised classification, as well as band combinations, which were applied to the stack band images in QGIS to discriminate some of the land classes from the two images (1986, 2007). The unsupervised classification was performed using the K-mean algorithm in QGIS to create 8 to 10 land classes, which were then reclassified based on their spectral similarity values to form five (5) land classes.

Table 3.1: Landsat images used and their characteristics.

Image acquisition date	Landsat Sensor	Cell size	Target WRS Path and Row	Projection
22/01/2022	OLI/TIRS 9	30	path = 194, row = 055	WGS 84 / UTM zone 30N
13/01/2007	ETM+	30	path = 194, row = 055	WGS 84 / UTM zone 30N
29/12/1986	TM 5	30	path = 194, row = 055	WGS 84 / UTM zone 30N

NDVI was calculated using the formula: $NDVI = \frac{(NIR-R)}{(NIR+R)}$, where R is red and NIR is near-infrared and has values that range between +1 and -1. Three classification values were set to categorize three land cover types namely, closed forest, open forest and Croplands and mixed vegetation. NDVI values between 0.2 and 0.4 were used for Croplands and mixed vegetation, between 0.4 and 0.6 were used for open forest and anything above 0.6 was considered a closed forest (EOS, 2019). The range used for Croplands and mixed vegetation was that the images (December and January) used in this study were between the two rainy seasons, during which Croplands and mixed vegetation i.e., maize and rice (main crop in the region), and mixed vegetation, such as grasslands

and recent fallow lands, exhibit characteristics akin to sparse vegetation. However, NDVI was also used to characterize non-vegetated areas such as build-up, water and bare land. NDVI values between -1 and 0.1 were considered non-vegetated (Hashim et al., 2019). The output of the two methods was compared to select areas of similarity from which 200 polygons were randomly digitized, i.e., 50 polygons each for the 4 land cover classes (Table 3.2.) with each polygon having more than 24 pixels.

However, for the year 2022, field data collection was performed to understand land-use within the study area and select locations for training datasets used for supervised classification. These locations were selected after meeting with the indigenous community members who know the history of their lands. With the help of a handheld GPS, coordinates of at least 20-squared polygons (at least 50 m x 50 m) for each land-use type i.e. 80 squared polygons and completed 200 polygons (30 extra polygons were created for each land-use type) were recorded using Google Earth Pro image (see Figure 3.2.).

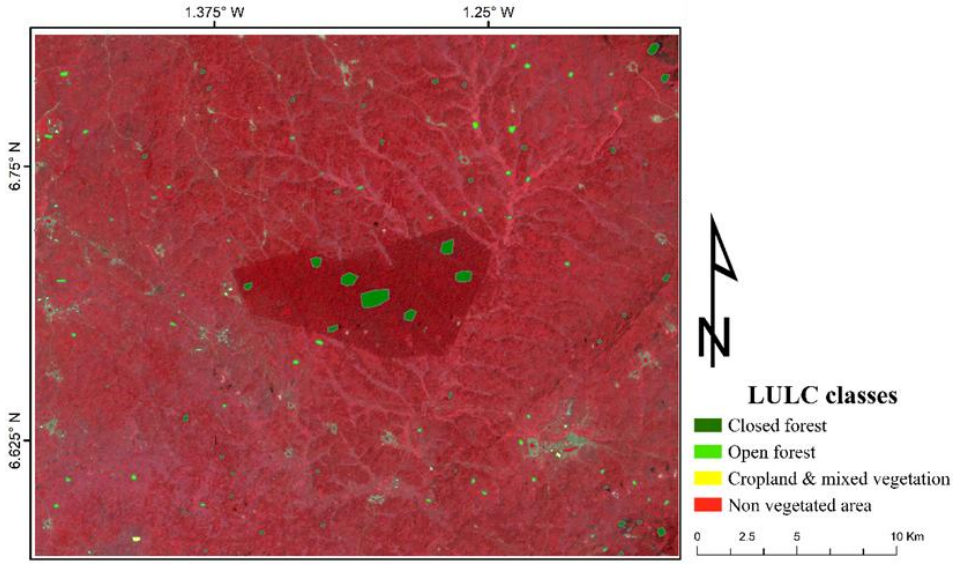

Figure 3.2: Training samples distribution on 1986 Landsat 5 image of the study area

3.2.3 Classification of Landsat Images

Supervised classification involves the supervision of the image by an analyst to (smoothen) the pixel categorization process by providing numerical descriptors of the

land cover classes to the computer algorithm, ensuring smoother classification (Lillesand et al., 2015).

Researchers in LULC change analysis utilize various classification algorithms for satellite image classification. These algorithms encompass both parametric approaches like supervised and unsupervised classification, as well as non-parametric supervised machine learning algorithms. Non-parametric classifiers have gained popularity due to their higher accuracy in image classification, as supported by some studies (Lu and Weng, 2007; Qian et al., 2015). While researchers have the freedom to select classifiers based on their judgment, the algorithm's classification accuracy plays a crucial role.

In this study, supervised classification was used, specifically the Random Forest algorithm was employed to classify images, which was done in the R 4.2.2 version. The polygons created (50 polygons) for each land-use type namely; closed forest, open forest, Croplands and mixed vegetation, and non-vegetated areas (see Table 3.2. for a description of the classes) were converted to centroid points, i.e., 200 centroid points using the "Feature to Point" tool in the ArcGIS software.

The Random Forest (RF) classification model was parameterised using the "randomForest" package in R. The process begins by creating a random subset of 1000 sample points of the training dataset (the 200 centroid points) to improve model generalization, from which 70% was used to train the algorithm and the remaining 30% for accuracy assessment of the classified images (see Table 3.3.). Key hyper-parameters from the algorithm, such as the number of trees, maximum tree depth and the number of features to consider at any given split, were set to 100, 20 and $\sqrt{\rho}$ respectively, where ρ is the number of features/bands. The other parameters were set to the default values in the "randomForest" package as described by Breiman (2001) and Griffiths et al. (2014), since they tend to have less impact on predictive accuracy. In this approach, each tree within the Random Forest contributes by voting for the most commonly occurring class based on the input, and the final decision is made through a majority vote across all the trees (Breiman, 2001). This algorithm generates a large number of classification trees (forests) automatically, with each tree based on a random selection of training samples and predictors.

Table 3.2: Definition of the Land-use/cover classes

Land categories	Definitions	Sources
Closed Forest	This encompasses all land with woody vegetation meeting the thresholds for forest land as defined in the national GHG inventory. It also includes vegetation systems currently below the following criteria: - Minimum Mapping Unit (MMU): 1.0 ha; - Canopy cover (CC): > 65 %; - Potential to reach a minimum height of 5 m at maturity (in situ).	(EPA, 2019; Koranteng, Adu-poku, et al., 2017)
Open forest	This includes perennial crops i.e., oil-palm and cocoa plantations, citrus and fallow areas with similar characteristics. These areas are not classified as Cropland and fall below the forest land threshold values based on the FAO definition in Ghana; CC: < 60 %, height: ≤ 5 m, MMU: > 0.5 ha.	(EPA, 2019)
Croplands and mixed vegetation	This includes annual and biennial croplands such as mono and mixed-cropped farms of cassava, maize, plantain, rice, and similar recent fallow areas with comparable vegetation characteristics.	(EPA, 2019)
Non-vegetated area	This comprises of Cities, towns, villages, and bare areas, rivers, ponds, and lakes.	(EPA, 2019; Hackman et al., 2017)

The spectral bands (original) were the predictors. Random Forest avoids the generalisation problems associated with single classification trees by creating many classification trees and thereby enhancing classification accuracy (Gislason et al., 2006). Each tree in the forest casts a unit vote for the most popular class. A majority vote of the trees determines the classification result. Random Forest performs internal validation (out-of-bag error rate) on training samples that are not utilised in tree building (Watts and Lawrence, 2008).

The results of the classification were post-processed in ArcGIS 10.3 and QGIS 3.18. The classified images were filtered to eliminate the "salt-and-pepper look" and improve the cartographic appearance. This was accomplished in ArcGIS 10.3 "majority filter" tool

using a 3 x 3 window size. A majority of cells that have the same value and are contiguous were applied to simplify the map and eliminate smaller patches of isolated cells. The final land-use maps (LUMs) were produced using the results of the filtering operation. After classification, change statistics were extracted from the 1986 – 2007 and 2007 – 2022 maps to create the two cross-tabulation matrices used in the change detection analysis.

3.2.4 Computation of Land-use Land-cover Changes and Intensity Analysis

3.2.4.1 *Land transition matrix*

Changes in LULC classification were identified through post-classification comparison of maps from three points in time. Two cross-tabulation matrices were created for the transitions; one for the 1986 – 2007 and another for the 2007 – 2022 intervals. In these matrices, rows display LULC types at time t (1986) and columns display the LULC types at time t_{+1} (2007). The inputs in the matrix (P_{ij}) represent the proportion of the study area transitioning from LULC type i at time t to LULC type j at time t_{+1}, where $\sum_i \sum_j P_{ij} = 1$.

Intensity analyses

To determine changes in LULC categories, a post-classification change detection method was employed. This approach quantified the number of pixels transitioning between land categories. By analysing these transitions, the annual percentage change was calculated, accounting for both losses and gains in LULC. Additionally, with the assistance of intensity analysis, changes in land categories at three distinct levels, namely time interval, categorical and transition levels, were assessed as described by Aldwaik and Pontius (2012). A hypothesised uniform change or intensity is contrasted with an observed change or transition at each level of the analysis. This subsection contains the notations used in the equations to calculate transitions at each level of the study.

The equation was built using the following variables; J number of categories, i index for a category at the initial time point for a particular time interval, j index for a category at the final time point for a particular time interval, m index for the losing category in the transition of interest; n index for the gaining category in the transition of interest, T number of time points, t index for the initial time point of interval $[Y_t, Y_{t+1}]$, where t ranges from 1 to $T - 1$, Y_t year at time point t; C_{ij} number of pixels that transition from

category *i* at time Y_t to category j at time $[Y_{t+1}]$; (S_t) annual intensity of change for time interval $[Y_t, Y_{t+1}]$, *(U)* value of uniform annual change/intensity for time-intensity analysis, (G_{tj}) annual intensity of gross gain of category *j* for time interval $[Y_t, Y_{t+1}]$;

L_{ti} annual intensity of gross loss of category *i* for time interval $[Y_t, Y_{t+1}]$, R_{tin} annual intensity of transition from category *i* to category *n* during time interval $[Y_t, Y_{t+1}]$ where $i \neq n$, (W_{tn}) value of the uniform intensity of transition to category *n* from all non-n categories at time Y_t during time interval $[Y_t, Y_{t+1}]$, (Q_{tmj}) annual intensity of transition from category *m* to category *j* during time interval $[Y_t, Y_{t+1}]$ where $j \neq m$, (V_{tm}) value of uniform intensity of transition from category *m* to all non-m categories at time Y_t, Y_{t+1} during time interval $[Y_t, Y_{t+1}]$.

Interval level

This level of analysis does not show specific changes in whether there is an increase or decrease in the land categories. However, it gives information on the time intervals during which the overall annual rate of change is relatively slow versus fast. In Equation 3.1, the observed change (S_t) computes the quantity of land cover change (encompassing changes in all LULC classifications) over the research period. Uniform yearly change or intensity (U) at the interval level was computed with Equation 3.2. The magnitude and rate of change were evaluated at the interval level over time for the two time periods (i.e., 1986 – 2007 and 2007 – 2022). The rate estimated as the yearly changes spread equally over the full-time span is known as uniform change at the interval level. When changes within each interval are spread uniformly across the geographic area, it is known as uniform change at the category level. If the observed change (S_t) exceeds the uniform change (U) at the interval level, the change is considered to be rapid. Otherwise, it is slow (Aldwaik and Pontius, 2012).

$$S_t = \frac{\left\{\sum_{j=1}^{J}\left[\left(\sum_{i=1}^{J} C_{tij}\right) - C_{tij}\right]\right\} / \left[\sum_{j=1}^{J}\left(\sum_{i=1}^{J} C_{tij}\right)\right]}{Y_{t+1} - Y_t} \times 100\% \qquad (3.1)$$

$$U = \frac{\sum_{t=1}^{T-1}\left\{\sum_{j=1}^{J}\left[\left(\sum_{i=1}^{J} C_{tij}\right) - C_{tij}\right]\right\} / \left[\sum_{j=1}^{J}\left(\sum_{i=1}^{J} C_{tij}\right)\right]}{Y_T - Y_1} \times 100\% \qquad (3.2)$$

Category level

Category level is computed using Equation 3.3, which calculates the gains (G_{tj}) for each category, while Equation 3.4 is used to compute the losses (L_{ti}) for each land category. Equation 3.1 provides the uniform intensity for time interval *t* at the category level, linking the interval level analysis to the category level analysis. If values of (G_{tj}) are equal for all j, they are equivalent to (S_t). Similarly, if (L_{ti}) values are equal for all i, they also equal (S_t).

At the category level, if the observed gains and losses exceed the uniform change (U) as defined in Equation 3.2, the categorical change is considered active. Conversely, if the observed change is less than the uniform change, the categorical change is classified as dormant.

$$G_{tj} = \frac{\left[\left(\sum_{i=1}^{J} C_{tij}\right) - C_{tjj}\right]/(Y_{t+1} - Y_t)}{\sum_{i=1}^{J} C_{tij}} \times 100\% \quad (3.3)$$

$$L_{ti} = \frac{\left[\left(\sum_{j=1}^{J} C_{tij}\right) - C_{tii}\right]/(Y_{t+1} - Y_t)}{\sum_{i=1}^{J} C_{tij}} \times 100\% \quad (3.4)$$

Transition level

The transition level describes the transition (R_{tin}) 'TO' a specific category from other categories, as calculated in Equation 3.5. The uniform intensity (W_{tn}) of transition to a category n from all other categories is determined using Equation 3.6. At this level, the uniform transition rate represents the quantity of land change evenly distributed among all categories available for transition (Aldwaik and Pontius 2012). If the land transition quantity from any category to *n* is below the uniform intensity (W_{tn}), category *n* avoids that category. Conversely, if the transition quantity is above the uniform intensity, category *n* targets that category.

$$R_{tin} = \frac{C_{tin}/(Y_{t+1} - Y_t)}{\sum_{j=1}^{J} C_{tij}} \times 100\% \quad (3.5)$$

$$W_{tn} = \frac{\left[\left(\sum_{i=1}^{J} C_{tin}\right) - C_{tnn}\right]/(Y_{t+1} - Y_t)}{\sum_{j=1}^{J}\left[\left(\sum_{i=1}^{J} C_{tij}\right) - C_{tnj}\right]} \times 100\% \quad (3.6)$$

On the contrary to transition 'TO', Equation 3.7 calculates transitions 'FROM' category *m* to other categories, with its uniform intensity determined by Equation 3.8.

When the quantity of land transition (Q_{tmj}) from *m* to another category is below the uniform transition intensity (V_{tm}), category *m* is avoided. Conversely, if the transition quantity exceeds the uniform intensity, category *m* is targeted by other land categories.

$$Q_{tmj} = \frac{[C_{tmj}/(Y_{t+1}-Y_t)]}{\sum_{i=1}^{J} C_{tij}} \times 100\% \quad (3.7)$$

$$V_{tm} = \frac{\left[\left(\sum_{j=1}^{J} C_{tmj}\right)-C_{tmm}\right]/(Y_{t+1}-Y_t)}{\sum_{i=1}^{J}\left[\left(\sum_{j=1}^{J} Ctij\right)-C_{tim}\right]} \times 100\% \quad (3.8)$$

3.2.5 Estimation of Deforestation Leakage

The land-use/cover maps created for this study (1986 – 2022) were used to calculate the average annual deforestation rate for BFR compared to its environs using ArcMap10.8. Deforestation was measured using the classification reports obtained after the post-classification process ("majority filter") with two methods. The first method, referred to as "deforestation (% forest)" (Equation 3.9), calculated the percentage of forested land from 1986 that was deforested by dividing the total closed forest loss (1986 – 2022) by the total closed forest area in 1986. The second method, "deforestation (% land)" (Equation 3.10), determined the percentage of terrestrial land deforested by dividing the total closed forest loss (1986 – 2022) by the total terrestrial area, as illustrated in Figure 3.3 (Ford et al., 2020; Lui and Coomes, 2016).

$$Deforestation\ (\%\ forest) = \frac{Total\ closed\ forest\ loss\ (1986-2022)}{Total\ closed\ forested\ area\ (1986)} \quad (3.9)$$

$$Deforestation\ (\%\ land) = \frac{Total\ closed\ forest\ loss\ (1986-2022)}{Total\ terrestrial\ area\ (1986)} \quad (3.10)$$

These two types of deforestation metrics were quantified because they offer distinct perspectives on the observed deforestation patterns. The % forest forestation offers insights into absolute rates of closed forest clearing, while, the % land metric places forest loss in the context of the existing forest cover, highlighting changes in the availability of forest resources over time. Leakage was defined as a higher average annual deforestation

rate in the areas surrounding the BFR compared to within the reserve itself (Ewers and Rodrigues, 2008).

3.3 Results

3.3.1 Land-use Land-cover Classification

The Random Forest classification technique yielded good accuracy. The overall accuracies and Kappa statistics for the three maps were 96% and 91%, 93% and 0.94, 0.86 and 0.89 for 1986, 2007 and 2022, respectively. The error matrix (Table 3.3) provides more details on the class performance.

3.3.1.1 *Land Intensity Analyses*

Interval and category level

The interval level analysis between 1986 and 2007 showed an observed yearly change of 2.06%, whereas between 2007 and 2022, the area changed by 1.04% with a uniform change of 1.64 (Figure 3.4). This level of analysis does not show specific changes of whether there is an increase or decrease in the land categories (closed forest, open forest, croplands and mixed vegetation and non-vegetated). However, changes at the category level were obtained from the interval level of analysis (see Eq. 3.3 and 3.4, linked with Eq. 3.1). The percentage loss in closed forests exceeded that of its gains at the category level in the first interval (see Figure 3.5). In both times, croplands and mixed vegetation, open forest, as well as non-vegetated area, were more likely to increase than decrease. In the first period, the net increase in non-vegetated area was more than that in croplands and mixed vegetation and open forest. Whereas during the second period, croplands and mixed vegetation showed a greater net gain compared to non-vegetated and open forest areas (see Figure 3.4).

Transition level analysis

This analysis level clarifies the transition between different LULC categories by considering whether a specific LULC type was targeted (playing the most significant role in the changes) or avoided (not a primary focus). An in-depth analysis of landscape transitions within two specific time intervals is provided in Table 3.5. In the first interval, 43% of the area experienced changes in LULC, in the second interval (or period) 16% of

the area experienced a LULC change. This change was translated in greatest loss depicted in closed forest and cropland and mixed vegetation with 75% and 60%, respectively. These losses led to a significant increase in both open forest and non-vegetated areas that expanded from 45,588 to 61,060 ha and 838 to 3,243 ha, respectively. In the same period, it was also observed an increase in cropland and mixed vegetation from 9,074 to 11,360 ha as seen in Table 3.5.

However, when looking at the second period (2007 – 2022) with an overall change of 16 %, a considerable reduction was observed in the rate of loss in the closed forest and cropland and mixed vegetation as compared to the first interval from 75% to 38% and from 60% to 34%, respectively. Furthermore, a fairly stable change can be noticed in open forest and cropland and mixed vegetation from 61,060 to 62,030 ha and from 3,243 to 3,213 ha, respectively.

It is noteworthy that in the second interval, the rate of loss decreased not only for closed forests but also for croplands and mixed vegetation, from 75% to 38% and 60% to 34%, respectively. This indicates potential changes in land-use patterns or ecological processes. Furthermore, significant shift in land transition patterns is highlighted in Table 3.5. and Figure 3.7. The magnitude of loss reduces from the first interval to the second.

Table 3.3: The error matrix for the years 1986, 2007 and 2022.

Land-use/cover (1986)	**Closed forest**	**Open forest**	**Croplands and mixed vegetation**	**Non-vegetated**	**User Total**	**User Acc**	**Producer Acc**
Closed forest	161	0	0	0	161	100.00	100.00
Open forest	0	84	2	0	86	97.67	93.33
Croplands and mixed vegetation	0	6	22	1	29	75.86	84.62
Non-vegetated	0	0	2	22	24	91.67	95.65
Producer Total	161	90	26	23	300		
Overall accuracy	***0.96***						
Kappa statistics	***0.94***						
2007							
Closed forest	132	8	1	0	141	93.62	99.25
Open forest	1	95	10	0	106	89.62	88.79
Croplands and mixed vegetation	0	4	20	2	26	76.92	62.50
Non-vegetated	0	0	1	26	27	96.30	92.86
Producer Total	133	107	32	28	300		
Overall accuracy	**0.91**						
Kappa statistics	**0.86**						
2022							
Closed forest	141	4	3	0	148	95.27	97.92
Open forest	3	114	5	0	122	93.44	94.21
Croplands and mixed vegetation	0	3	11	1	15	73.33	55.00
Non-vegetated	0	0	1	14	15	93.33	93.33
Producer Total	144	121	20	15	300		
Overall accuracy	**0.93**						
Kappa statistics	**0.89**						

Croplands and mixed vegetation, for example, gained mostly from open forests in both periods. This shows that when compared to all other land-use categories, open forest was the most common kind of LULC converted into Croplands and mixed vegetation in both time frames. Various stages of transition from and to other LULC types are seen in Figure 3.6.

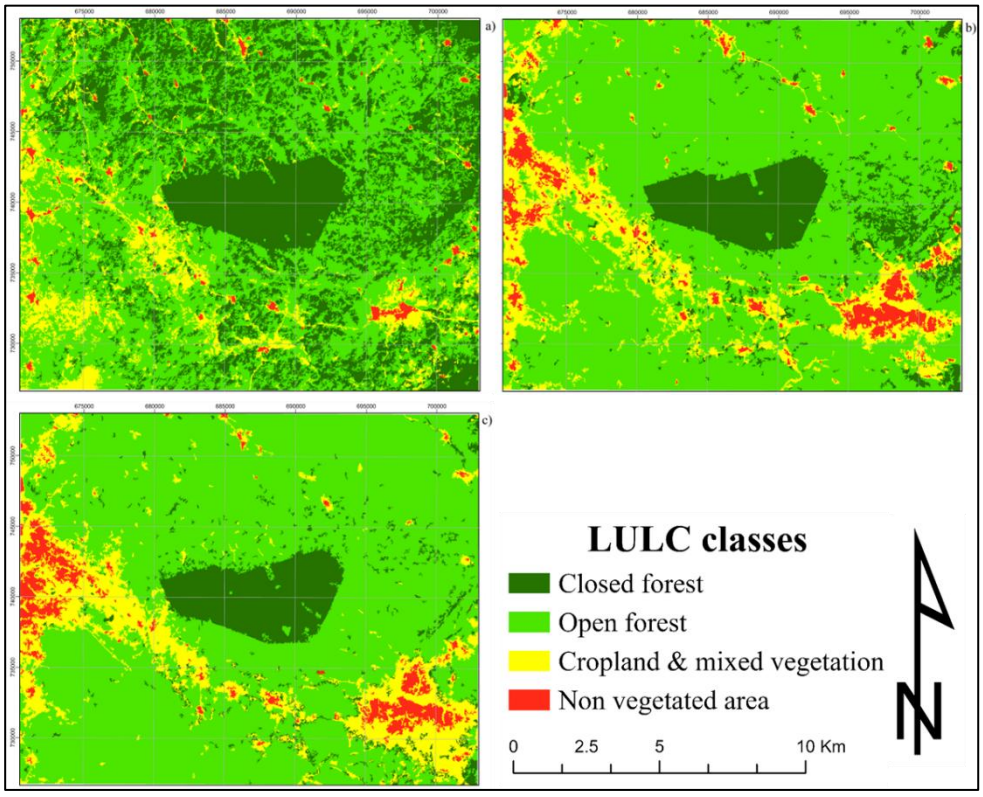

Figure 3.3: Land-use map of the study area for the years 1986 (a), 2007 (b), and 2022 (c).

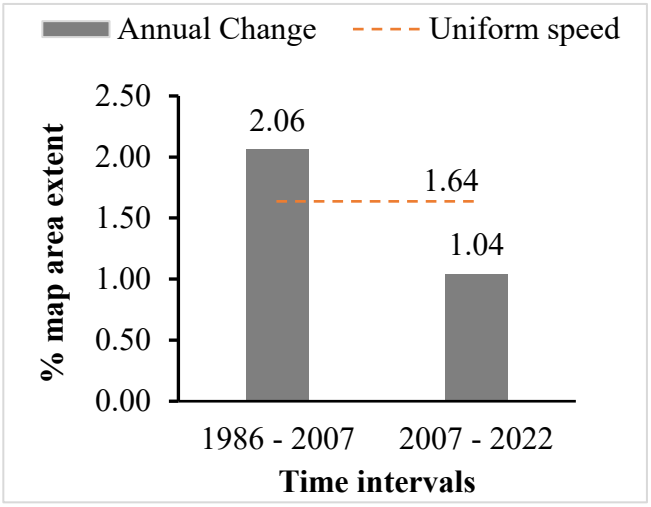

Figure 3.4: Interval level analysis

Table 3.4: Land-use change from 1986 – 2007 and 2007 – 2022.

Land-use/cover	1986 (ha)	2007 (ha)	2022 (ha)	1st interval net change (ha)	2nd interval net change (ha)	1st interval net change (%)	2nd interval net change (%)	Annual rate of change 1st interval (%)	Annual rate of change 2nd interval (%)
Closed forest	29,805.21	9,641.88	8,100.18	-20,163.33	-1,541.70	-23.64	-1.81	1.13	0.12
Open forest	45,587.61	61,060.14	62,029.62	15,472.53	969.48	18.14	1.14	0.86	0.08
Croplands and mixed vegetation	9,074.25	11,360.25	11,961.81	2,286.00	601.56	2.68	0.71	0.13	0.05
Non-vegetated	837.81	3,242.61	3,213.27	2,404.80	-29.34	2.79	-0.02	0.13	0.00
Total	85,304.88	85,304.88	85,304.88						

Table 3.5: Land-use land cover transition matrix for two-time intervals: 1986 – 2007, 2007 – 2022 and 1986 – 2022, the numbers represent the percentage of pixels transitioning between categories, with gains and losses calculated by deducting transitions within the same category.

2007							
	Land-use/cover	**Closed forest**	**Open forest**	**Croplands and mixed vegetation**	**Non-vegetated**	**Total**	**Gross loss (%)**
1986	Closed forest	7480.98	20670.21	1436.49	217.53	29805.21	74.9
	Open forest	1834.83	36532.89	6158.34	1061.55	45587.61	19.86
	Croplands and mixed vegetation	319.41	3828.96	3648.69	1277.19	9074.25	59.79
	Non-vegetated	6.66	28.08	116.73	686.34	837.81	18.08
	Total	9641.88	61060.14	11360.25	3242.61	85304.88	
	Gross gain (%)	22.41	40.17	67.88	78.83	**43.32% Change**	
2022							
2007	Closed forest	6012.09	3283.83	339.3	6.66	9641.88	37.65
	Open forest	1620.63	56147.13	3213.27	79.11	61060.14	8.05
	Croplands and mixed vegetation	446.04	2579.49	7506.9	827.82	11360.25	33.92
	Non-vegetated	21.42	19.17	902.34	2299.68	3242.61	29.08
	Total	8100.18	62029.62	11961.81	3213.27	85304.88	
	Gross gain (%)	25.78	9.48	37.24	28.43	**15.64% Change**	
2022							
1986	Closed forest	6553.26	21090.96	1890	270.99	29805.21	78.01
	Open forest	1237.68	36715.23	6401.25	1233.45	45587.61	19.46
	Croplands and mixed vegetation	303.12	4195.71	3417.03	1158.39	9074.25	62.34
	Non-vegetated	6.12	27.72	253.53	550.44	837.81	34.30
	Total	8100.18	62029.62	11961.81	3213.27	85304.88	
	Gross gain (%)	19.10	40.81	71.43	82.87	**44.63% Change**	

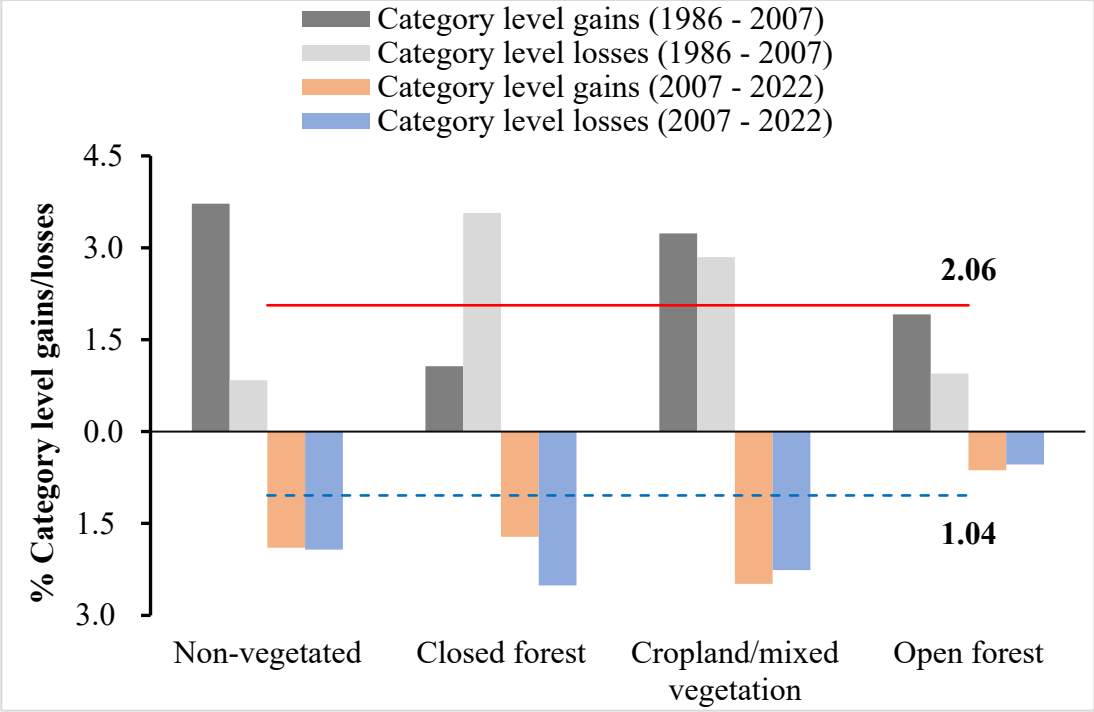

Figure 3.5: Category level analysis

3.3.2 Deforestation Rate and Potential Driving Forces

The deforestation rates calculated throughout the study reveal a total annual deforestation (% forest) rate between 1986 and 2022 of 0.71 % per annum, of which 0.06% and 0.64% occurred within the BFR and the surrounding areas of BFR, respectively. This result suggests a lower deforestation rate in the BFR than in the environs. This is evidence of leakage in the BFR environs, which experienced a more rapid decline in closed forest cover compared to the forest reserve.

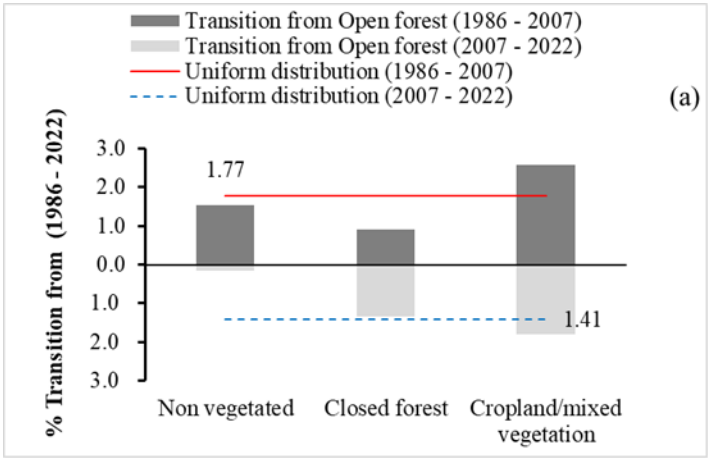
Transition from Open forest (1986 - 2007)
Transition from Open forest (2007 - 2022)
Uniform distribution (1986 - 2007)
Uniform distribution (2007 - 2022)
(a)
% Transition from (1986 - 2022)
3.0
2.0
1.0
0.0
1.0
2.0
3.0
1.77
1.41
Non vegetated
Closed forest
Cropland/mixed vegetation

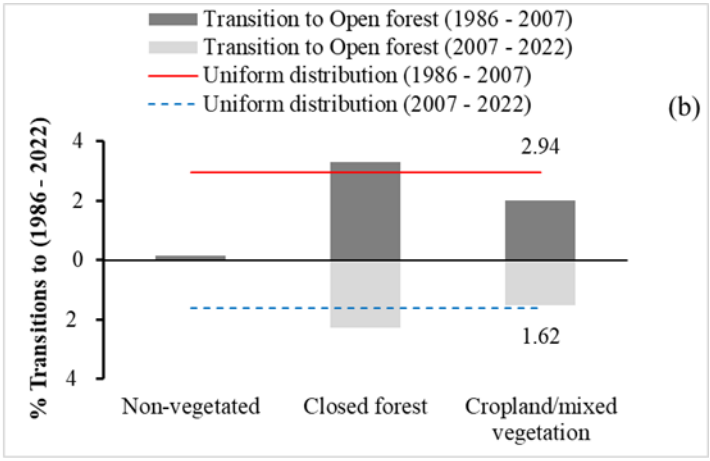
Transition to Open forest (1986 - 2007)
Transition to Open forest (2007 - 2022)
Uniform distribution (1986 - 2007)
Uniform distribution (2007 - 2022)
(b)
% Transitions to (1986 - 2022)
4
2
0
2
4
2.94
1.62
Non-vegetated
Closed forest
Cropland/mixed vegetation

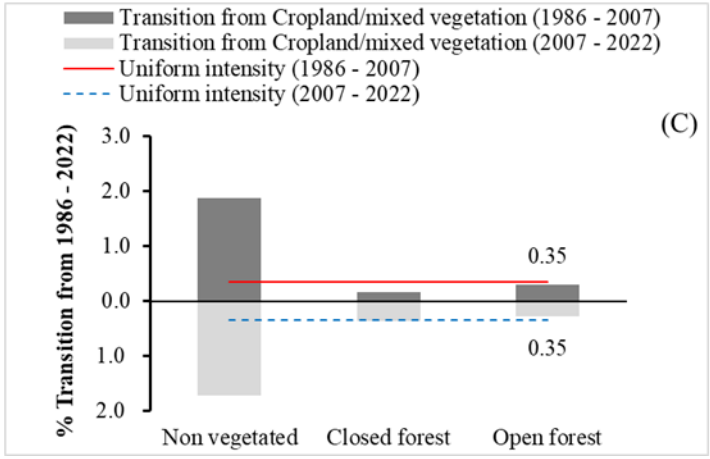
Transition from Cropland/mixed vegetation (1986 - 2007)
Transition from Cropland/mixed vegetation (2007 - 2022)
Uniform intensity (1986 - 2007)
Uniform intensity (2007 - 2022)
(C)
% Transition from 1986 - 2022)
3.0
2.0
1.0
0.0
1.0
2.0
0.35
0.35
Non vegetated
Closed forest
Open forest

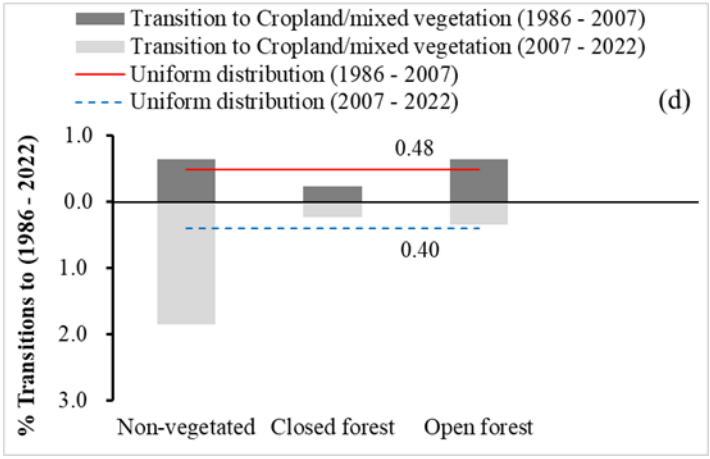
Transition to Cropland/mixed vegetation (1986 - 2007)
Transition to Cropland/mixed vegetation (2007 - 2022)
Uniform distribution (1986 - 2007)
Uniform distribution (2007 - 2022)
(d)
% Transitions to (1986 - 2022)
1.0
0.0
1.0
2.0
3.0
0.48
0.40
Non-vegetated
Closed forest
Open forest

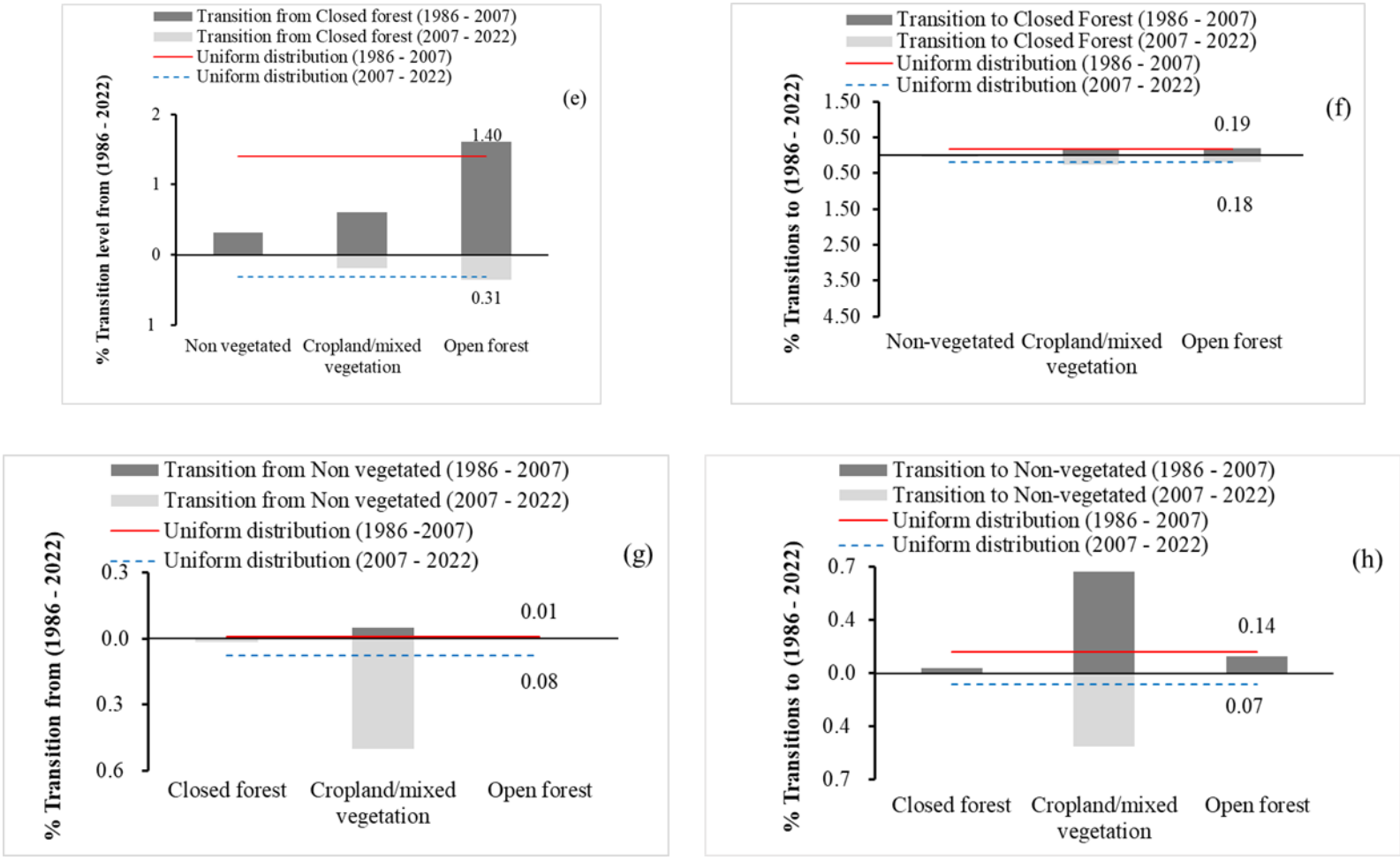

Figure 3.6: Analysis of transition intensity (percentage of category) from and to Open Forest, Croplands and mixed vegetation and forest and Non-vegetated area across two time intervals: 1986 – 2007 and 2007 – 2022.

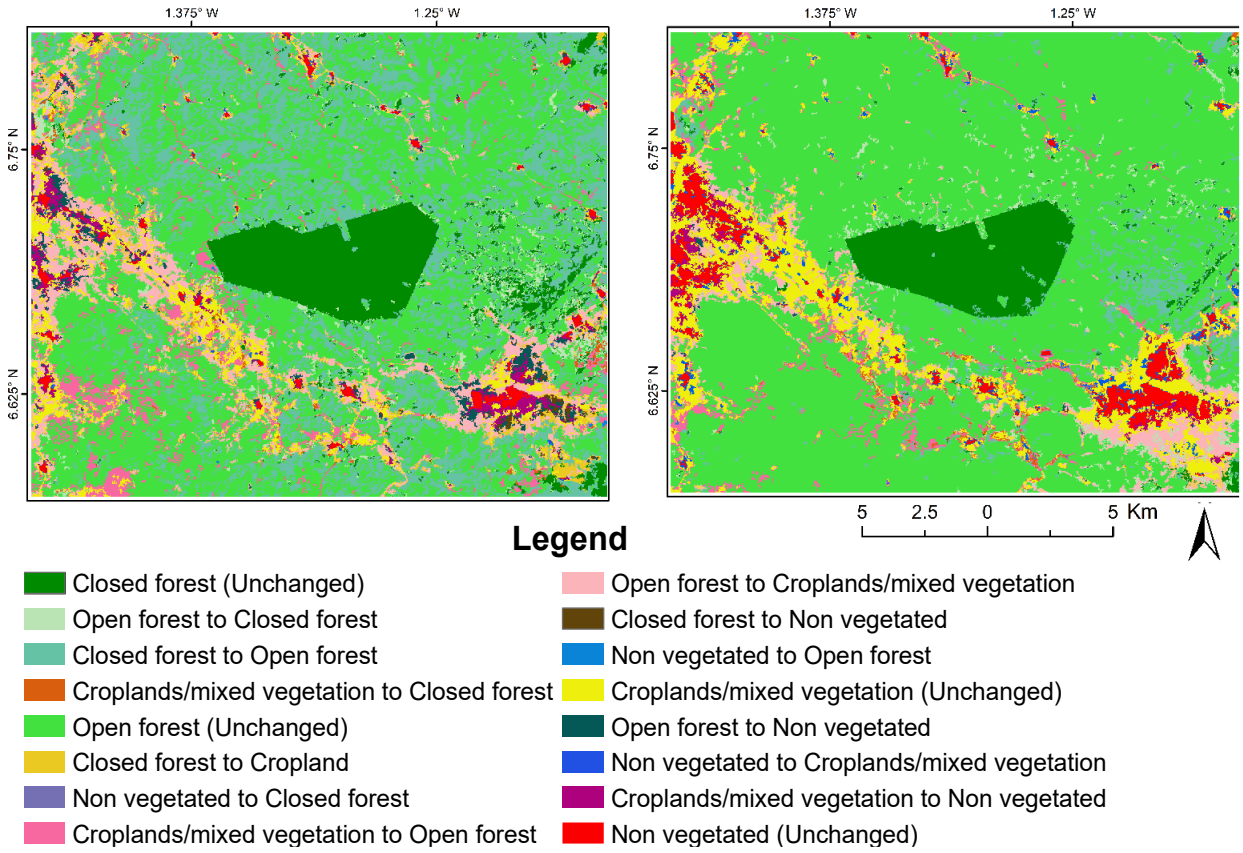

Figure 3.7: Change map of the study area between 1986 – 2007 (left image) and 2007 – 2022 (right)

Table 3.6: Land summary of deforestation rates from 1986 to 2022 for the designated BFR
and its environs.

Regions closed forest	**1986**	**2007**	**2022**	**% change (1986 - 2022)**	**% Annual rate of change**
BFR	5420.18	5415.94	5296.69	**2.26**	**0.06**
Surrounding area of BFR	24317.12	4192.27	2742.11	**23.18**	**0.64**
Total study area	29737.30	9608.21	8038.80	25.44	0.71

Note: Deforestation rates are presented as both the average annual percentage of land deforested (% land) between 1986 – 2007 and 2007 – 2022 and the average annual percentage of forest deforested (% forest) from 1986 – 2007 and 2007 – 2022.

3.4 Discussion

3.4.1 Land-use/cover Classification and Change Detection

The results of the land-use/cover classification in this study are consistent with the standard value in the study done by Campbell (2002) with good overall accuracies and kappa statistics, which enables further analysis and the formulation of valid conclusions. Observations of the LULC for 1986, 2007 and 2022 reveal a progressive decrease in closed forest loss in the BFR environs over the period. Notably, deforestation-induced forest loss in the study area predominantly occurred outside the boundaries of the designated forest reserves.

The LULC maps obtained at three different time points displayed four distinct land categories, namely closed forest, open forest, croplands and mixed vegetation, and non-vegetated areas (primarily comprising buildings and roads). However, a noticeable trend observed was a decline in the closed forest category, with a corresponding increase in open forest and croplands and mixed vegetation over the study period 1986 – 2023 (Table 3.4. and Figure 3.3). The analysis of gross change rates revealed significant differences between the two-time intervals (Table 3.5). Furthermore, the transition tables indicated that the loss of closed forests was accompanied by the expansion of both open forests and croplands and mixed vegetation. However, the magnitude of change was found to be higher during the first-time interval compared to the second, while transitions from closed forest and non-vegetated areas to croplands and mixed vegetation decreased (Table 3.4). The outcomes of this study align with the findings of a similar study by Tekle and Hedlund (2000), who observed a rise in the size of settlements at the expense of forests in the Kalu district of Ethiopia. Similarly, Mark and Kudakwashe (2010) observed a decline in forest cover and an increase in agricultural land in their investigation of the Shurugwi District in the Midlands province of Zimbabwe. The conversion of significant portions of closed canopy forests into open canopy forests within the surrounding of the BFR can be attributed to various underlying factors, such as a decline or inadequacy in forest conservation efforts, rapid socioeconomic developments and institutional changes (Addo-Fordjour and Ankomah, 2017; Ankomah et al., 2019; Baffour-Ata et al., 2021). A recent study on the Kyekye, admitted community within the Tano-Offin Forest Reserve,

located in the Nkawie Forest District, revealed similar trends (Oduro et al., 2021). The study showed that livelihood activities, including agricultural expansion, settlement development and harvesting of woody resources serve as direct drivers of change that flow from the indirect causes. These activities have significantly contributed to a consistent decline in closed forest cover, leading to an increase in open forests and Croplands and mixed vegetation (Oduro et al., 2021).

3.4.2 Land-use land-cover Changes and Intensity Analysis

Previous studies in other countries have compared the intensity analysis method with alternative approaches, such as the Markov transition matrix. These studies, including Aldwaik and Pontius (2012) and Mwangi et al. (2017), have consistently demonstrated that intensity analysis is a highly efficient and effective method for analysing LUCs. Based on these findings, the present study opted to utilize the intensity analysis method to examine transitional changes among the prominent land categories during the two selected time intervals. This approach is crucial for gaining insights into the transformations and transitions within the LULC patterns. Understanding these changes and transitions will support the development of policies and interventions aligned with United Nation's Sustainable Development Goals (SDGs) to promote sustainable development (Christensen and Arsanjani, 2020).

The intensity analysis conducted at the category level revealed noteworthy patterns in LULC. Non-vegetated areas demonstrated active gains throughout all time intervals while experiencing active losses specifically in the second interval. This trend can be attributed to the upsurge of rural-urban migration, leading to a significant increase in built-up areas within the study region (Nyamekye et al., 2020). The active loss of Non-vegetated areas can primarily be attributed to the expansion of croplands and mixed vegetation, driven by agricultural activities (Nyamekye et al., 2020).

Croplands and mixed vegetation exhibited active gains in both intervals, likely driven by increasing food demand due to population growth in the study area, with an increase from 124,176 inhabitants to 244,646 inhabitants in the year 2000 and 2021, respectively, coupled with consistent reduction in yields (GSS, 2005; 2021). In the case of closed

forest, it displayed active losses in both intervals but became an active gainer in the second interval. This later gain in forested land can be attributed to reforestation efforts undertaken by various projects and government initiatives and some agroforestry practices, which transform the cropland into a forest after some years.

For example, the National Forest Plantation Development Programme (NFPDP) aimed to accelerate the establishment of new forest plantations by setting a yearly target of 20,000 hectares. These efforts began to demonstrate impacts on vegetation cover in different sites, including the moist semi-deciduous forest zone surrounding the study area (Addo-Danso, 2010; Bosu, 2010; Oduro, 2016).

The transition intensity analysis revealed disparities in the transited class and the corresponding year. It evidenced a reduction in the overall change intensity during the second interval, as depicted in Figure 3.4. In the initial time interval, the expansion of croplands and mixed vegetation influenced both non-vegetated areas and open forests, while the impact on open forests was comparatively less in the subsequent interval, as illustrated in Figure 3.6d. These findings indicate that the observed changes were inconsistent between the two intervals, primarily driven by the expansion of croplands and mixed vegetation, which is supported by previous vegetation studies (Bessah et al., 2019; Shoyama et al., 2018).

Furthermore, the results underscore the ecological importance of the decline in closed forest cover, as it exhibited the most substantial degree of reduction relative to its state in 1986. The intensity of closed forest loss was more prominent during the initial time interval. Additionally, the study revealed heterogeneous effects of open forest expansion on different vegetation types, with closed forests identified as the most susceptible to the ongoing expansion of open forests.

The consistent occurrence of transitions between non-vegetated and croplands and mixed vegetation during the two analysed time intervals can be attributed to the constraints imposed by urban growth in Ghana, which has limited the expansion of agricultural lands (Toku et al., 2021). The transitions, gains and losses observed predominantly result from the expansion of non-vegetated areas, often at the expense of croplands and mixed

vegetation. It is essential to address the loss of croplands and mixed vegetation from non-vegetated areas (particularly from settlements) as this trend can be attributed to population growth over the years (Bessah et al., 2019; Nyamekye et al., 2020; Shoyama et al., 2018).

The gain in non-vegetated areas is closely linked to significant urban development in the study area, driven partially by the conversion of croplands and mixed vegetation close to towns (Aspinall, 2004; Koranteng et al., 2015; X. Li et al., 2013; Müller et al., 2010; Nyamekye et al., 2020).

3.4.3 Drivers of Deforestation Leakage

Overall, the results of this study indicate a higher occurrence of deforestation leakage from the BFR over the study period (1986 - 2022), with the annual rate of deforestation of 0.06% and 0.64 % for the PA and its environs, respectively (Table 3.6). The observed leakage in the study period could be explained by the fact that farmers who have been displaced due to urbanization or peri-urban migration seek alternative Croplands and mixed vegetation, leading to the conversion of forest lands in the surrounding areas of the BFR, particularly open forests, in areas located beyond the reach of urbanization. The new Croplands and mixed vegetation are however later replaced with non-vegetated (bare land) when they become unfertile land resulting in the expansion of non-vegetated areas in the surroundings of the BFR. The increase in non-vegetated areas is particularly concentrated along the Kumasi-Accra Road network, traversing the study area.

This finding aligns with the trends documented by Ford et al. (2020), who documented 55 instances of deforestation leakage from PAs in the tropics, with agriculture expansion driving forest loss in buffer zones in over 35 cases. Although PAs are typically not created to directly mitigate detrimental land-uses beyond their borders, the overall success of conservation efforts may still depend on managing activities beyond the PA boundaries (DeFries et al., 2010; Laurance et al., 2012). However, in most related studies, a drastic decrease in the protected area forest cover was observed due to deforestation induced by human encroachment into the forest for either built-up (settlement) or farming. From their study in the Ashanti region by analysing patterns of deforestation within some PA to identify the main drivers of forest cover loss in the region, Acheampong et al. (2019)

reported that agricultural expansion was a major threat to forest cover in the region. Brobbey et al. (2020) also conducted a similar study on three protected areas in Ghana and found agricultural expansion and infrastructure development to be the proximate causes of deforestation. These are driven by population growth, and low productivity of cash crops such as cocoa due to unfertile land. Their study linked the poor fertility and low productivity of cocoa farms as reasons why farmers encroach into the Forest Reserves of Krokosua, Tano Offin and Sui River to increase productivity.

Despite the problem of encroachment of deforestation activities into some forest reserves, the BFR has over the years received relatively good protection. One of the main reasons for its effective conservation is the recognition of its high ecological and tourism value. This has led to constant control by the Forestry Commission (FC) and high research interest in the area evidenced by the long-term presence of researchers. Guards from the Forestry Commission of Ghana regularly monitor the area to detect and prevent illegal logging and other deforestation activities such as mining and hunting. Additionally, the long-term presence of researchers since 1946 (Djagbletey et al., 2018) has contributed to a "science safeguarding effect", where scientists act as de facto park guards (Laurance, 2013).

3.5 Conclusions

The implementation of intensity analysis in the study area revealed significant changes across the land-use classes. The study revealed an overall increased rate of LULCC, highlighting extensive land development across the analysed intervals. Notably, the croplands and mixed vegetation and non-vegetated classes recorded the largest gains, while the closed forest class consistently experienced losses in both time intervals. The gains in the non-vegetated class primarily originated from croplands and mixed vegetation, while closed and open forests were comparatively avoided. However, active transitions from closed forest and open forest to croplands and mixed vegetation were observed in both intervals. Moreover, throughout the three time points, there was active transitioning between the croplands and mixed vegetation and non-vegetated classes.

The research highlighted effectiveness of using contemporary Landsat products in improving the understanding and assessment of conservation success of the protected area of Bobiri Forest Reserve in Ghana. Furthermore, the study unveiled a higher occurrence of deforestation leakage within the environs of the protected area of BFR. Nevertheless, the protected area itself curtails deforestation within its borders, as indicated by an observed annual deforestation rate of 0.06% throughout the entire study period, compared with a much higher deforestation rate outside the protected area (0.64%) than what would be expected without protection.

Considering the likelihood that the Protected Area (PA) of the Bobiri Forest Reserve (BFR) will continue to play a crucial role in conservation, implementing policy measures specifically geared towards creating a legal boundary as a buffer zone of at least 10 km radius from the BFR and provide measures to restore the closed forest cover within the designated boundary is recommended. This is particularly important to the overall conservation goal of the area as it would help prevent/reduce deforestation leakage within the buffer zone and reduce the substantial threat of exposing the PA itself to various possible encroachment and other climatic threats. Additionally, the global protected area network is formally established in international law through Target 11 of the 2010 Convention on Biological Diversity. However, focusing merely on protecting the boundary of a protected area does not necessarily translate to positive impacts on habitat and biodiversity, if the PA shifts threats to areas where biodiversity is more highly vulnerable. Investigating and managing this potential relocation effect should be a primary focus of research as more protected areas are established. The study provides valuable insights that can support a more comprehensive approach to protected area management, ensuring both long-term protection and maximum benefits from these areas. These findings are particularly relevant for land and resource managers, conservationists, researchers, and policymakers.

CHAPTER 4 : SEASONAL DYNAMICS OF SOIL CO_2 EFFLUX UNDER DIFFERENT LAND-USE SYSTEMS IN A MOIST SEMI-DECIDUOUS FOREST IN GHANA: INSIGHTS FOR CLIMATE CHANGE MITIGATION

Abstract

Background:

Carbon dioxide (CO_2) is a major greenhouse gas driving climate change. In Ghana, the Agriculture, Forestry, and Other Land Use (AFOLU) sector contributes to national CO_2 emissions while also offering opportunities for carbon sequestration. This study assessed seasonal variations in soil respiration rates (SRR) across four land-use types, including forest, fallow, maize, and rice fields within a semi-deciduous forest zone in Ghana. The aim was to provide baseline data and identify key soil factors that influence SRR to support mitigation strategies.

Methods:

Soil respiration rate was measured monthly over one year using a closed-chamber technique. Concurrently, soil physico-chemical properties such as organic matter (OM), pH, texture, and moisture (SM) were recorded. Stepwise multiple regression and correlation analyses were conducted to explore relationships between SRR and soil variables.

Results:

SRR varied across seasons and land-use types, with higher emissions during the wet season. Fallow and cropland areas (maize and rice fields) recorded the highest CO_2 efflux, while closed forests showed the lowest emissions, likely due to minimal disturbance. Among the soil variables assessed, OM, pH, silt content, and SM showed stronger associations with SRR. The final regression model explained 58% of the variation in SRR.

Conclusion:

This study shows that SRR vary by land-use type, with higher emissions observed in disturbed systems such as fallow and croplands, and lower emissions in undisturbed forest areas. These findings underscore the critical role of forest conservation and sustainable land management in mitigating greenhouse gas emissions and strengthening ecosystem resilience in tropical regions. To effectively reduce emissions from the AFOLU sector, policies should promote practices such as reforestation, agroforestry, and reduced soil disturbance that enhance soil carbon retention and support sustainable land-use transitions.

Keywords: Climate change, AFOLU, Assessing soil respiration rate, tropical ecosystems, soil moisture, Ghana

4.1 Introduction

Climate change remains one of the most pressing global environmental challenges of the 21st century, driven primarily by increased concentration of greenhouse gases (GHGs) in the atmosphere, notably Carbon dioxide (CO_2), methane (CH_4) and nitrous oxide (N_2O). Carbon dioxide is the most significant of these gases, accounting for approximately 76% of total GHG emissions globally (IPCC, 2021). Anthropogenic activities, such as fossil fuel combustion, deforestation and industrial processes, have significantly elevated atmospheric CO_2 levels, contributing to global warming and altering climatic patterns (Pachauri and Meyer, 2014). Therefore, understanding the dynamics of CO_2 emissions from various sources and sinks is crucial for developing effective mitigation strategies to meet international climate targets, such as those outlined in the Paris Agreement.

In Africa, CO_2 emissions have been rising steadily, although they remain lower than global averages, largely due to rapid economic development, urbanization and changing land-use practices (Atedhor, 2023). West Africa, particularly Ghana, has seen significant increases in CO_2 emissions, primarily from the energy sector and agriculture, forestry and other land-use (AFOLU) sector (EPA, 2024). According to the Ghana Environmental Protection Agency (EPA) 2024 report, from the estimated national GHG emissions of 51.78 million tonnes of carbon dioxide equivalent (51.78 $MtCO_2e$), about 51.2% are from the energy sector, 38.3% from the AFOLU sector, 7.3 % from the waste sector and 3.2 % from the industrial processes and product use (IPPU) sector (EPA, 2024). This data indicates that the AFOLU sector is the second largest source of GHG emissions in Ghana, primarily due to deforestation, agricultural expansion and land degradation. Additionally, the Food and Agriculture Organization of the United Nations (FAO) has identified agricultural expansion as a major driver of deforestation and forest degradation, leading to significant GHG emission (FAO, 2020).

The AFOLU sector serves as both a source and a sink of CO_2. Activities such as slash-and-burn agriculture, conversion of forests to croplands and inappropriate land management practices release significant amounts of CO_2 into the atmosphere (Anyanwu et al., 2023; Houghton and Goodale, 2004). In contrast, well-managed forests and agricultural lands can act as carbon sinks, sequestering CO_2 and thus

mitigating climate change. Soil respiration rate (SRR), a process in which CO_2 is released from the soil surface due to microbial decomposition of organic matter and root respiration, constitutes a substantial component of terrestrial CO_2 fluxes (Raich and Tufekcioglu, 2000). Global soil respiration contributes an estimated 60 – 90 Pg C yr^{-1} to atmospheric CO_2, which is approximately ten times greater than emissions from fossil fuels (Bond-Lamberty and Thomson, 2010). Therefore, understanding soil respiration rate, particularly across different LULC types, is crucial for accurate carbon budgeting and effective climate mitigation in the AFOLU sector.

Monitoring soil CO_2 emissions is not only important for scientific understanding but also for policy formulation and implementation. Ghana, as a signatory to the Paris Agreement, has committed to reducing GHG emissions through its Nationally Determined Contributions (NDCs) (Ghana Government, 2015). Part of this commitment involves improving the management of forest and agricultural lands to enhance carbon sequestration and reduce emissions. Accurate data on soil CO_2 fluxes is essential for developing and refining national emission inventories, and for monitoring progress towards this international commitment. This monitoring will also aid in aligning with global climate goals set forth by the United Nations Framework Convention on Climate Change (UNFCCC).

In Ghana, different methods have been used to measure SRR, each with its advantages and limitations. The most commonly used is the static alkali absorption chamber method for trapping CO_2 flux (Parkin et al., 1997). In this method, CO_2 emitted from the soil is absorbed by a strong alkali solution, such as sodium hydroxide (NaOH), placed inside a sealed chamber that is inverted into the soil. The absorbed CO_2 reacts with NaOH to form sodium carbonate (Na_2CO_3), and the amount of CO_2 trapped is later quantified through laboratory titration (Anokye et al., 2021; Koomson, 2013; Maccarthy et al., 2018). This method is relatively simple and cost-effective, but it requires repeated manual sampling, making it labour-intensive and potentially prone to human error.

Although limited research has been conducted on the use of automated soil respiration systems with infrared gas analysis equipment in Ghana, such as the brief study by Dicko (2016), these systems offer significant advantages, including high temporal resolution and reduced labour. However, their use is often constrained by high costs

and logistical challenges, particularly in remote areas where powering and calibrating the equipment is problematic. In Ghana, most existing studies cover short measurement periods, ranging from a few weeks (Dicko, 2016; Maccarthy et al., 2018) to nine months (Koomson, 2013), which may not adequately capture seasonal variability. Therefore, long-term and continuous monitoring is needed to gain a comprehensive understanding of *SRR* and its seasonal dynamics across Ghana's diverse landscape.

Soil respiration is a complex biochemical process governed by various environmental and soil physio-chemical factors, with climatic conditions playing a critical role. Among these, temperature and moisture are key regulators of *SRR* as they directly influence microbial activity and root respiration, which are the primary contributors. Elevated temperatures enhance microbial metabolic rates and enzymatic activity, resulting in accelerated organic matter decomposition and subsequent CO_2 release (Davidson and Janssens, 2006). However, this effect is moderated by soil moisture; both excessively dry and waterlogged conditions can inhibit microbial activity and reduce soil respiration (Smith, 2008). In addition to climatic conditions, soil physio-chemical properties such as pH, texture and soil organic matter (SOM) content are crucial determinants of soil respiration. Higher SOM provides more substrate for microbial decomposition, thereby increasing *SRR* as microbes break down the organic material into simpler compounds, releasing CO_2 in the process (Raich and Tufekcioglu, 2000). Similarly, soil pH affects the composition and activity of microbial communities, while soil texture influences aeration and moisture retention, both of which are critical for microbial and root respiration processes (Bi et al., 2018). Understanding the interplay between these variables is essential for accurately predicting SRR across different LULC types in Ghana's semi-deciduous forest zone.

Therefore, this study aims to provide baseline data on *SRR* from forest, fallow (open forest) and cropland (maize and rice) in the semi-deciduous forest zone of Ghana to understand the dynamics of *SRR* across different land-use types. The present study aims to address the following research questions: (1) How does seasonal variation influence *SRR* across different LULC types? (2) Are there significant differences in *SRR* among various LULC types, topographical features, and habitat types? And (3) Which soil physicochemical and environmental variables are most effective in predicting variations in *SRR* across these LULC types? To answer these questions, a

combination of field measurements and laboratory analyses were employed. Soil respiration rate was monitored using an infrared gas analyser to detect the CO_2 concentration over time across different land-use types.

4.2 . Materials and Methods

4.2.1 Site Description and Plot Selection

The research was conducted within a protected area, the Bobiri Forest Reserve (BFR), and surrounding areas in the moist semi-deciduous forest of Ghana (Figure 3.1). Spanning over a total area of 853 km^2, the study area includes the BFR and its surrounding areas and lies within the Ejisu and Juabeng Municipalities of the Ashanti Region. The BFR covers over 54 km^2 (Dembélé et al., 2024; Hall and Swaime, 1981; Hawthorne and Abu-Juam, 1995) and is surrounded by communities in the Ejisu Municipal of Ashanti region namely Kubease, Akuokrom, Bomfa, Duampopo, Hwereso, Konongo, New Koforidua, Nobewam, Odumasi, Lowcost, Besease, Donaso, Boankra and Edwenase (Dembélé et al., 2024). The reserve is divided into management units designated for various purposes, including production, tourism, research and conservation. Notably, it features a butterfly sanctuary and a strict nature reserve (Djagbletey et al., 2018).

The area experiences a humid semi-equatorial climate characterized by a bimodal rainfall pattern. The moist semi-deciduous zone has a bimodal rainy season with the major rainy season occurring from April to July, while the minor rainy season occurs from September to November. This is followed by a long dry season from December to March and a shorter one in August. Climatic variables have been monitored at Ghana Forestry Research Institutes (CSIR – FORIG), located approximately 35 km away from the BFR, over a period of 22 years from 2002 to 2023. Annual rainfall varies from 1,189.0 mm to 1,450 mm for the year 2023 and 2018, respectively, with the mean annual being 1,441.64 ± 215.43 mm yr^{-1}. The mean annual temperature is 24.65 ± 0.67 ℃, with the coolest month being August with a mean temperature of 22.48 ± 3.62 ℃ and the hottest month being February with a mean temperature of 25.66 ± 3.10 ℃.

Four land-use types were selected for the study based on the classified satellite images from 1986, 2007 and 2022, as developed in Chapter 3. These images represent the dominant LULC classes in the region; closed forest, open forest, cropland and mixed

vegetation (Dembélé et al., 2024). However, for specificity, the LULC classes were reclassified based on the specific vegetation types observed within the study plots. Closed forests and open forests were represented by forest and fallow land-use types, respectively. For the cropland and mixed vegetation class, two major food crops commonly grown in the study region, namely maize and rice, were selected.

The forest plots were located within the BFR research working cycle. The BFR was established on 11th November, 1939 under the Forest Ordinance Act 1939, however, operations started in 1946. The soil within the research area of the BFR is not subject to any specific management practices, though the primary forest management strategies implemented include silvicultural interventions, such as enrichment planting and liberation thinning (Djagbletey et al., 2018). The fallow plots selected for this study range in age from 7 to 15 years old. These plots were previously used for cultivating food crops like maize, plantain, cassava and cocoyam, but are currently left uncultivated. The selection of croplands was based on the region's staple crops, specifically maize and rice, that are cultivated twice a year. Maize is grown from May to July and again from September to November, while rice is cultivated from May to August and from October to January. The maize plots have been under continuous cultivation for over 15 years, and the rice fields for more than 20 years. Farmers also reported that no chemical fertilizers are used on the maize fields, but chicken manure is applied once a year, typically before the major rainy season. For the rice fields, chemical fertilizers, especially urea, are applied around 45 to 50 days after planting, during the panicle initiation stage (Dogbe et al., 2015). Furthermore, both maize and rice farmers use chemical pesticides for weed and pest control as part of their crop management practices.

4.2.2 Land-use Selection and Experimental Layout

A total of 14 plots, each measuring 50 x 50 meters, were established in four different land-use types. A schematic representation of the experimental design is presented in Figure 4.1.

The selection criteria of the sites for the soil respiration measurement were as follows:

- Topography: two plots were chosen for each Upland (UP) and lowland (LL) area to assess the impact of elevation on *SRR* for all land-use types, except rice

fields. In the study region, most rice cultivation occurs in lowland areas, so no highland rice plots were included (Table 4.1.);

- Distance between plots: to ensure sufficient heterogeneity within each land-use category, plots were spaced at least 200 meters apart.
- Habitat type: within each plot, two dominant habitat types were identified, and three PVC rings (or collars with 25 cm in diameter and 15 cm in height) were inserted into the soil in each habitat type for measuring *SRR*.

Forest plots: Three collars were installed in each of the two habitat types; bare soil under the canopy (shaded by trees) and bare soil in the inter-canopy area (exposed to sunlight).

Fallow plots: The chosen habitat types were bare soil and soil covered with grass.

Maize and Rice fields: The selected habitat types were bare soil and areas with maize or rice plants.

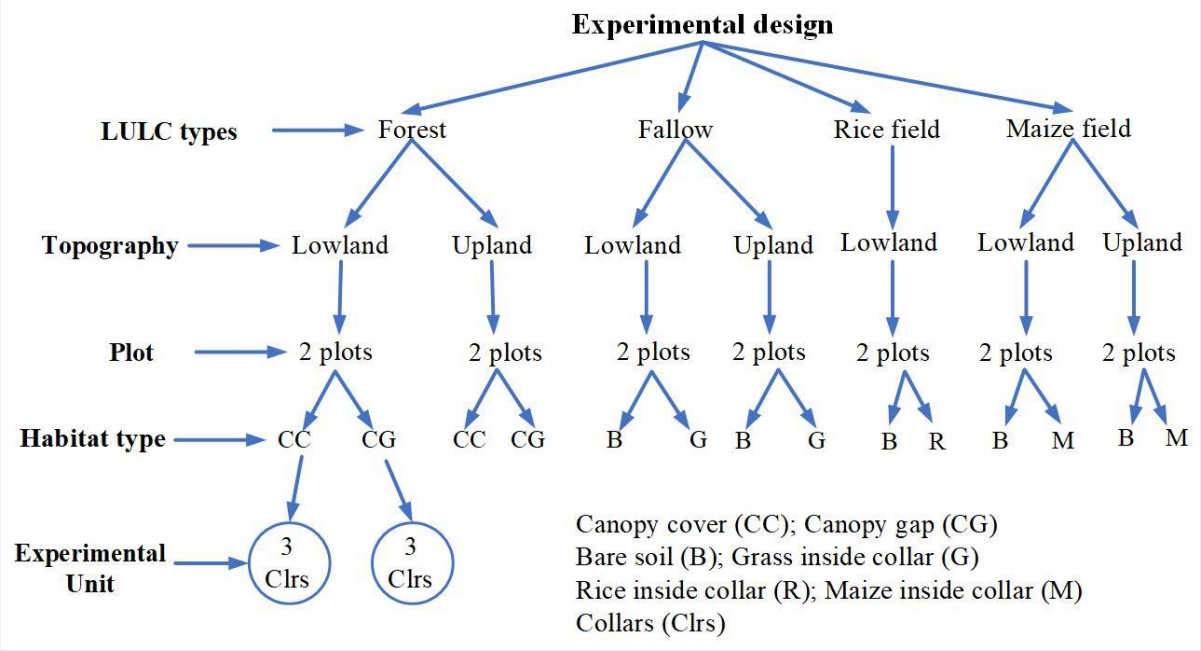

Figure 4.1: Experimental design for measuring soil respiration

This design enabled a comprehensive assessment of *SRR* different land-use types, topographical settings, and habitat variations, providing valuable insights into the environmental and management factors influencing *SRR*.

4.3 . Data Collection

4.3.1 Soil Greenhouse Gas Measurement

A closed chamber method was employed to measure *SRR* across the selected land-use types. Prior to starting the measurement, collars were installed 72 hours in advance to minimize soil disturbance and remain on the field for the entire study period. The collars are made up of short polyvinyl chloride (PVC) pipes of dimension 25 cm diameter and 15 cm in height. These were inserted into the soil, leaving 5 cm above the surface to provide a stable base for the chambers. Each plot had six collars installed, with three collars allocated per habitat type.

Table 4.1: Coordinates of the selected plot for the four land categories

Land categories	Topography	Plot	Longitude	Latitude	Altitude
Forest	Lowland	1	-1.34186	6.68722	266
Forest	Lowland	2	-1.34667	6.68767	267
Forest	Upland	1	-1.34939	6.68672	289
Forest	Upland	2	-1.34861	6.68481	309
Fallow	Upland	2	-1.36412	6.66202	254.2
Fallow	Upland	1	-1.35889	6.66889	258.3
Fallow	Lowland	1	-1.35454	6.66941	258.5
Fallow	Lowland	2	-1.36551	6.66038	263.1
CL (Maize)	Lowland	1	-1.35254	6.67146	233.1
CL (Maize)	Lowland	2	-1.34784	6.65478	249.2
CL (Maize)	Upland	1	-1.3495	6.65645	256.5
CL (Maize)	Upland	2	-1.34763	6.65484	257.1
CL (Rice)	Lowland	1	-1.36151	6.66833	249.4
CL (Rice)	Lowland	2	-1.35256	6.6719	238.4

Note: CL = Cropland

The respiration chambers are also made of PVC and have the same diameter as the collars. However, two chamber heights of 40 cm and 100 cm were available for the measurement depending on the habitat type. Each chamber was equipped with one or two small fans, depending on its height, to ensure air homogenization within the chamber. The sensors were mounted on top of the chamber to monitor CO_2 gas

accumulation, air temperature, air pressure and relative humidity. A CO_2 sensor probe, Vaisala GMP252 (Vaisala, 2024) with a range from 0 to 10,000 ppm and a three-in-one sensor, Tekbox TBSHTP05 sensor (Tekbox Digital Solutions, 2024), for measuring relative humidity (RH), air temperature and air pressure were installed in the chamber. The Relative humidity (RH) sensor has tolerance level of ±2 % RH, and a measurement range of 0 – 100%. The Barometric Pressure sensor has a tolerance of ± 0.5hPa, with a measurement range of 300 – 1250 hPa. The operating range of the temperature sensor is from – 20°C to + 55°C. All sensors were connected to a GP2 datalogger and the data recording of the various parameters was set at one-minute intervals. Once the chamber was closed, the recording process began and continued for seven minutes. To ensure accuracy, the first and last minutes of the recorded data were discarded to avoid noise, and only data from 2^{nd} and 6^{th} minutes (i.e., 5 data points) were used. For the analysis, only linear regression results with an R^2 value of 90% or higher between CO_2 concentration and time were considered, as shown in Figure 4.2 (Dossa et al., 2015). In addition to the above-mentioned recorded parameters, volumetric soil moisture content and temperature were simultaneously measured using a soil probe (WET 150 sensor) inserted near the collar at a depth of 5.0 cm

4.3.2 Soil Sampling and Physiochemical Analysis

Soil samples were collected from all 14 selected plots within the study area for the analysis of physio-chemical properties. The sampling design was based on the habitat types within each plot, with two types of samples collected for analysis of composite and single samples.

The samples were collected from the topsoil to a depth of 10 cm, to ensure consistency across sampling points. For composite samples, three soil samples were collected from different location within each habitat type (adjacent to the collars) using a core sampler. These samples were thoroughly mixed in a bucket to make a uniform composite sample. From the mixed sample, 1.0 kg subsample was taken for analysis. For the single samples, a sample was collected from each habitat type (also adjacent to the collar), using a core sampler. The samples were weighed immediately after collection and the fresh weight determined and recorded.

Physio-chemical analysis:

The collected soil samples were analysed to determine their physio-chemical properties. The Physical properties measured were soil water, bulk density (BD), total soil porosity (TSP), and water-filled pore space (WFPS), using the protocols described in (Landon, 1991). However, the chemical properties including soil texture, soil pH, total nitrogen (%TN), organic carbon (C) and organic matter, Available phosphorus (P_{avail}) and electrical conductivity (EC) were determined following the protocols described in Motsara and Roy (2008) and Nelson and Sommers (1982).

4.4 . Soil respiration rate calculation

The soil respiration rate was calculated using the following equation developed by Kahmark et al. (2020) and Zaman et al. (2021):

$$F = \frac{\alpha_v MPV}{RTA} \times 0.0024 \qquad (4.1)$$

Where:

- F = CO_2 flux in kilogram per hectare per day
- α_v = Volume-based CO_2 slope (ppm h^{-1})
- M= Molecular weight of CO_2 = 44.01 $g\ C\ mol^{-1}$
- P= Atmospheric pressure = $1{,}010\times10^3$ Pa
- R= Universal gas constant = 8.314 J $mol^{-1}\ K^{-1}$
- T= Field temperature in Kelvin (°C + 273)
- V= Chamber volume (m^3)
- A= Soil surface area covered by the chamber (m^2)
- 0.0024= Conversion factor for hours to days and m^2 to ha

The Eq. 4.1. calculates the *SRR* in kilograms per hectare per day using a static chamber system. The flux is derived by determining the slope of CO_2 concentration changes over time (α_v), a sample of slope calculation and is illustrated in Figure 4.2. The value adjusted for atmospheric conditions (pressure and temperature), molecular properties of CO_2, and chamber area. The formula incorporates conversion factors to account for time (from minutes to days) and area (from square meters to hectares), while converting mass units from micrograms to kilograms. This provides a standardised way to express *SRR* over a defined area and timeframe, useful for comparing fluxes across land-uses or environmental conditions

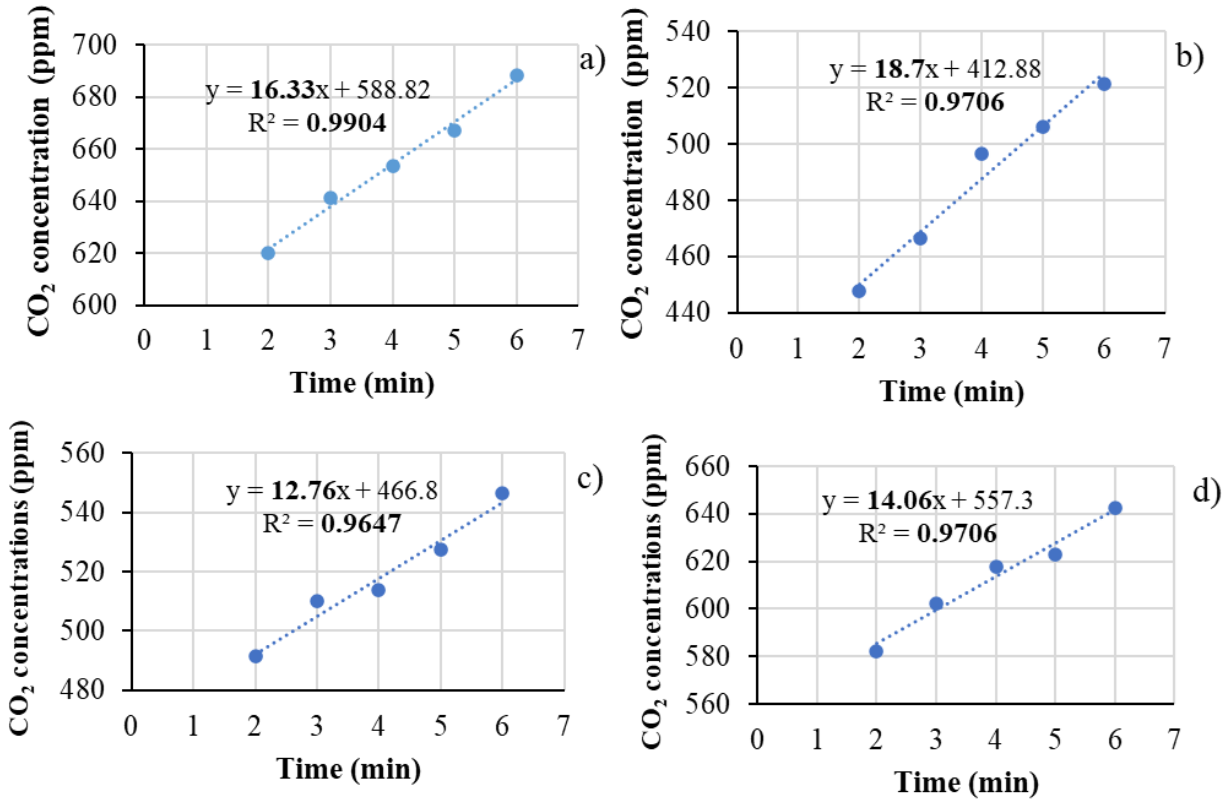

Figure 4.2: Sample calculation demonstrating the linear regression of CO_2 concentration over time to determine the slope and the coefficient of determination (R^2) for each land-use type: (a) Forest, (b) Fallow, (c) Maize field and (d) Rice field.

4.5 . Soil Respiration Model Development

Soil respiration was modelled using both linear and nonlinear regression approaches. A stepwise multiple regression analysis was conducted with four predictor variables, comprising both soil biophysical properties and environmental factors. Three model types were employed: linear, exponential and logarithmic. The selected variables were chosen based on their strong relationships with soil respiration. The detailed model structures are presented in Table 4.2. To evaluate the performance of these models in estimating soil respiration rates, three statistical indicators were used: the Akaike Information Criterion (AIC), the coefficient of determination (R^2), and percentage Bias (%Bias).

The AIC evaluates the trade-off between model accuracy and complexity by applying a penalty for overfitting, with lower values indicating a better-fitting model (Sutherland et al., 2023). The R^2 quantifies the proportion of variance in the observed

data that is explained by the model, with values closer to 1 reflecting greater explanatory power (Chicco et al., 2021). Percentage bias measures the systematic deviation between predicted and observed values, where values near zero indicate minimal bias, positive values suggest overestimation and negative values indicate underestimation (Moriasi et al., 2015). Collectively, these indicators provide a comprehensive assessment of model performance, ensuring accuracy, efficiency and reliability in model selection.

Table 4.2: Equations of multiple linear and non-linear regression

Model types	Equation	References	Eq
Linear	$y = \beta_0 + \beta_1 x_1 + \beta_2 x_2 + \cdots \beta_n x_n + \varepsilon$ Where $\beta_0, \beta_1, \beta_2$ and β_n are coefficients for the predictor x_i, and ε is the error.	(Kutner, 2005)	1
Exponential	$y = ae^{(\beta_1 x_1 + \beta_2 x_2 + \cdots + \beta_n x_n)}$ Where a is a constant, $\beta_0, \beta_1, \beta_2$ and β_n are coefficients for each predictor x_i.	(Huang et al., 2009)	2
Logarithmic	$y = \beta_0 + \beta_1 \log(x_1) + \beta_2 \log(x_2) + \cdots \beta_n \log(x_n)$ Where $\beta_0, \beta_1, \beta_2$ and β_n are coefficients for the predictors.	(Tiao et al., 1998)	3

4.6 Data Analyses

The data was log-transformed to perform a factorial analysis of variance (ANOVA), which was used to determine the effect of seasonal variation on *SRR* across the four land-use types. Additionally, a two-sample t-test (assuming unequal variance) was conducted to determine significant differences in *SRR*, soil moisture and temperature between the wet and dry seasons across the different land-use types.

A multifactorial ANOVA was also performed to estimate the influence of land-use types, topography and habitat types on *SRR*. Tukey's honestly significant difference (HSD) test was used to identify significant differences among the means at a 5% significance level. Furthermore, a pairwise correlation matrix was computed to examine the relationships between various bio-physio-chemical parameters and *SRR*, providing insight for variable selection in multiple linear and nonlinear regressions. Predictors such as soil moisture, temperature, pH, organic matter and texture were

analysed to assess their effects on *SRR*. All statistical analyses were performed using R statistical software (version 4.4.1), Excel and SAS OnDemand for Academics.

4.7 . Results

4.7.1 Effect of Topography on Soil Respiration Rate

The effect of topography on SRR was evaluated across different land-use types, as illustrated in Figure 4.3. The results present the mean soil respiration and associated standard errors for various LULC types across lowland and upland topography. In forests, mean soil respiration was significantly higher in the upland (46.61 ± 1.79 kg CO_2 ha^{-1} d^{-1}) compared to the lowland (41.25 ± 29.52 kg CO_2 ha^{-1} d^{-1}), with the large standard error in the lowland indicating greater variability in measurements. On fallow lands, there was no significant difference in mean soil respiration between upland (68.68 ± 1.72 kg CO_2 ha^{-1} d^{-1}) and lowland (69.73 ± 28.30 kg CO_2 ha^{-1} d^{-1}). However, the higher standard error in the lowland suggests greater variability. Similarly, in maize fields, mean soil respiration showed no significant difference between the upland (48.85 ± 1.16 kg CO_2 ha^{-1} d^{-1}) and lowland (47.40 ± 20.57kg CO_2 ha^{-1} d^{-1}), with the upland displaying lower standard error, indicating more consistent measurements. In the case of rice fields, data were available only for the lowland region, with a mean soil respiration of 58.48 ± 21.31 kg CO_2 ha^{-1} d^{-1}. The results indicate that upland regions tend to have more consistent soil respiration measurements, as reflected by lower standard errors, while lowland regions exhibit greater variability, particularly for forest, fallow and maize land-use types.

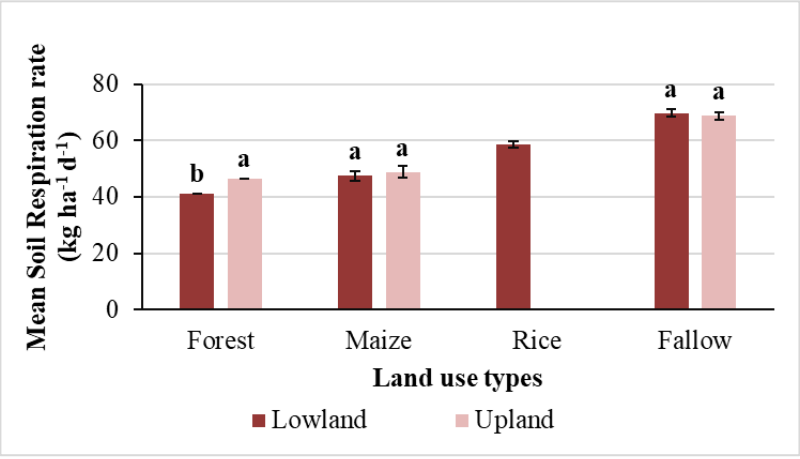

Figure 4.3: Variation of soil respiration between topography for each land-use type

4.7.2 Seasonal Variation in Soil Respiration Rate, Moisture and Temperature

The seasonal variation in *SRR* differed across the four land-uses (Figure 4.4). For the fallow land-use, the highest respiration rate was exhibited in January, with a rate of 88.36 kg CO_2 ha^{-1} d^{-1}, for the forest land-use it was in March and June, with the value of 58.82 and 58.52 kg CO_2 ha^{-1} d^{-1}, respectively, for the maize land-use it was in October and June with the rate of 59.79 and 57.17 kg CO_2 ha^{-1} d^{-1}, respectively, whereas for the rice land-use it was in May with the rate of 85.80 kg CO_2 ha^{-1} d^{-1} (Figure 4.4). The lowest soil respiration rate for the fallow land-use was exhibited in August with a rate of 56.12 kg CO_2 ha^{-1} d^{-1}, for the forest land-use it was in July with the rate of 17.46 kg CO_2 ha^{-1} d^{-1}, for the maize land-use it was in February with rate of 24.56 kg CO_2 ha^{-1} d^{-1}, whereas for the rice land-use it was in July with the rate of 34.46 kg CO_2 ha^{-1} d^{-1} (Figure 4.4).

Pattern of the seasonal variation in soil temperature was similar among the various land-uses. The lowest soil temperature in all the land-uses occurred in August, with the values for Fallow, Forest, Maize and Rice land-uses being 27.71, 25.03, 27.69 and 27.93 ^{o}C, respectively. However, the highest temperature occurred in different months. The highest value of 38.73°C was exhibited by the Fallow land-use in February, followed by 38.09 ^{o}C in January, 37.11 ^{o}C in April and 30.29 ^{o}C in March for Maize, Rice and Forest land-uses, respectively. The lowest soil temperature was exhibited in the Forest land-use, followed by an increasing order by Fallow, Maize and Rice Land-uses, with the values being 27.17, 30.39, 32.94 and 34.39 ^{o}C, respectively (Figure 4.4).

Seasonal variation in soil moisture content for all the land-uses followed a similar trend. The soil moisture exhibited a steady negative or positive change from July towards September, and then abrupt negative change towards the lowest in January/February. The soil moisture then steadily increased towards June/July following the rainfall pattern. The soil moisture was highest in June for the Fallow land-use (31.64%), in August for the Forest land-use (22.35%), in June for the Maize land-use (37.85%) and in July for the Rice land-use (66.84%) (Figure 4.4).

Soil respiration rates across various land-uses exhibit significant variability due to factors such as soil moisture and temperature, land management practices, and ecological cycles. For example, fallow land showed peak respiration rate during

January 2024 and June 2024, aligning with dry season decomposition and increased microbial activity at the onset of the wet season, respectively (Figure 4.4). Conversely, respiration rate was lower in August and October 2023, possibly due to a transition in vegetation stages. In forest land-use, emissions spike in March 2024 and June 2023, likely driven by the decomposition of accumulated organic materials and optimal conditions (soil moisture) for microbial activity during the wet season's peak. However, in July 2023 and February 2024 the respiration rate reduced, likely due to stabilized decomposition rates and the dry season's suppressive effects on microbial processes. Rice land-use reached peak respiration rate in May 2024 and January 2024, exacerbated by wet season conditions and residual decomposition in flooded fields, while unexpectedly lower emissions in July and August 2023 may result from stabilized anaerobic decomposition or improved management practices. Similarly, maize fields record high emissions during the beginning of the wet season in October and due to the high soil moisture content in August, with lower emissions noted at the end of the wet season in November and during the dry season in February (Appendix 6).

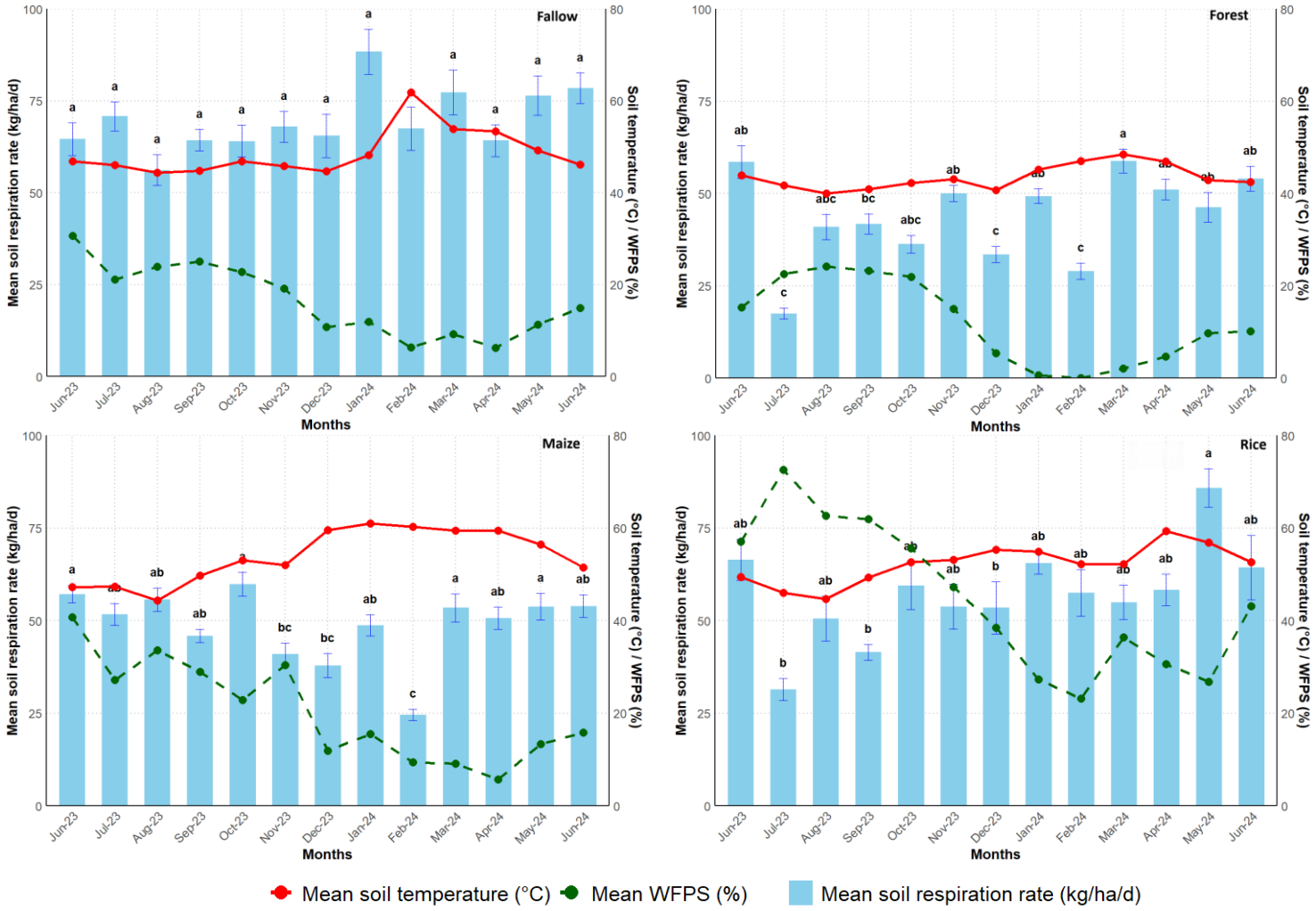

Figure 4.4. Seasonal variation in soil respiration rate, temperature and moisture across land-use types, (a) Forest land, (b) Fallow, (c) Maize field, (d) Rice field.

4.7.3 Extent of Change from Previous Month

Excluding the fallow land, the soil respiration rate of the forest, maize and rice land-uses decreased from June to July 2023. However, the extent of the decrease differed among the three land-uses with the values being -70.17%, -9.56% and -52.63%, whereas from July to August the trend reversed with the extent of increase being 134.29%, 7.62% and 60.58% for the forest, maize and rice land-use, respectively. For that of the fallow land-use, the extent of increase was 9.58%, but the trend reversed from July to August with the extent of decrease being 20.70%. From August to September, there was an increase in forest (2.11%) and fallow (14.53%) land-uses, whereas there a decrease the maize (17.59%) and rice (17.99%) land-uses (croplands). The trend reversed from September to October where that of the forest and fallow land-uses decreased (13.13% and 0.44%, respectively), and that of maize and rice land increased (30.40% and 43.42%, respectively). From October to November, that of forest and fallow land-uses increased (37.88% and 6.16%, respectively), whereas that of maize and rice land-uses decreased (-31.51% and -9.57%, respectively). From November to December there was reduction in the SRR for all the land-uses, with the extent of reduction being -33.01%, -3.65%, -7.44% and -12.27%, as well as from January to February which was -41.14%, -23.72%, -49.56% and -12.27% for the forest, fallow, maize and rice land-uses, respectively. There was an increase in the *SRR* from December to January for all the land-uses with the extent being 46.98%, 34.98%, 28.47% and 22.55% for the forest, fallow, maize and rice, respectively. From February to March, there was an increase in the *SRR* for all the land-uses with the exception of rice land-use which exhibited a reduction. However, the reverse occurred from March to April when there was reduction in all the land-uses with the exception of the rice land-use which exhibited an increase. From April to May only the Forest showed a reduction, whereas only the rice land-use exhibited a reduction from May to June (Figure 4.5).

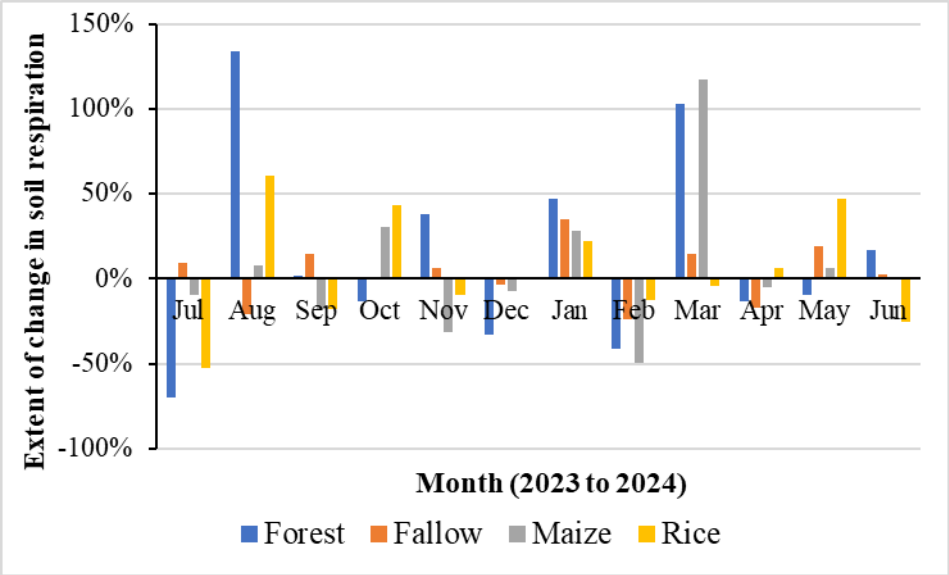

Figure 4.5: Extent of change in soil respiration rate from that of previous month in the four land-uses.

4.7.4 Soil Characteristics

The variation in soil nutrients and physicochemical properties across different LULC types reveals significant differences in organic matter content, bulk density, pH and total nitrogen. Organic matter was highest in fallow soils (3.48 ± 0.15 %) and forest soils (3.19 ± 0.13 %), while lower levels were observed in maize fields (1.56 ± 0.07 %) and rice fields (2.48 ± 0.15 %). Bulk density was lowest in forest (1.25 ± 0.05 g cm^{-3}) and fallow soils (1.24 ± 0.05 g cm^{-3}) but higher in maize (1.39 ± 0.06 g cm^{-3}) and rice fields (1.40 ± 0.09 g cm^{-3}), indicating greater soil compaction in cultivated fields. Soil pH was slightly acidic across all LULC types, with the highest value recorded in rice fields (6.01 ± 0.36), followed by fallow (5.73 ± 0.25), maize (5.66 ± 0.24), and forest soils (5.47 ± 0.22). Similarly, total nitrogen content was highest in forest soils (0.23 ± 0.01%) and fallow soils (0.19 ± 0.01 %), while maize (0.11 ± 0.005 %) and rice fields (0.10 ± 0.006 %) had the lowest values. Overall, forest and fallow lands maintain higher levels of organic matter and nitrogen, whereas agricultural fields exhibit reduced values and higher bulk density, likely a result of cultivation practices and soil compaction. These results are illustrated in Figure 4.6.

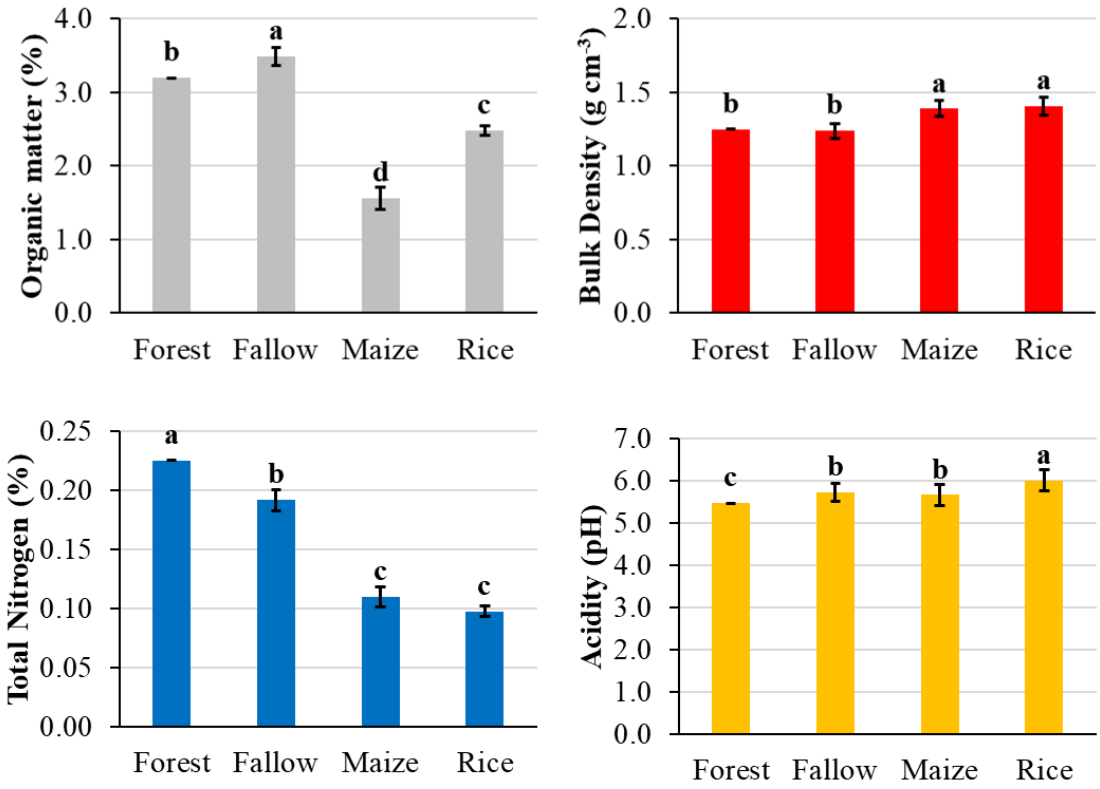

Figure 4.6: Variation of soil nutrients and physicochemical properties across the different land-use types

4.7.5 Interaction Between Respiration Rate and Land-use

The analysis of variance conducted on *SRR* across the four land-use types over 13-month period (from June 2023 to June 2024) revealed significant influences from both the type of land-use and the month (Table 4.3). There is a demonstration of a profound effect of land-use type, on the *SRR*, with F= 119.36, indicating that the variance in emissions across these categories is statistically significant ($p < 2e^{-16}$). This suggests that each land-use type contributes differently to the overall respiration rate, with potentially different management practices. The monthly analysis further demonstrates the seasonal dynamics affecting *SRR*, with F= 13.51 ($p < 2e^{-16}$), confirming significant monthly variations. This temporal pattern likely reflects changes in soil moisture and temperature that influence biological and chemical processes in the soil.

Moreover, the interaction between land-use and seasonal variation, denoted by F= 4.35 ($p = 3.44\ e^{-16}$), indicates that the effect of land-use on *SRR* varies throughout the

year. This could be due to different management practices and growth cycles of each land-use type during various months. For instance, rice fields may exhibit higher *SRR* during wet months due to flooding, whereas forest and fallow lands might see increased emissions during high biomass decomposition periods.

Table 4.3: Analysis of variance for soil respiration rate by land-use type and month

Source	Df	Sum Sq	Mean Sq	F value	Pr (>F)
LUT	3	209,838	69,946	119.355	$< 2e^{-16}$ *
Months	12	94,989	7,916	13.507	$< 2e^{-16}$ *
LULC × Months	36	91,819	2,551	4.352	$3.44e^{-16}$ *
Residuals	1915	1,122	586		

Df: degree of freedom, Sum Sq (Sum of Squares), Mean Sq (Mean Square), sig. 0.05 (*)

4.7.6 Effect of Land-use Change, Topography and Habitat Types on Soil Respiration Rate

A multifactorial analysis of variance (ANOVA) was conducted to assess the effects of LULC, topography and habitat type on *SRR*. The ANOVA also explored interactions between these factors to understand their combined effects on emissions. The statistical outcomes of this analysis are summarized in Appendix 4. The results indicated both LULC and habitat factors had significant effect on soil respiration rate, with $F = 104.90$, $p < 2e^{-16}$ and $F = 25.05$, $p = 6.65e^{-16}$, respectively, highlighting the role of land-use and habitats in soil CO_2 dynamics. The pairwise comparisons further highlight these differences, with fallow land exhibiting the highest emissions, significantly higher than those from forests, maize and rice (Figure 4.7). This variation could be attributed to the age of the fallow land and the rapid decomposition of organic matter in these plots. Additionally, agronomic practices such as NPK fertilizer application in rice fields and organic manure application in maize also influence emission profiles compared to forest areas.

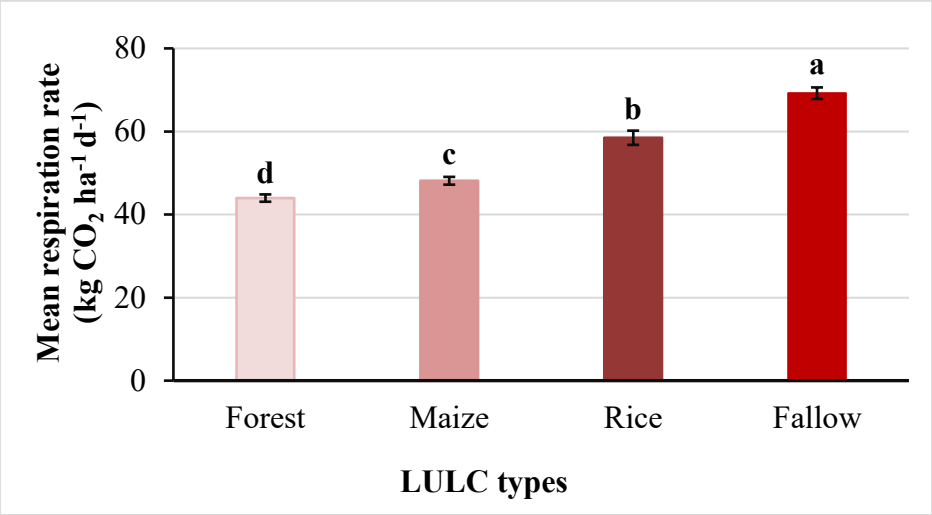

Figure 4.7: Mean respiration rate by land-use land cover type

The comparative mean respiration rate across the four different LULC types is illustrated in Figure 4.7. It demonstrates that fallow land exhibits the highest respiration rate, with a mean value of more than 69 ± 0.05 kg ha^{-1} d^{-1}, significantly higher than the other types. Rice and Maize fields also show substantial emissions with their mean values of 58.48 ± 1.72 kg ha^{-1} d^{-1} and 48.13 ± 0.94 kg ha^{-1} d^{-1}, respectively, and were statistically significant difference from forest plots, which have recorded the lowest emissions 43.96 ± 0.88 kg ha^{-1} d^{-1}.

The results indicate that uncultivated soil, when left fallow for several years, becomes rich in organic matter. Coupled with exposure to sunlight, these conditions create an ideal environment for the decomposition of organic matter, significantly increasing *SRR*. Rice fields, typically cultivated under flooded (rainfed) conditions, exhibit higher emissions than maize and forest lands, likely due to the anaerobic decomposition processes that prevail under such conditions. In contrast, forest lands, which are characterized by greater biomass, less disturbed soils, and reduced exposure to sunlight critical for microbial activity, display the lowest emissions among the land-use types.

The ANOVA results indicate a significant difference in emissions across various habitat types within different land-use categories. The highest emissions are observed in grass habitats on fallow plots, with levels approaching 80 kg ha^{-1} d^{-1}. This suggests that grass habitats, characterized by abundant plant material, likely facilitate higher rates of organic matter decomposition, significantly increasing *SRR* (Figure 4.8).

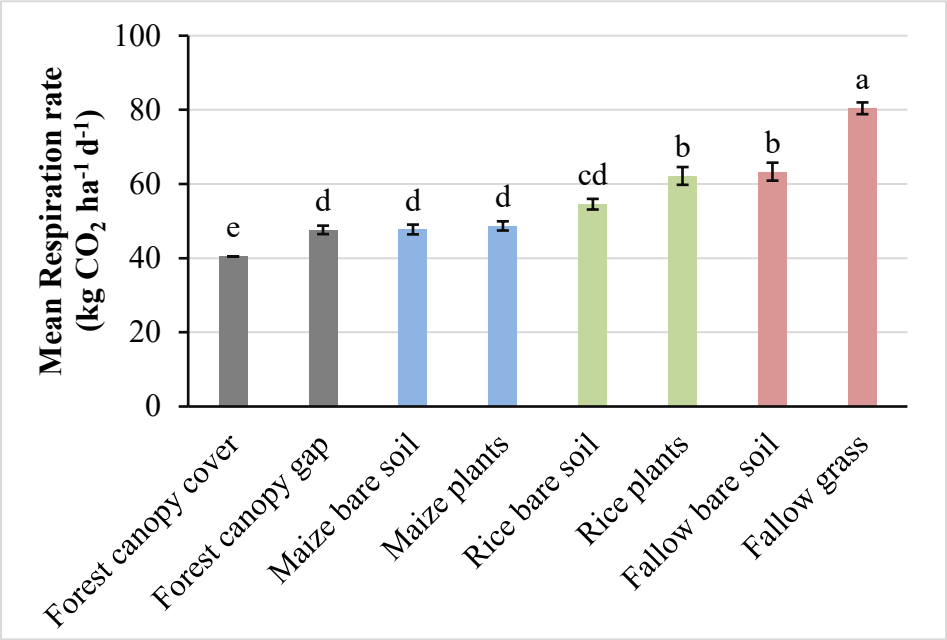

Figure 4.8: Mean respiration rate by LULC types

Conversely, the lowest respiration rate was observed in forest plots with canopy cover with 40.46 ± 1.15 kg ha^{-1} d^{-1}. This suggests that areas under a forest canopy, where little to no sunlight reaches the soil surface, exhibit lower emissions compared to areas with canopy gaps where the soil is exposed to sunlight. The limited sunlight in canopy cover restricts the energy i.e., soil temperature available for microbial activities necessary for the breakdown of organic matter, leading to reduced *SRR*. Intermediate emissions are observed in agricultural lands, with Maize Plants and Rice Plants displaying significant differences. This variation suggests that these crop types have differing impacts on soil CO_2 dynamics during active cultivation. Bare land types across both Maize and Rice show no significant differences in emissions, although Maize Bare tends to emit less than Rice Bare. This pattern may reflect the influence of residual soil moisture and management practices, such as fertilizer application, on the *SRR*.

Topography did not show a significant effect on respiration rate, with F = 2.99, and a p = 0.083, suggesting a potential role in influencing how environmental conditions affect soil processes. This indicates that while topography may not be the primary driver of SRR, it could still play a role in shaping the environmental conditions that affect soil dynamics. Additionally, the combined effects of land-use type and habitat type, as well as land-use type and topography, did not show significant results (p >

0.05). Therefore, the main effects of land-use and habitat type on *SRR* are not affected by these factors.

This highlights the dominance of LULC and habitat type in influencing the rates of respiration, independent of the variations in topography.

4.7.7 Modelling Soil Respiration Rate

Soil Characteristics of the Land-use Types

The soil bio-physio-chemical properties of the land-use types analyses are presented in Tables 4.4 and Figure 4.6. Overall, soil bulk density (BD) decreased from cropland to less disturbed forest, with the highest values recorded in the rice and maize fields, showing no significant difference between them. In contrast, the forest and fallow land that exhibited the lowest bulk density values, also showed no significant difference ($p < 0.05$) at the 0 – 10 cm depth. The soil texture was sandy loam in all three land-use types, except for the forest, which had a sandy texture. Soil pH varied across land-use types, with the rice field recording the highest pH and the forest the lowest. No significant difference was observed between the pH levels of maize and fallow lands.

Table 4.4: Soil physical characteristics in the land-use types

Soil depth (cm)		Land-use type				Pr(>F)
		Fallow	Forest	Maize	Rice	
0 - 10	Bulk density (g cm^{-3})	1.24^{b}	1.25^{b}	1.39^{a}	1.4^{a}	$2e^{-16}$ *
	% SAND	77.53^{b}	88.75^{a}	77.7^{b}	77.65^{b}	$2e^{-16}$ *
	% CLAY	8.89^{c}	4^{d}	11.18^{a}	10.36^{b}	$2e^{-16}$ *
	% SILT	13.57^{a}	7.26^{c}	11.12^{b}	11.99^{b}	$2e^{-16}$ *
	Texture	Sandy loam	Sand	Sandy loam	Sandy loam	

Soil organic matter (SOM) content was significantly different across the land-use types and was the highest from the decreasing order fallow, forest, rice and maize. The forest land had the highest amount of nitrogen content followed by fallow, but no significant difference was observed between maize and rice nitrogen content. Nitrogen content in the forest was twice higher than in the croplands and more than 17% greater than in the fallow. Soil available P was highest in the forest with more than 45 %, 99 % and 99% higher in the fallow, maize and rice land-use, respectively.

Relationship Between Soil Parameters and Carbon Dioxide Emission

The relationships between various bio-physio-chemical parameters and soil respiration rate were analysed using the respiration rate, related to the soil variables

collected during the data collection period. These relationships are illustrated in Figure 4.9. The correlation matrix indicates that apart from soil organic matter (OM) and pH that showed significant relationship and yet weak 0.43 and 0.40, respectively with respiration rate, all other variables collected did not show significant relationship. Additionally, variables such as silt, soil moisture (SM), and soil temperature (ST) also showed positive correlations with respiration rate, but these relationships are from weak to poor and not statistically significant, with coefficients of 0.36, 0.26 and 0.16, respectively. This suggests that OM, pH and Silt are likely more relevant predictors of *SRR* in this dataset than soil temperature and moisture alone.

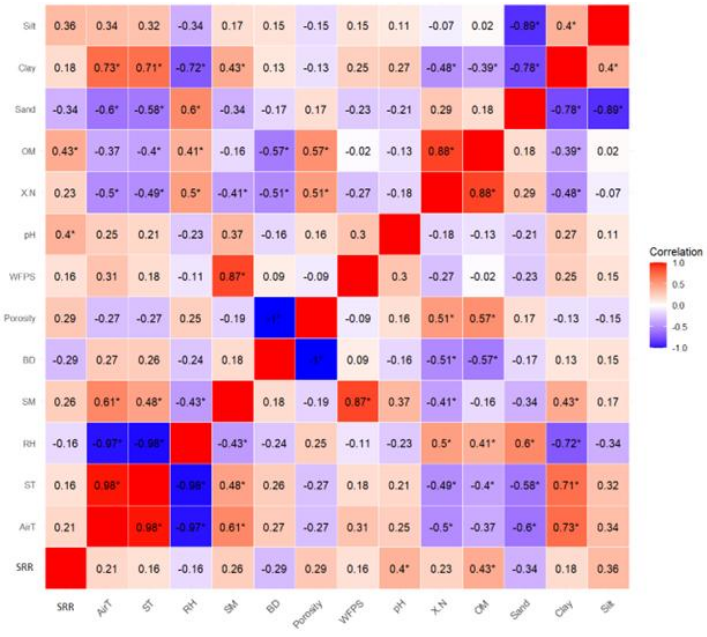

Figure 4.9: Pairwise correlations matrix of soil bio-physio-chemical parameters and soil respiration rate (SRR).

Stepwise Regression Analysis of Soil Respiration Predictors

The step-wise multiple regression analysis was performed to determine the influence of organic matter (OM), pH, silt, and soil moisture (SM) on *SRR*. These predictors were selected based on the pairwise correlation in Figure 4.9. The performance of the four regression models including Linear, Logarithmic, Exponential, and Mixed models was evaluated for predicting soil respiration rates based on edaphic factors (OM, pH, Silt and SM) using stepwise multiple regression techniques. The results revealed that linear models exhibited the weakest performance, with R^2 values peaking at 0.40 and *RMSE* remaining high (8.79 - 11.17), indicating a limited capacity to explain *SRR*. In contrast, the logarithmic models performed better, achieving an R^2

of 0.53 and a reduced *RMSE* of 8.48 when all predictors were included, with no apparent bias. The exponential models showed moderate improvement, with an R^2 of 0.49 and an *RMSE* of 8.79, although slight systematic errors were observed in the %Bias values. However, the mixed models outperformed all others, achieving the highest R^2 (0.58), the lowest *RMSE* (8.03), and the best AIC (58.69), along with minimal %Bias (0.0027). This higher performance demonstrates the mixed model's ability to capture the complex relationships between predictors and *SRR*. Therefore, the mixed model incorporating OM, pH, Silt and SM is recommended for its accuracy, efficiency, and minimal bias. The different modelling outputs are in the Table 4.5.

Table 4.5: Stepwise non-linear multiple regression models of soil respiration rate on edaphic variables

Models	Variables	Multiple Regression Model	R^2	RMSE	AIC	%Bias
Linear	OM	$SR = 44.583 + 3.607OM$	0.152	11.17	212.93	0.00
Linear	OM, pH	$SR = -23.596 + 4.087OM + 11.778pH$	0.339	9.66	207.09	0.00
Linear	OM, pH, Silt	$SR = -25.741 + 3.988OM + 10.889pH + 0.705Silt$	0.408	8.95	204.96	0.00
Linear	OM, pH, Silt, SM	$SR = -21.652 + 4.134OM + 9.589pH + 0.657Silt + 0.185SM$	0.403	8.79	205.99	0.00
Logarithmic	OM	$SR = 46.630 + 8.963log\ (OM)$	0.144	11.44	214.25	0.00
Logarithmic	OM, pH	$SR = -74.982 + 11.249\ log\ (OM) + 69.037log\ (pH)$	0.377	9.76	207.67	0.00
Logarithmic	OM, pH, Silt	$SR = -78.030 + 11.962\ log\ (OM) + 60.840\ log\ (pH) + 7.540log\ (Silt)$	0.509	8.66	203.21	0.00
Logarithmic	OM, pH, Silt, SM	$SR = -75.134 + 12.311\ log\ (OM) + 52.862\ log\ (pH) + 6.569\ log\ (Silt) + 4.558\ log\ (SM)$	0.530	8.48	204.05	0.00
Exponential	OM	$SR = 45.331exp^{(0.0652OM)}$	0.195	11.10	212.58	-0.03
Exponential	OM, pH	$SR = 54.0392exp^{(0.0957OM+0.086pH)}$	0.358	9.91	208.48	0.07
Exponential	OM, pH, Silt	$SR = 53.7944exp^{(0.097M+0.094pH+0.072Silt)}$	0.473	8.98	205.14	0.01
Exponential	OM, pH, Silt, SM	$SR = 53.7554exp^{(0.103OM+0.083pH+0.067Silt+0.034SM)}$	0.495	8.79	206.01	0.01
Mixed	OM	$SR = 45.3313\ exp^{(0.0663OM)}$	0.20	11.10	58.60	0.03
Mixed	OM, pH	$SR = (0.856\ exp^{(0.0663OM)})(55.9370\log(pH) - 44.0498))$	0.39	9.69	57.77	-0.04
Mixed	OM, pH, Silt	$SR = (0.\ 0161exp^{(0.0741OM)})(55.9370\log(pH) - 46.3181)(7.8634\log(Silt) + 36.9390)$	0.56	8.24	56.50	0.03
Mixed	OM, pH, Silt, SM	$SR = (0.\ 000377exp^{(0.0771OM)})(55.9370\log(pH) - 36.2977)(6.3644\log(Silt) + 36.9390)(3.2327\log(SM) + 24.48)$	0.58	8.03	58.69	0.00

4.8 . Discussion

4.8.1 Seasonal Variation and Soil Respiration Rate

Seasonal variations have a significant impact on *SRR* due to changes in environmental factors such as ST and SM, which influence biological processes, including the activity of soil microorganisms and plant roots (Davidson and Janssens, 2006). These effects are particularly pronounced in tropical regions like Ghana, where there are distinct wet and dry seasons, with soil moisture playing a critical role.

The influence of seasonal dynamics on *SRR* has been clearly demonstrated in studies specific to seasonal changes in temperate, sub-tropical and boreal regions (Kong et al., 2022; Oechel et al., 2014; Veldkamp et al., 2003; Vicca et al., 2012). Favourable soil moisture and temperature might lead to higher microbial and root activity, as observed in Appendix 5 and Figure 4.4. The potential increase in biological activity leads to higher rates of OM decomposition and consequently higher *SRR* in the wet season. Studies have shown that peak microbial activity often coincides with peak soil moisture during the wet seasons, leading to increased *SRR* (Pingintha-Durden et al., 2007; Vicca et al., 2012). Furthermore, the stagnation of water in the field can raise soil moisture levels, creating anaerobic areas, especially in rice fields. This can lead to increased CO_2 production and the emission of potent greenhouse gases (Nieveen et al., 2005). Conversely, during the dry season, lower soil moisture and higher temperatures may limit microbial activity and root growth, resulting in lower *SRR*. This is reflected in Appendix 5, where respiration rates were generally higher during the wet season, although the difference between the two seasons was not statistically significant. There is evidence in the literature that soil microorganisms require certain levels of moisture and temperature to maintain metabolic activity. Though, most of these studies reflect the temperate and sub-tropical climate conditions (Borken and Matzner, 2009; Davidson et al., 2012; Xu and Shang, 2016) that are significantly different from the tropical climate in terms of temperature and moisture fluctuation.

However, the current results show that in tropical regions like Ghana, although a slight increase in respiration rate was observed during the wet season, likely due to significant soil moisture influencing *SRR*, no clear trend was observed in the variation of SM and ST with the emission across land-use types (as seen in Appendix 5 and Figure 4.4). Similar results were found in Ameyaw (2015) and Manu (2023) who also

monitored soil respiration from the forest land and different Cocoa agroforestry systems in Ghana using an infrared gas analyser (EGM – 5). They found no significant relationship between *SRR* and SM and ST. In contrast to the study by Anokye et al. (2021), which assessed soil respiration across three land-use types, namely forest, oil palm plantation and arable land, using the gas entrapment method over a short period (30 days each in the dry and wet seasons, with sampling every 48 hours), their findings highlighted that both soil moisture and temperature contribute to *SRR* in both seasons. However, soil temperature showed a stronger and more significant relationship with *SRR*, with correlation coefficients between 0.74 and 0.83 for the dry and wet seasons, respectively. In comparison, the correlation between soil moisture and *SRR* was weaker, ranging from 0.4 to 0.49 in the dry season and 0.52 to 0.67 in the wet season. While their study recorded a significant relationship between SM and ST, the specific threshold at which these factors, especially SM, may drive autotrophic and heterotrophic respiration given the limited temperature variation in tropical regions affects decomposition and overall respiration remains poorly understood and requires further investigation.

4.8.2 Effect of Land-use Change, Topography and Habitat Types on Soil Respiration Rate

Variation of Carbon Dioxide Across Land-use Types

A multifactorial analysis of variance (ANOVA) was performed to determine the effect of land-use, habitats and topography on SRR. The results reveal significant effects of land-use and habitat types on SRR, while topography had no significant influence.

Carbon dioxide emission is known to vary significantly across different vegetation types or land-use types (Don et al., 2011; Mboyerwa et al., 2022). The Fallow land-use exhibited the highest *SRR* (Figure 4.7) possibly due to accumulation of soil organic matter (SOM) (Figure 4.6), which decomposes rapidly when exposed to favourable conditions such as sunlight and aeration. Yang et al. (2022) and Liu et al. (2022) reported that when fallow land remains uncultivated with no management practices for several years, it accumulates significant amounts of organic matter. This organic matter is then broken down by microbial activity, especially under favourable conditions of soil moisture, temperature, sunlight and aeration, leading to a sharp increase in *SRR*. The results of the study show that fallow land could emit more than 69 kg CO_2 ha^{-1} d^{-1}, which is significantly higher than the other land-use types. Furthermore, the lower bulk

density in fallow plots (Figure 4.6), as reported by Kumar et al. (2020) and Silva et al. (2011), improves aeration, which enhances microbial access to organic carbon and accelerates the decomposition of organic matter. Consequently, microbial respiration increases, leading to greater CO_2 release. Collectively, these findings show that fallow lands, with their high organic matter content and favourable conditions for decomposition, are significant contributors to *SRR*.

In croplands, particularly in rice fields, the *SRR* was significantly high, although not as high as in fallow lands (Figure 4.7). The distinct environmental conditions in rice fields, characterized by alternating periods of flooding and drought, create a complex dynamic that influences CO_2 release. During flooded periods, rice fields emit primarily methane (CH_4) due to anaerobic decomposition processes. However, during dry periods when the fields are drained, aerobic conditions prevail, leading to increased SRR (Boateng et al., 2017; Mboyerwa et al., 2022). In the current study, the rice fields were rainfed. It is uncertain whether anaerobic conditions persisted throughout the wet season. However, the maximum soil moisture recorded was below 70%, indicating that the soil was not fully saturated, with air-filled pores still present. Full saturation, which occurs at 100% soil moisture, provides ideal conditions for anaerobic decomposition processes, including methanogenesis (Islam et al., 2020). Given the observed moisture levels, it is likely that the soil respiration measured during the data collection period was predominantly due to aerobic decomposition, as oxygen was still available in the unsaturated soil pores, promoting the release of CO_2 over CH_4 (Islam et al., 2020; Kögel-Knabner et al., 2010). In maize plots, the levels of *SRR* were lower compared to fallow lands and rice fields. The highest bulk density (BD) values were recorded in the maize crop land-use, but had the lowest levels of organic matter and nitrogen, and this might have accounted for the reduced *SRR*. High BD soils typically have limited pore space, which restricts aeration and reduces microbial activity, slowing down the decomposition of organic matter and thereby limiting CO_2 production (Franzluebbers, 2002; Todisco et al., 2022). Furthermore, low organic matter and nitrogen content can restrict the availability of microbial substrates, further decreasing *SRR* (Rodrigues et al., 2023).

Forest land recorded the lowest *SRR* among the four land-use types. This could be explained by the role of forests as significant carbon sinks, where the soils maintain

relatively stable organic matter pools. In addition, forest soils typically experience minimal disturbance, resulting in lower bulk density (BD) and higher organic matter content compared to croplands (Hidalgo et al., 2007; Rodrigues et al., 2023). In forest ecosystems, the decomposition of organic matter occurs at a slower rate due to high lignocellulosic content in forest litter, lower temperatures, and the protective effect of the canopy cover (Jandl et al., 2007). The canopy reduces sunlight penetration to the soil surface, limiting microbial activity compared to the more exposed, aerated, and disturbed soils found in agricultural systems (Davidson et al., 2006).

Variation of Carbon Dioxide Across Habitat Types

There were significant differences in soil *SRR* across various habitat types (Figure 4.8). These differences are influenced by vegetation type, soil conditions, and land management practices, with each habitat type exhibiting distinct emission patterns. Since an opaque chamber was used, all observed *SRR* are due to dark respiration, which includes both heterotrophic respiration (from soil microorganisms) and autotrophic respiration (from plant roots), but not photosynthesis (Lambers and Oliveira, 2019).

Fallow grass habitats recorded the highest levels of soil *SRR*, approaching 80 kg CO_2 $ha^{-1}day^{-1}$. This is likely due to a combination of significant root respiration and microbial respiration. Since no light entered the chamber, dark respiration from plant roots contributed substantially to the total *SRR*. Studies by Raich and Tufekcioglu (2000) suggest that grasslands, and this study fallow, have well-established root systems that tend to exhibit higher respiration rates due to both root activity and the decomposition of organic material. Fallow bare soil and rice plant habitats showed similar emissions, slightly lower than those of the fallow grass (Figure 4.8). In the fallow bare soil, *SRR* is primarily driven by microbial activity decomposing organic matter. Rice plants, however, contribute through both root respiration and microbial decomposition. However, the temporary waterlogged conditions in rice fields can create anaerobic zones, thus limiting aerobic respiration and potentially reducing *SRR* compared to drier systems (Islam et al., 2020; Lloyd and Taylor, 1994).

Emissions from rice bare soil were significantly lower than those from fallow habitats but statistically similar to emissions from maize habitats, including maize bare soil and maize plants. This may be attributed to microbial decomposition. Although maize roots contribute to respiration, the overall root biomass and organic inputs are lower than in

perennial systems like fallow grass, which recorded 1.56% and 3.48% of organic matter content, respectively. Moreover, frequent disturbances in maize fields during seeding and pesticide applications can disrupt microbial communities, reducing *SRR* (Ciais et al., 2010). It is also important to note that maize plants were affected by fall armyworms and other herbivores during their vegetative stage, which occurred less than a month after seeding. Moreover, those that survived could not be monitored after 45 to 50 days of planting, as their height and width exceeded the chamber size used for measurements (25 cm diameter and up to 140 cm height). These factors likely explain the similar SRR recorded across the maize habitat types.

Forest soils under canopy cover and canopy gaps displayed the lowest *SRR*, particularly in canopy cover areas. Forest soils generally have slower decomposition rates due to lower temperatures and higher moisture that reduce microbial activity (Subke et al., 2006; Tong et al., 2024). Although more sunlight may stimulate root and microbial activity in the canopy gap, dark respiration measurements suggest that total root biomass may be lower than in open fallow or cropland.

Variation of Carbon Dioxide Across Topography

The results show that topography has a non-significant effect on soil *SRR* ($F = 2.99$, $p = 0.083$). This is even though topography is usually considered to be a critical factor in determining soil moisture, temperature and organic matter distribution. This finding contrasts with earlier research by Davidson and Janssens (2006), who argued that topographical variations, such as slope and elevation, create microclimatic conditions that significantly impact soil carbon cycling and microbial activity. Sloped terrains, for example, may have different moisture retention capacities and erosion patterns, which in turn affect organic matter decomposition rates and *SRR* (Żarczyński et al., 2023). Steeper slopes generally experience greater runoff, leading to reduced moisture retention and possibly lower microbial activity. However, the lack of a significant difference in *SRR* across topography may be due to plot selection which was based on altitude. As shown in Table 4.1, the altitude difference between lowland and highland plots is less than 10 meters on average for both maize and fallow land-use, except in the forest land. In contrast, the forest plots had an altitude difference exceeding 30 meters between lowland and highland plots. This higher altitude variation within the forest plots may explain why significant differences were observed between the forest

topography, while no significant difference was found in maize and fallow topography as captured in (Figure 4.3).

4.8.3 Selection of Models for Predicting Soil Respiration

Soil organic matter (OM) and pH were positively correlated with mean annual *SRR* for the four land-use types (Figure 4.6). Similar observations were reported by Biasi et al. (2005) who demonstrated that higher SOM and optimal pH levels enhance microbial activity, thereby increasing *SRR* through the decomposition of OM. Mo et al. (2007) reported that SOM and pH significantly influence *SRR* by promoting microbial respiration in tropical forest soils. Furthermore, Wang et al. (2021) and Zhang et al. (2016) observed a close link between SOM, pH, and soil *SRR*, as these factors support microbial metabolic processes crucial for CO_2 production across various land-use types.

The results from the stepwise regression analyses revealed a complex interaction between *SRR* and the various soil parameters used (Table 4.5). The mixed models of SM and ST could not explain and predict soil respiration. Although, studies have reported that SM and ST are key factors regulating CO_2 production and emissions from soil surfaces (Anokye et al., 2021; Cui et al., 2020). However, in this study, no strong relationship of *SRR* to SM and ST was observed, with correlation values of 0.26 and 0.16, respectively (Figure 4.9). Similar findings were reported by Manu (2023) based on annual data from forest and cocoa agroforestry systems in Ghana, suggesting that the relationship between *SRR* and these factors may vary depending on temporal scale. Specifically, season and duration of data collection can significantly affect *SRR*. In tropical regions, SM will likely has a stronger influence on this interaction than ST as there is less temperature fluctuation in the tropics (Barry and Chorley, 2009).

Conclusions and Way Forward

The study assessed seasonal variations in soil respiration rates across four land-use types, including forest, fallow, maize and rice in a moist semi-deciduous forest in Ghana. The results reveal that *SRR* were highest in fallow, followed in a decreasing order by rice, maize and forest land-uses, despite the forest having high soil organic matter content. This could be attributed to minimal soil disturbance in forested areas together with the lower sunlight reaching the forest floor. These results underscore the importance of preserving forest reserves and promoting agroforestry systems to mitigate GHG emissions. The study also found that *SRR* from the rice paddies field occurred primarily during aerobic conditions as the soil was not fully saturated to enable anaerobic decomposition to take place which promotes methane emission. Seasonal variability significantly influenced *SRR* across land-use types, with higher emissions recorded during the wet season across all land-use types. However, no consistent relationship was observed between *SRR* and soil temperature or moisture. A regression model was developed using *SRR* and soil physio-chemical properties including soil moisture, organic matter content, pH and silt, which collectively explained approximately 58% of the observed variability in *SRR*.

Future research should investigate the role of additional soil parameters, such as soil microbial biomass carbon and nitrogen, in driving *SRR*. Furthermore, studies should focus on understanding the contributions of soil moisture and temperature to the overall emissions, as their relationships were not established in this study. Expanding the scope of GHG analysis to include methane and nitrous oxide, using advanced tools such as gas chromatographs, is also crucial for a more comprehensive understanding of emissions dynamics across land-use types. These efforts will enhance the design of targeted strategies for managing GHG emissions in tropical ecosystems.

CHAPTER 5 : MODEL-BASED ANALYSIS OF LAND-USE/LAND COVER AND ASSOCIATED SOIL RESPIRATION IN A MOIST SEMI-DECIDUOUS FOREST OF GHANA

Abstract

Tropical forests play a critical role in mitigating climate change by sequestering carbon and providing essential ecosystem services. However, these forests, particularly in the Global South, face significant threats from land degradation driven by land-use changes, such as deforestation, which contribute to carbon emissions. This study projects land-use/land-cover changes in the Bobiri Forest Reserve, a moist semi-deciduous forest, and surrounding areas in Ghana under a business-as-usual scenario, with 2022 as the baseline for projections through 2050, using the Dinamica EGO model. Additionally, soil respiration rate (*SRR*) associated with these land-use changes were estimated using a forest-based regression model. The results reveal that closed forest covers are decreasing at an alarming rate of over 36% as compared with the reference year 2022, while cropland and mixed vegetation and non-vegetated areas are projected to increase by about 20% and 40%, respectively. The model results also showed a potential reduction in the Bobiri Forest Reserve protected area. Regarding future *SRR*, the model achieved R^2 values of 0.97 for both 2022 and 2050, with open forests projected to emit the highest levels of 55 kg CO_2 ha^{-1} d^{-1} by 2050. These findings highlight the importance of managing land-use changes to mitigate CO_2 emissions. Future studies should explore alternative scenarios, such as integrated land management or land degradation scenarios, and compare different modelling approaches using IPCC Tier 1 default values alongside country-specific Tier 2 or 3 emission factors.

Keywords: Land-use/land cover projection, Soil respiration rate, Dinamica EGO, forest-based regression model, Bobiri forest reserve, Ghana, IPCC

5.1 Introduction

Forested landscapes are vital for combating climate change, by sequestering carbon and providing essential ecosystem services that support adaptation and resilience. Conserving these landscapes is therefore a powerful strategy for combating global environmental challenges. In this context, the conservation of tropical forests, particularly in the Global South, has received significant emphasis (Ingalls and Dwyer, 2016). Tropical forests are pivotal in maintaining the Earth's climate system, serving as regulating of solar radiation, driving of hydrological processes, and maintaining of critical biogeochemical cycles. They are also substantial carbon reservoirs, storing approximately 360 pentagrams of carbon (PgC) in their vegetation. It is observed that when combined with the carbon stored in tropical forest soils, this total reaches approximately 800 PgC, an amount nearly equivalent to the total carbon present in the atmosphere (Artaxo et al., 2022).

That notwithstanding, tropical forest systems face severe degradation from anthropogenic drivers. This degradation has profound impacts on global carbon and hydrological cycles, threatens biodiversity on a massive scale, and undermines the livelihoods of communities that depend on these forests (Gibson et al., 2011). Among the primary drivers of tropical forest degradation are land-use/land-cover changes (LULCC), wood extraction, hunting, atmospheric alterations, and climate change. LULCC emerges as the most significant driver, with wide ranging consequences (Wright, 2010). Particularly the conversion of forests to non-forest areas through deforestation, due to the expansion of cropland, are estimated to be the largest contributor to global carbon emissions (Houghton et al., 2012).

Advancements in land-use modelling offer a powerful instrument for understanding the processes driving LULCC by analysing a wide range of socioeconomic, policy and environmental factors (Cheng et al., 2020). In addition to analysing historical developments, these models offer the possibility to simulate alternative future development pathways in the form of scenarios and test the stability of interconnected ecological systems, facilitating the development of robust scenarios to address the complexities of land-use systems. Such approaches have significantly advanced applications in land-use planning, optimized land resource allocation and improved natural resource management (Maeda et al., 2010).

Numerous models used for simulating LULCC are now available, generally categorized into two types; quantitative and spatial structure projection models (Boajie et al., 2018). Quantitative models, such as the Grey Model, Markov Chain, System Dynamics and Artificial Neural Networks, focus on numerical forecasts. Spatial structure projection models, including Multi-Agent and Cellular Automata approaches as well as advanced modelling frameworks such as CLUE-S, SLEUTH, and Dinamica EGO, go further by dynamically visualizing land-use changes, providing valuable insights into spatial patterns of change (Cheng et al., 2020; Rodrigues and Soares-Filho, 2018).

Despite advancements in geospatial technologies, land-use transitions and forest loss in many forest reserves across Ghana persist at an alarming rate (Dembélé et al., 2024). This ongoing degradation is closely linked to declines in biodiversity and critical ecosystem functions, such as carbon sequestration. Key drivers of this pressure include population growth, agricultural expansion, urban development, and shifting lifestyles, all of which intensify the pressure on limited land and natural resources (Dembélé et al., 2024). Model-based scenario analysis provides valuable information on the functioning of the observed land-use system as a basis for designing integrated land management systems that balance current and future land-use demands for different purposes (e.g. food, carbon storage and nature protection) effectively (Wolff et al., 2020).

Dinamica EGO modelling framework was employed to simulate land development scenarios within the Bobiri Forest Reserve (BFR) and forest fringe areas. Dinamica EGO is a versatile tool capable of constructing various environmental simulation models, including complex spatial dynamic models (Rodrigues and Soares-Filho, 2018). The framework has been widely applied in numerous studies, addressing diverse topics such as deforestation, urban growth, and both agricultural expansion and abandonment (Cheng et al., 2020; Maeda et al., 2010).

Building on a historical land-use map (LUM) in and around the BFR, this research focuses on projecting future LULCC of the BFR and its surrounding environs in the semi-deciduous forest zone in Ghana for the year 2050 under a business-as-usual (BAU) scenario and estimates the associated soil CO_2 emissions resulting from these projected LULCC. The choice of 2050 as the projection year aligns with global climate goals, including the Paris

Agreement, which targets carbon neutrality by mid-century to limit global warming to 1.5 ℃ (IPCC., 2018). Additionally, it also corresponds with Ghana's Nationally Determined Contributions (NDCs), which prioritize sustainable land management and emissions reductions (Republic of Ghana, 2021). Furthermore, this timeline supports the evaluation of how current land management practices align with the Sustainable Development Goals (SDGs), particularly Goal 13 on climate action. The BAU scenario provides an exploratory pathway to assess potential future impacts, based on historical trends in the region (Wolff et al., 2020). Its assumptions are informed by a comprehensive review of studies supplemented by focus group discussion and quantitative interviews conducted with farmers in the region (Boateng, 2023; Dembélé et al., 2024; Djagbletey et al., 2018).

5.2 Materials and Methods

5.2.1 Description of the Study Area

Located between latitudes 6◦ 33′ 15″ and 6◦ 48′ 85″ N and longitudes 1◦ 25′ 95″ and 1◦ 11′ 35″ W, with a land area of approximately 853.42 km^2. The study was done within the protected area of the Bobiri Forest Reserve (BFR) and its surrounding environs as seen in Figure 5.1., in the moist semi-deciduous forest zone of Ghana.

The BFR is over 54 km^2 (Dembélé et al., 2024; Hall, and Swaime, 1981) (Figure 5.1) and is surrounded by the communities of Kubease, Akuokrom, Bomfa, Duampopo, Hwereso, Konongo, New Koforidua, Nobewam, Odumasi, Lowcost, Besease, Donaso, Boankra and Edwenase in the Ejisu Municipality of the Ashanti Region. The reserve is divided into management units that include a butterfly sanctuary, a research site, and a production area. These units collectively support production, tourism, research and conservation functions (Djagbletey et al., 2018).

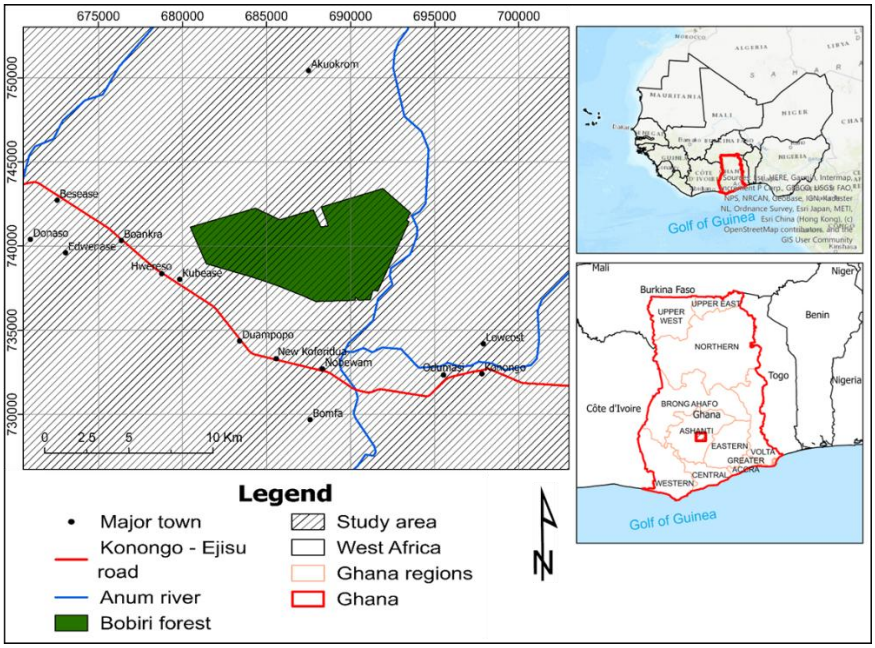

Figure 5.1. Location of the study area: the Bobiri Forest Reserve (BFR) and its surrounding environs located in the Ashanti region of Ghana (Chapter 3)

5.2.2 Satellite Imagery and Processing Landsat

Remote sensing, GIS techniques, and the Dinamica – EGO modelling software were combined to assess drivers of LUC in the study area and to simulate future land-use scenarios (Garcia et al., 2007).

The modelling process was based on two historical images for the years 1986 and 2022 developed by Dembélé et al. (2024). The overall accuracies and kappa statistics of these maps were 96%, 93%, and 0.94, 0.89, respectively. These images are shown in Figure 5.2 (a) and (b), the classification details for the land-use categories are provided in Table 5.1. Additional information regarding the map processing, classification methodology and accuracy assessment can be found in Dembélé et al. (2024) (Chapter 3).

The land-use/land cover maps for 1986 and 2022 were reclassified to distinguish the protected area of Bobiri Forest Reserve (BFR) from the other closed forest areas with similar vegetation cover. This resulted in five land-use classes including Closed Forest, Open Forest, Cropland mixed vegetation and non-vegetated area and Protected area. The reclassification was performed using the "Reclassify Selective Areas" tool in ArcGIS Pro. The land-use/land cover maps (Figure 5.2a and 2b) and the reclassified maps (Figure 5.2c and 2d) illustrate these modifications.

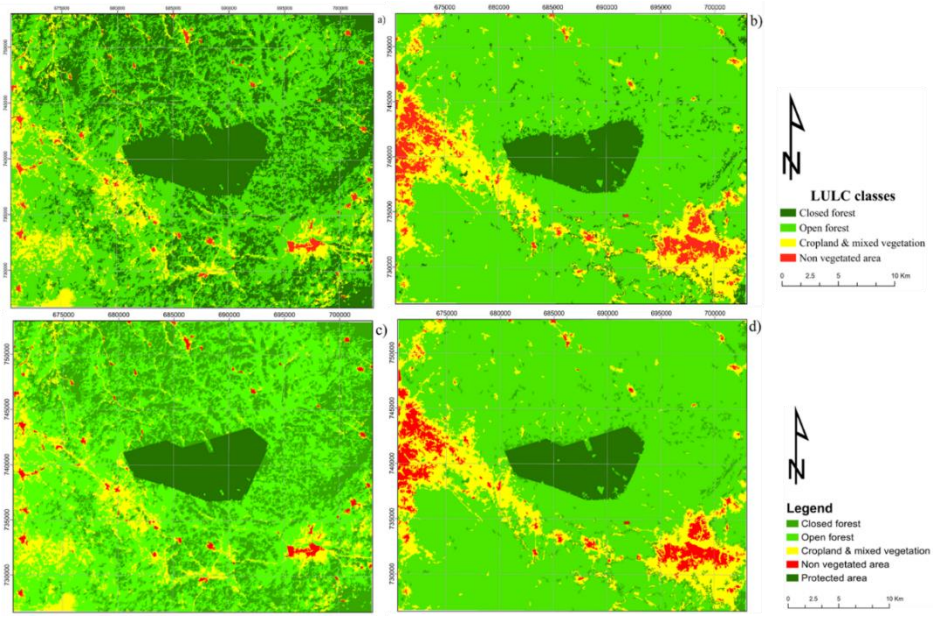

Figure 5.2. Land-use land cover maps a and b are the respective 1986 and 2022 maps and c and d are the reclassified maps (Dembélé et al., 2024)

Table 5.1: Definition of the LULC classes

Land categories	Definitions	Sources
Closed Forest	This encompasses all land with woody vegetation meeting the thresholds for forest land as defined in the national GHG inventory. It also includes vegetation systems currently below the following criteria: - Minimum Mapping Unit (MMU): 1.0 ha - Canopy cover (CC): > 65 % - Potential to reach a minimum height of 5 m at maturity (in situ).	(EPA, 2019; Koranteng, Adu-poku, et al., 2017)
Open forest	This includes perennial crops i.e., oil-palm and cocoa plantations, Orange and fallow areas with similar characteristics. These areas are not classified as Cropland and fall below the forest land threshold values based on the FAO definition in Ghana:	(EPA, 2019)

	Canopy cover: < 60 %, Height: ≤ 5 m, MMU: > 0.5 ha	
Croplands and mixed vegetation	This includes annual and biennial croplands such as mono and mixed-cropped farms of cassava, maize, plantain, rice, and similar recent fallow areas with comparable vegetation characteristics.	(EPA, 2019)
Non-vegetated areas	This comprises of Cities, towns, villages, and bare areas, rivers, ponds, and lakes.	(EPA, 2019; Hackman et al., 2017)
Bobiri Forest Reserve (BFR)	Represents the boundary of the protected area of BFR, which contains both closed and open forests	(Dembélé et al., 2024)

5.3 The Modelling Process

In this study, two spatially explicit modelling tools were combined and adapted to the case study region. The first model was Dinamica-EGO for calculating spatially explicit projection of LULCC dynamics until 2050. Building on the generated LUMs, a machine learning modelling approach was employed in ArcGIS Pro version 3.0 to estimate the spatial distribution of soil respiration resulting from LULCC (Esri, 2023).

5.4 The Dinamica EGO Model

Dinamica EGO is an integrated object-oriented geographic modelling software developed in C++ and Java. It functions as a spatial-dynamic model capable of simulating both the numerical and geographical allocation of LULCC, influenced by various environmental, socioeconomic and political factors (Cheng et al., 2020; Shehzad et al., 2014). The model operates on the cellular-automata fundamentals and characteristics (Feng, 2017).

The modelling process relies on LUMs from two selected years 1986, representing the initial landscape, and 2022, the final landscape. These maps capture historical land-use transitions in the study area and provide a foundation for future scenario projection. Key steps in this process include calculating the land-use transition matrix and transition probabilities, calculating the weight of evidence coefficients, setting transition rules,

calibrating internal parameters and model projection (Cheng et al., 2020). The workflow for this modelling process is illustrated in Figure 5.3.

5.5 Model Setup and Calibration

i. Calculation of the Land-use Transition Matrix

The transition matrix is a square matrix that describes changes between different land-use categories in the system within a given period in this case, between 1986 and 2022. Transition volumes represent the cumulative percentage of all variables from the previous time step. The single-step matrix (P) represents the ratio of land-use changes to its categories in the initial year. When divided into multiple time steps (n), the relationship between the multiple–step transition matrix (P_t) and P is given as:

$$P = (P_t)^n \quad (5.1)$$

In the simulation process, multiple-step matrices allow for the incorporation of factors such as policy changes, natural events, or other variables influencing land-use transitions over different periods, thereby controlling land-use transition rates (Clark et al., 2010).

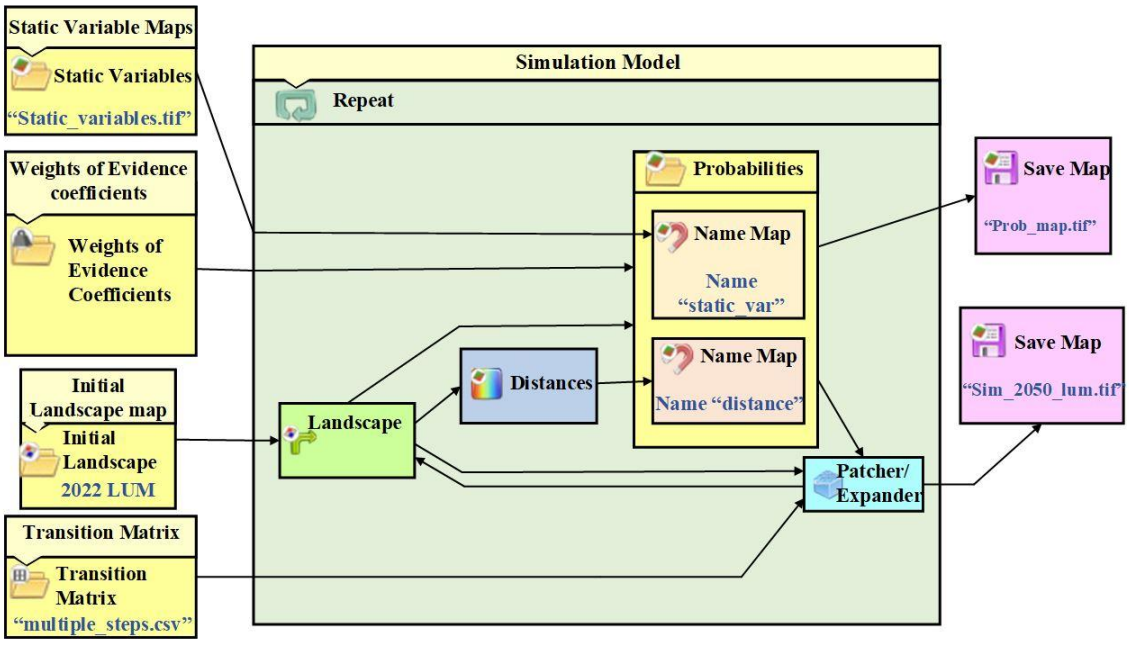

Figure 5.3: Workflow of the Dinamica EGO (Environment for Geoprocessing Objects) modelling process (Soares-Filho et al., 2002). The flowchart shows the key steps involved in simulating land-use changes, including the integration of static variable maps, weights of evidence coefficients, transition matrices and initial landscape maps. Outputs include the probability map and the final simulated LULC map.

A multiple-step matrix used in the simulation to incorporate annual changes within the study period (1986 – 2022), allowing for a more accurate representation of the temporal dynamics. Details of the transition matrix are presented in Table 5.2.

ii. Calculation of Transition Probability

The transition probability in Dinamica EGO quantifies the likelihood that a driving factor will cause a change in a specific land-use type. Driving factors are categorized into two types; dynamic variables, which change as the cell states evolve during the iterative simulation process, and static variables, which remain constant throughout the simulation. The model processes a set of raster data cubes as inputs and generates new raster outputs. For this study, the static variables were selected based on data availability and include the following; Digital Elevation Model (DEM), slope, relief, shading, aspect and proximity to roads.

These static variables were derived from the 30-meter Shuttle Radar Topography Mission (SRTM-1) dataset, obtained from the NASA EarthData platform(https://www.earthdata.nasa.gov/sensors/srtm).

The dynamic variables include data related to the distances to closed forest, open forest, cropland and mixed vegetation, non-vegetated areas and protected area. These variables are updated during the iterative modelling process to reflect spatial changes in land-use types. This ensures that the simulation accounts for temporal dynamics and interactions among the various land-use categories.

Table 5.2: Multiple-step transition matrix from 1986 to 2022

From*	To*	Change rate (%)
Closed forest	Open forest	0.1024173
Closed forest	Non-vegetated area	0.0002732
Open forest	Closed forest	0.0023968
Open forest	Cropland and mixed vegetation	0.0075938
Open forest	Non-vegetated area	0.0003109
Open forest	Bobiri Forest Reserve (BFR)	0.0000096
Cropland and mixed vegetation	Closed forest	0.0049764
Cropland and mixed vegetation	Open forest	0.0209342
Cropland and mixed vegetation	Non-vegetated area	0.0073218
Non-vegetated area	Cropland and mixed vegetation	0.0183925
Bobiri Forest Reserve (BFR)	Open forest	0.0008792

iii. Weights of Evidence Calculation

The Dinamica EGO software applies the Weights of Evidence (WoE) method, a statistical approach based on Bayes' theorem, to determine the change probabilities. This method evaluates the influence of spatial variables on land-use transitions independently, without accounting for interactions among variables in the combined solution (Agterberg, 1992; Bonham-Carter, 1994; Cheng et al., 2020; Soares-Filho et al., 2002). To determine the prior probability of a land-use change event ($P(D)$), the study site is divided into $N(T)$ cell units,

where D represents the land-use change event to be projected, and $N(D)$ denotes the number of cells undergoing LULCC. The prior probability of LULCC is calculated as:

$$P(D) = \frac{N(D)}{N(T)} \quad (5.2)$$

This calculation provides the baseline probability of a land-use transition occurring before incorporating the effects of spatial variables. The WoE method then refines this probability by calculating the weights associated with the presence or absence of specific evidence factors, enable a robust spatial analysis of LUC dynamics (Cheng et al., 2020).

The odds ratio, $O(D)$, quantifies the probability of a LUC event (D), occurring relative to it not occurring, expressed as:

$$O(D) = \frac{P(D)}{1-P(D)} \quad (5.3)$$

The driving factors of LUCs were treated as evidence factors, where B represents the presence of a specific evidence factor and $\bar{B}$ its absence. The weight of evidence (W^+) area calculated using the following formulas:

$$W^+ = \ln \frac{P(B/D)}{P(B/\bar{D})} \quad (5.4)$$

$$W^- = \ln \frac{P(\bar{B}/D)}{P(\bar{B}/\bar{D})} \quad (5.5)$$

Where:

D: represents the event that a predicted LUC occurring;

$\bar{D}$: represents the event that a predicted LUC not occurring;

B: represents the presence of the evidence factor;

$\bar{B}$: represents the absence of the evidence factor.

The contrast (C) defined as: $C = W^+ - W^-$. The contrast measures the relationship between the presence of event D and the evidence factor B . If C is close to zero, the factor has little or non-existent influence on LUC.

When multiple evidence factors $(B_1, B_2, \ldots B_m)$ independently affect the occurrence of event D, the combined odds ratio can be expressed as:

$$\ln O(D|\, B_1 \cap B_2 \ldots \cap B_m) = \sum W^+ + \ln O(D) \quad (5.6)$$

The posterior likelihood of a change from land-use type i to j, given the presence of all specific under the condition that all specific evidence factors $B_1, B_2, \ldots B_m$ at a location (x, y), is calculated using the logistic function:

$$P(i \Longrightarrow j|B_1 \cap B_2 \ldots B_m) = \frac{e^{\sum W^+}}{1+e^{\sum W^+}} \quad (5.7)$$

The logistic function ensures that the probability value remains within the range between 0 and 1.

Continuous variables such as elevation, slope and distance are categorised using a method developed by Goodacre et al. (1993). This method assumes that spatial correlations remain consistent over short distances. Each category is assigned a weight, quantifying its influence on LUCs (Soares-Filho et al., 2002).

The Cramér's V test and Joint-Uncertainty information are utilised to evaluate the independence of each driving factor, which is a critical assumption for the WoE method (Bonham-Carter, 1994). These tests evaluate the degree of correlation between driving factors to ensure they do not introduce redundancy or bias into the model.

The analysis revealed a strong correlation between the DEM and Relief variables across most land-use transitions. Based on Cramér's coefficient, the relief variable was identified as redundant and subsequently excluded from the model. This step ensured that the remaining driving factors were independent, thereby enhancing the robustness and accuracy of the WoE analysis.

iv. Setting Model Transition Rules and Calibration of Internal Parameters

In the Dinamica-EGO model, transition rules define how cell states change during the simulation process. The expansion pattern of cells is influenced by several key factors, including cell diffusion rules, patch size, patch standard deviation, and the isometric coefficient, among others. The model utilizes two primary cell transition functions namely Expander and Patcher (Chadid et al., 2015; Soares-Filho et al., 2002).

The Expander function facilitates the growth of existing land-use patches by expanding into adjacent cells. This is particularly useful for simulating scenarios where established land-use areas, including agricultural fields or urban zones, gradually grow outward into nearby

areas. In contrast, the Patcher function creates new patches by generating "seeds" and growing them into cohesive clusters. This mechanism is critical for simulating the formation of new patches in the landscape (Soares-Filho et al., 2002). By leveraging these functions, the model can replicate the LUC dynamics, balancing area expansion with the emergence of new areas.

v. Model Projection and Validation

The Dinamica-EGO model uses algorithms to project LUCs by scanning the initial LUM to identify cells with the highest likelihood of transition. These cells are organised into a ranked data array. From this array, cells are randomly selected from top to bottom, with the degree of randomness controlled by an adjustable stochastic selection mechanism. This mechanism allows the simulation to vary between deterministic and stochastic behaviour, enhancing its adaptability to different scenarios (Cheng et al., 2020; Soares-Filho et al., 2002).

In the final step, the selected transitions are implemented on the LUM, updating the spatial configuration of land-use. The initial calibration parameter in the simulation is the percentage of change assigned to each of the two transition functions, i.e., Expander and Patcher. The Expander function facilitates the growth of existing patches, making it particularly suitable for scenarios where landscape changes predominantly involve the expansion of established areas. In contrast, the Patcher function generates new patches by growing "seeds", it is used when new patch formation is a key feature of the landscape dynamics (Chadid et al., 2015; Soares-Filho et al., 2002).

Following the calibration of these percentages, the next step involves specifying the mean and variance of the new patch sizes. These parameters can be configured independently for both the Expander and Patcher functions, allowing for precise modelling of land-use dynamics. Additionally, the model incorporates the Patch Isometry parameter, which influences the shape of patches. A high value indicates compact and cohesive patch formations, while lower values result in more fragmented and irregular patch shapes (Soares-Filho et al., 2002).

vi. Validation of the Simulated Land-use Map

The validation of the simulated LUM involves an iterative calibration process to ensure the model accurately represents the observed land-use dynamics. Initial parameter values including mean patch size, variance and Patch Isometry are set based on the guidelines provided by Dinamica (2024) on the pattern of change and empirical knowledge derived from previous research conducted within the study area (Boateng, 2023; Dembélé et al., 2024; Djagbletey et al., 2018).

The calibration process begins by running the model using the 1986 LUM as a starting point to simulate the 2022 land-use scenario. The resulting simulated map was then visually compared to the reference 2022 LUM. In cases where discrepancies between the simulated and reference maps are observed, parameter values are adjusted. This iterative process aimed to enhance the model's ability to replicate the spatial patterns observed in the reference map (Hagen, 2003). The calibration was repeated iteratively, with parameter adjustments after each simulation, until the simulated map was closely aligned with the reference map. This alignment is illustrated in Figure 5.4. In Figure 5.4 (b), colours approaching 1 (red and dark areas) indicate strong similarity with the reference map, whereas, colours close to 0 (blue areas) represent discrepancies between the simulated and reference maps.

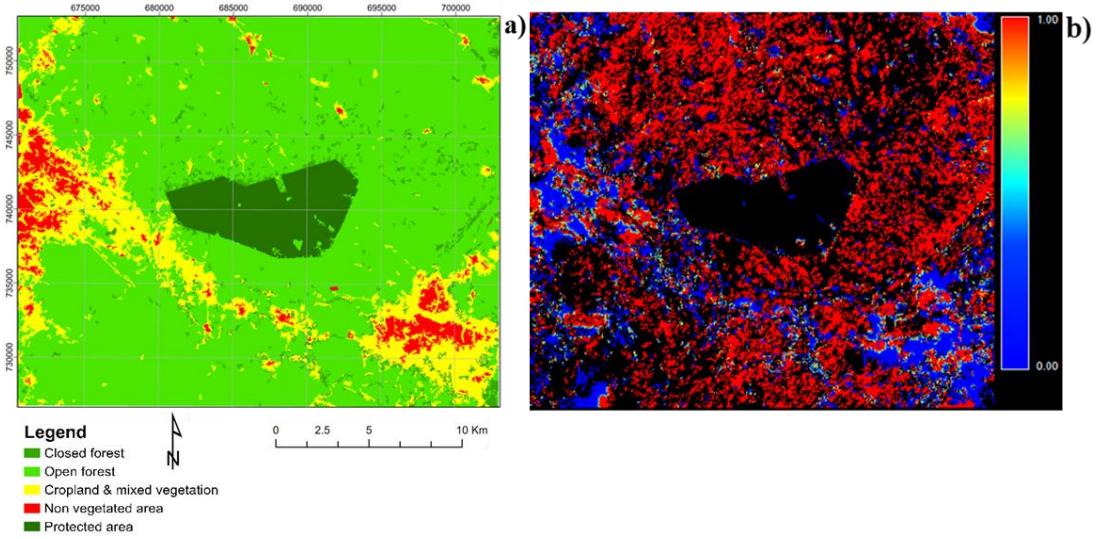

Figure 5.4: Calibration of the model to simulate the 2022 image. Panel (a) represents the reference 2022 and (b) shows the simulated 2022 image. The colour scale in panel (b) indicates the degree of similarity between the simulated and reference maps.

5.6 Modelling Soil Respiration Rate using Forest-based Regression Model in ArcGIS Pro

The Forest-based Regression tool in ArcGIS Pro uses the Random Forest algorithm to predict continuous outcomes based on input features. In regression, the model is trained using predictor variables including land-use types, and a continuous response variable, namely soil CO_2 emission (Breiman, 2001). The Random Forest algorithm constructs multiple decision trees, each based on random subsets of the training data and predictor variables and aggregates the outputs of these trees to produce a robust and accurate prediction. This ensemble approach minimises overfitting and improves the model's ability to handle complex, non-linear relationships between predictor variables and the response variable (Cutler et al., 2007).

Once trained, the Random Forest regression model is used to predict the response variable for new or unseen data, such as projected future LUMs (Liaw and Wiener, 2002). The model generates continuous values, which makes it versatile for predicting CO_2 emissions (Georgiadis and Wang, 2021). One of the key advantages of Random Forest regression is its ability to handle a large number of predictors while capturing complex interactions between them. Additionally, it is well-suited for managing missing or noisy data, which is often a challenge in geospatial analyses involving environmental datasets (Liu et al., 2018). These strengths make Random Forest an effective method for modelling soil CO_2 emissions and understanding their relationship with LUCs.

5.6.1 Forest-based Regression Model Parameterization in ArcGIS Pro

To optimise the performance of the random forest regression model, several key parameters were configured during the training process. One of the most important parameters is the number of trees, which was set to 100 trees as a default value. This parameter determines the number of decision trees created in the forest model. While increasing the number of trees typically improves model accuracy, it also increases computational time, requiring a balance between predictive accuracy and computational efficiency (Breiman, 2001). Typical values for the number of trees range between 50 and 100, although higher values may be used if sufficient computational resources are available (Cutler et al., 2007).

Another important parameter is the maximum tree depth, which controls how deep the decision trees can grow. A deeper tree can capture more complex relationships between predictor variables and the response variable, but also increases the risk of overfitting (Liaw and Wiener, 2002). A maximum tree depth was set to 5 as the land-use types that are used as predictor variables are not many. In practice, a typical value for maximum depth ranges between 5 and 20, depending on the dataset's complexity. Additionally, parameters such as minimum samples per leaf and number of features per split, which control the complexity and randomness of the trees were left at their default values. These parameters ensure that each leaf node contains a minimum number of data points and restrict the number of features to be considered for each tree split, reducing the likelihood of overfitting and maintaining diversity among trees in the forest (Georgiadis and Wang, 2021). The model parameters were fine-tuned through a trial and error-process to achieve optimal performance while balancing accuracy and computational efficiency (Liu et al., 2018).

5.6.2 Land-use Land-cover Scenario Development and Assumptions

Land-use change is a process that is influenced by demands multiple spatial scales. In an increasingly interconnected world, decisions made at one spatial scale can have effects at other spatial scales, leading to feedback on land-use decisions and trade-offs for the well-being of people and nature. In Ghana, the dynamics of LUC are expected to be driven by increasing demand for food and fibre as a result of population growth (Meyfroidt et al., 2013; Wolff et al., 2020). The case study region, the protected area of the BFR and its environs, is no exception to these changing dynamics. Historical data reveals significant LULCC in the region between 1986 and 2022. During this period, closed forest (CF) cover declined by more than 88%, while the protected area (PA) decreased by about 2.3%. Simultaneously, non-vegetated (NV) areas, open forest (OF) and cropland mixed vegetation (CMV) increased to over 283%, 36% and 31% respectively (Dembélé et al., 2024).

Given these historical trends, a future projection for 2050 was made using the business as usual (BAU) scenario based on the observed trends from 1986 to 2022. Under this scenario, some changes are expected in the land-use trends observed between 1986 and 2022 in the BFR and its environs. Population growth and the increasing demand for agricultural

produce are expected to drive LULCC, resulting in continued deforestation and land conversion. Closed forest cover is projected to decline further, potentially exceeding the historical 88% reduction. The PA of BFR may experience a moderate decrease in the forest cover similar to the 2.3% reduction observed in previous decades. Conversely, NV areas, OF and CMV are expected to see substantial increases, likely exceeding the rates of expansion recorded in the past. These changes are likely to exacerbate biodiversity loss, habitat degradation, and carbon emissions in the region (Dembélé et al., 2024).

Although the focuses on one BAU scenario, participatory processes were incorporated into the validation of the scenario assumptions to align projections with local realities and stakeholder input. These processes included qualitative focus group discussions, quantitative surveys and expert consultations. In 2022, focus group discussions were conducted in Kubease and Krofrom, engaging 15–20 participants per community, including smallholder farmers and community leaders, with diverse representation across gender and age groups. Discussions explored topics such as climate change perceptions, farming conditions, adaptation strategies and barriers to technology adoption. These qualitative insights offered a nuanced understanding of how socio-economic and environmental changes are experienced at the local level.

In 2023, a structured quantitative survey involving 159 respondents from the same communities was conducted using simple random sampling. The survey assessed climate change awareness, its impacts on crop yields, and the adoption of climate-smart agricultural practices. Together with expert consultations involving forestry professionals from the Forestry Research Institute of Ghana and other organizations, these data ensured that the BAU scenario reflects not only historical trends but also local realities and expert knowledge.

By integrating these participatory processes into the BAU scenario, this study captures both top-down policy perspectives and bottom-up community concerns, providing a robust framework for projecting future land-use patterns in the BFR and its environs. While additional scenarios, such as integrated land management or participatory policy interventions, will be explored in other studies, this approach lays the foundation for

aligning projections with sustainable development goals and resource management strategies.

5.6.3 Assumptions for Projecting Soil Respiration Rate under the BAU Scenario

In the forest-based regression modelling process, three land-use types (LUTs) were used as predictors for soil respiration rates namely; closed forest, open forest and cropland and mixed vegetation. Soil respiration data were collected from June 2023 to June 2024 from 14 plots evenly distributed among the LUTs, with 4 plots each for closed forest, open forest and 6 plots for cropland and mixed vegetation. This sampling strategy ensured balanced representation across the LUTs, providing a robust dataset for capturing variations in soil respiration rate specific to each land-use type. It is important to note that the SRR dataset used in this study only accounted for net CO_2 emissions, with no consideration of CO_2 uptake.

To project *SRR* across the study area under the Business-as-Usual (BAU) scenario, the model assumes that the *SRR* data from the sampled plots accurately represent the average variation across the entire study area. Additionally, since the LULC map was developed for 2022 and *SRR* data were collected between June 2023 and June 2024, it is assumed that land-use patterns did not change significantly during this period, which allows the model to use the 2022 LUM to estimate *SRR* for both 2022 and the projected 2050 LUMs.

This assumption is fundamental for scaling plot-level measurements to the broader landscape, particularly in areas where direct *SRR* data are not available. By relying on the representativeness of the sampled data, the model can estimate emissions across the entire study area while accounting for the spatial and ecological heterogeneity inherent in the different LUTs.

This approach ensures that the model provides a comprehensive and practical framework for predicting future *SRR* under the BAU scenario. It captures the interplay between land-use dynamics and emissions trends, offering valuable insights into the potential outcomes of maintaining current land-use practices in the study area.

5.7 Results and Discussion

This section presents the validation of the calibrated model, the 2050 LULC projections derived from the BAU scenario, and the estimated *SRR* resulting from the projected 2050 LUM. The validation of the simulated map was conducted first to ensure the model's accuracy before proceeding with the future projection and subsequent emissions estimation.

5.7.1 Validation of the Calibrated Model

The LUM was analysed using pairwise comparisons with maps of differences; (i) between the initial 1986 LUM and a simulated 2022 map, and (ii) between the initial 1986 LUM and the reference map (2022). This assessment addresses two key issues. First, an overall two-way similarity measure was applied to the entire map by analysing one type of change at a time, regardless of the total number of cells across different categories. Second, this method eliminates the inherited similarity between the initial and simulated maps by excluding the null cells in the total count, ensuring a precise evaluation of the transitions (Almeida et al., 2008). This validation approach is useful for comparing maps that may not match perfectly on a cell-by-cell basis but exhibit similar spatial patterns within localised neighbourhoods (Soares-Filho et al., 2002).This method uses a similarity index (FSI), calculated within a gradually expanding window (Hagen, 2003) as illustrated in Figure 5.5. The FSI results indicated that the simulated 2022 map achieved a spatial fit of over 65% at the highest resolution of 1m. As the window size increased to 11 m, the fitting improved to over 80%. These results align with the recommended FSI thresholds: at least 50% for the 1m resolution and a minimum 80% for the 11m resolution (Almeida et al., 2008; Hagen, 2003; Soares-Filho et al., 2002).

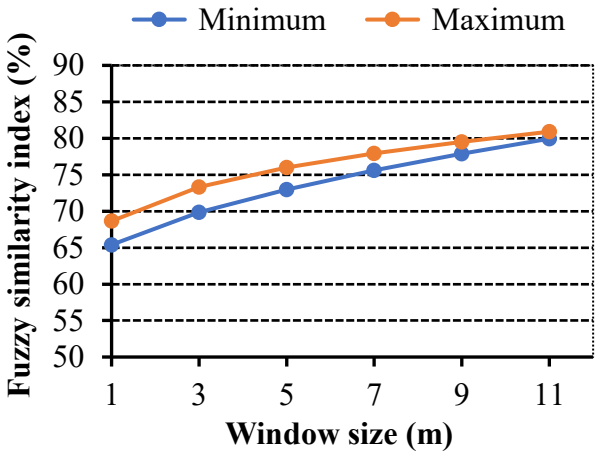

Figure 5.5: Fuzzy similarity indices calculated for different window sizes during the model fitting evaluation. The minimum and maximum FSI values are plotted against window sizes. The results indicate a spatial fit of over 65% at the highest resolution (1m) and over 80% as the window size increases to 11m. using multiple-size windows obtained in the model fitting evaluation.

Since Dinamica EGO is a stochastic model, the final model was run 20 times to account for uncertainties in the spatial distribution of LULC classes. The map statistics from the simulated 2022 LUM were compared with the reference map statistics to estimate the percentage deviation of each land-use land cover class (Soares-Filho et al., 2002). The maximum deviation observed was approximately 11.75% across all LULC classes, with the largest deviation occurring in the closed forest class. This indicates that the model underestimated the closed forest area by about 11% compared to the reference year. The LULC classes of open forest, non-vegetated areas, and the protected area of the Bobiri forest reserve were all slightly underestimated, with deviations of -1.39%, -1.15% and -0.45% respectively. Conversely, the cropland mixed vegetation class was overestimated by approximately 10.49% when compared to the reference 2022 map (Table 5.3).

Table 5.3: Comparison of area statistics for LULC classes map in the reference year 2022 and the simulated map

LULC	CF	OP	CMV	NVA	PA-BFR
Area 2022 reference map (ha)	2,806.20	62,029.62	11,961.81	3,213.27	5,293.98
Area 2022 simulated map (ha)	2,476.44	61,164.9	13,217.04	3,176.37	5,270.13
% deviation	-11.75	-1.39	10.49	-1.15	-0.45

CF: Closed forest; OP: Open forest; CMV: Cropland and mixed vegetation; NVA: Non-vegetated area; PA-BFR: Protected area of Bobiri forest reserve

5.7.2 Projection of 2050 under the BAU Scenario

The model, calibrated with the 2022 LUM as the baseline, was employed to simulate the land-use pattern for 2050 under the BAU scenario. This scenario assumes that current land-use trends and practices will continue without intervention. The resulting projection, as illustrated in Figure 5.7c, highlights potential landscape changes that may occur if these trends persist.

Table 5.4: Statistics of the projected 2050 land-use map

LULC 2050	Area (ha)	% change from 2022 LUM
Closed forest	1,775.52	36.73
Open forest	59,357.79	4.31
Cropland and mixed vegetation	14,449.59	-20.80
Non-vegetated areas	4,538.07	-41.23
Protected Area of Bobiri Forest Reserve	5,183.91	2.08

The results presented in Figure 5.6c and Table 5.4 indicate a continuous decline in closed forest (CF) areas, with an approximate deforestation rate of 37% projected over 28 years period between 2022 and 2050. Both open forest (OF) and the protected area of Bobiri forest reserve (PA-BFR) also exhibit reductions in forest cover, with change rates change rates of 4.31% and 2.08%, respectively. The reduction in forest cover within the PA-BFR forest aligns with previous findings by Dembélé et al. (2024), who emphasised the need for

policy measures to safeguard the BFR zone and its buffer areas. Such measures are essential to prevent biodiversity loss, forest cover depletion and land degradation. However, the projected scenario underscores the consequences of insufficient policy action. Conversely, non-vegetated area (NVA) and cropland and mixed vegetation (CMV) showed considerable expansion, with projected increases of approximately 20.8% and 41.2%, respectively. The increase in CMV could be attributed to Ghana's rising population levels, as reported by the Ghana Statistical Service (GSS, 2021) and the United Nations population prospects for Ghana (UN, 2022). This growing population is expected to drive increased demand for agricultural products to meet food security requirements, contributing to the expansion of CMV in the study area.

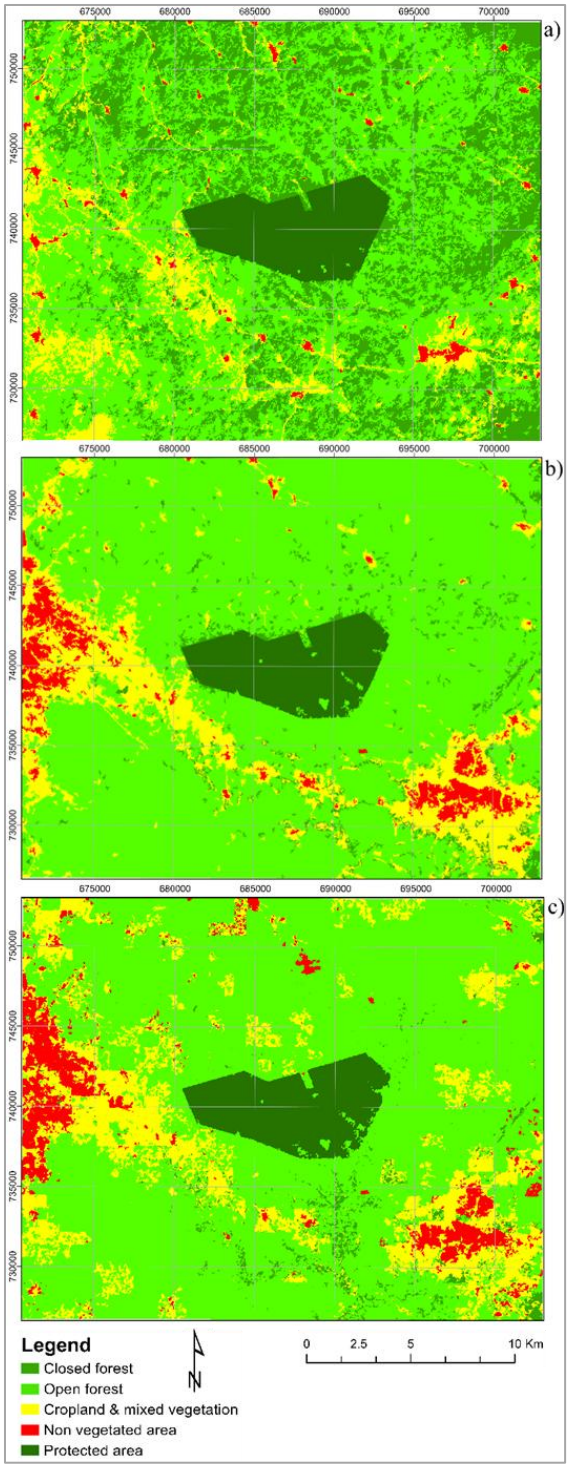

Figure 5.6: Land-use maps for the initial landscape 1986 (a), the final landscape 2022 (b) and the projected landscape for 2050 under the Business-as-Usual scenario (c). The maps illustrate the spatial distribution of land-use categories, including closed forest, open forest, cropland and mixed vegetation, non-vegetated areas, and the protected area of the Bobiri Forest Reserve.

5.7.3 Estimation of Soil Respiration Rate Resulting from the Projected LUM

The forest-based regression model predicted the spatiotemporal evolution of SRR from 2022 to 2050 (Figure 5.7). The model achieved a coefficient of determination (R^2) value of 0.97 for the predicted *SRR*, indicating that it is suitable for being applied for regional analysis both the 2022 LUM and the projected 2050 LUM, as shown in Appendix 6. This high R^2 value suggests that the model effectively captures the relationship between land-use patterns and *SRR*, providing high predictive accuracy for future projections.

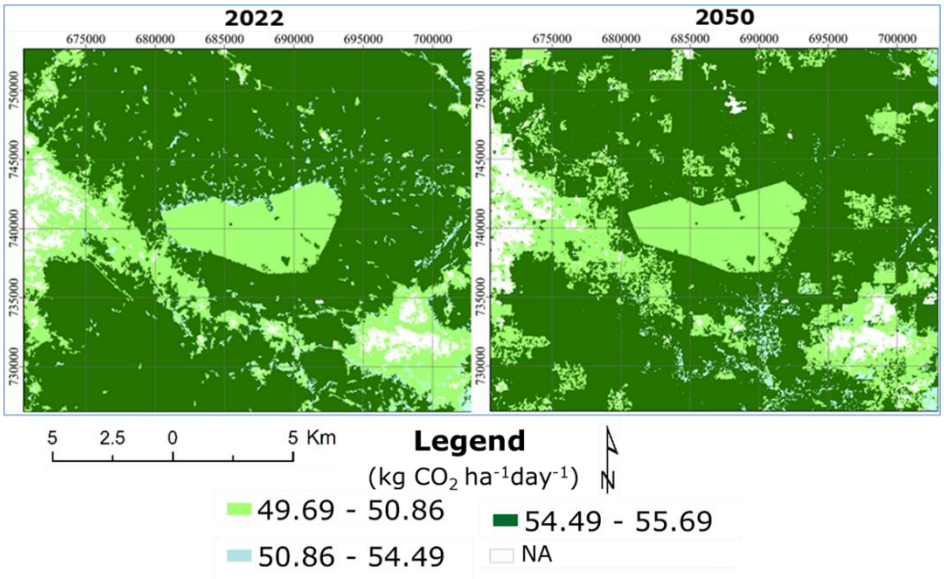

Figure 5.7: Predicted soil respiration rate (kg CO_2 $ha^{-1}day^{-1}$) for the years 2022 (a) and 2050 (b) based on the forest-based regression model. The maps illustrate spatial variations in emissions, with darker green shades representing higher *SRR*. The legend indicates emissions range from the highest to the lowest. NA areas correspond to regions with no available data.

The current and projected land-use and *SRR* data spanning from 2022 to 2050 were used to determine the relationship between land-use patterns and *SRR* across different land-use categories.

The predicted 2022 *SRR* map (Figure 5.7a) shows the spatial variation of *SRR*, with lighter green shades indicating lower emissions and darker green areas representing higher emissions. White areas, labelled as “not available” (NA), correspond to areas where no data was collected and align with the non-vegetated areas in Figure 5.6b and 6c. The colour scale highlights areas with emissions below 50.89 kg CO_2 $ha^{-1}day^{-1}$ are coloured in light

green, emissions between 50.89 and 52.09 in medium green, and those exceeding 52.09 but not more than 55.69 in darker green. The darker green tones are predominantly associated with open forest areas, fallow lands or vegetation with similar vegetation structures as shown in Appendix 7. The open forest soils recorded the highest emissions, further highlighting the strong relationship between land-use and carbon emissions. However, the predicted 2050 *SRR* map (Figure 5.7b) shows the projected *SRR* for the future. It can be observed significant expansion of darker green areas representing approximately 70% of the entire study area (Table 5.4). The projected increases in high-emission areas suggest that continued LULCC, including deforestation and agricultural expansion, will contribute to a rise in CO_2 emissions by 2050. These changes in spatial distribution and emission levels underscore the impact of land-use practices on *SRR* over time.

The findings align with several studies that examined the relationship between LULC and carbon emissions. Georgiadis and Wang (2021) reported that LULC changes, particularly the conversion of forests to open forests or agricultural lands, significantly increase *SRR*. Similar results were observed by Liu et al. (2018) and Kumar et al. (2020), who identified open forests and agricultural lands as major sources of CO_2 emission. These emissions are driven by factors including soil disturbances from agricultural practices, changes in vegetation structure and increased availability of soil organic matter, which accelerates decomposition rates. The projected increase in *SRR* observed in the study area, particularly in the open forest and cropland and mixed vegetation areas, reflects these dynamics and emphasises the ongoing impact of deforestation and cropland expansion on carbon emissions.

Moreover, the use of a forest-based regression model to predict emissions based on LULC maps is supported by Yang et al. (2024), who employed a similar modelling approach to project future *SRR* across different LULC types. Their study highlighted the importance of including spatial data to accurately predict the effects of land-use on carbon emissions. Furthermore, Liaw and Wiener (2002) and Breiman (2001), emphasised the robustness of Random Forest algorithms to handle complex environmental datasets and produce accurate predictions of *SRR* from various land-use types. This methodology is particularly effective

in scenarios where direct emissions data are unavailable, as it enables the scaling of plot-level measurements to larger landscapes.

Conclusions

This future LULCCs under the BAU scenario using DINAMICA EGO modelling software was projected, with 2022 as the baseline for projections through 2050. A forest-based regression model was then applied to predict soil respiration rate for both the 2022 and the projected 2050 LUMs.

The results revealed that without interventions to recover closed forest cover, the area of closed forests is projected to decrease by over 36% by 2050 compared to the 2022 reference map. In contrast, cropland and mixed vegetation as well as non-vegetated areas, are projected to increase by more than 20% and 40%, respectively, likely driven by the growing demand for food due to population growth. Additionally, the projected LUM indicates a potential reduction in the protected area of Bobiri Forest Reserve, which has remained nearly intact for the past 36 years.

This research provides relevant information for land-use planning and carbon management strategies, particularly in regions undergoing significant LULCs. It underscores the necessity of implementing sustainable land-use policies that prioritize forest conservation and mitigate the expansion of high-emission land-use categories, such as open forests and croplands. Furthermore, the modelling approach used in this study offers a valuable tool for projecting future LULC changes and associated carbon emissions based on land-use changes, contributing to long-term environmental management and climate mitigation strategies.

Limitations and Future Recommendations

A key limitation of this is the absence of alternative scenarios, such as integrated land management or land degradation scenarios, that consider current policies, projects, and programs in Ghana aimed at reforestation and mitigating climate change impacts. Future research should incorporate these alternative scenarios alongside the BAU scenario to evaluate the potential influence of restoration activities and sustainable land-use practices on future land development and associated emissions.

Furthermore, this study focused solely on *SRR* and did not account for emissions from above and below-ground vegetation. Including these components in future models would provide a more comprehensive understanding of carbon fluxes across different land-use categories. Vegetation, particularly biomass and root systems, play a critical role in carbon sequestration, and emissions, integrating these factors would therefore improve the accuracy of overall greenhouse gas (GHG) projections.

Moreover, while this study utilised the ArcGIS forest-based regression model to simulate *SRR*, future studies could compare emission factors (EFs) across IPCC Tiers, specifically Tier 1 values to Tier 2 or Tier 3 for the land-use types under study. Tier 1 EFs rely on global default values, making them easy to implement, however, often lack precision for local contexts. Tier 2 improves accuracy by incorporating country-specific emission factors and activity data, reflecting regional characteristics. Tier 3 provides the highest resolution and reliability through advanced modelling or direct measurements.

Such comparisons would provide an opportunity to validate the model's predictions and determine whether using Tier 1 EFs results in overestimations or underestimations of emissions. This approach would improve the accuracy of emission projections and offer more robust insights for land-use and climate change policy development.

CHAPTER 6 : GENERAL DISCUSSION

The primary aim of this study was to establish baseline data and analyse the evolution of soil CO_2 emissions in the Agriculture, Forestry, and Other Land-use (AFOLU) sector in Ghana. Each of the specific objectives was successfully addressed. The first specific objective (SO1) focused on land-use/cover (LULC) change analysis (see Chapter 3) providing a solid foundation by documenting historical land-use changes and their impact on the local environment. Assessment of the effect of seasonality and land-use change on soil respiration rate (SRR) variability from the SO2 (see Chapter 4), deepened understanding of how environmental factors and land management practices influence CO_2 fluxes. Finally, the SO3 focused on projecting future LULC change and association CO_2 emissions under the business-as-usual (BAU) scenario provided essential data to inform land-use planning and climate change mitigation strategies.

6.1 Comparison of the Findings with Existing Literature

The findings of this study are consistent with several studies in this field but also provide new insights into the specific dynamics of the semi-deciduous forest zone in Ghana. For illustration, the intensity analysis method used to assess land-use change is supported by existing research that highlights its efficiency compared to other methods, such as the Markov transition matrix (Aldwaik and Pontius, 2012; Mwangi et al., 2017). The observed trends in deforestation and agricultural expansion are consistent with global patterns of land conversion, particularly in tropical regions where forests are increasingly replaced by agricultural land (Lambin and Meyfroidt, 2011; Georgiadis and Wang, 2021).

The findings of seasonal variability in relation to SRR are consistent with global studies indicating that higher organic matter is likely associated with enhanced microbial activity and CO_2 emissions during the wet season, particularly in tropical climates (Davidson and Janssens, 2006; Vicca et al., 2012). However, the study also challenges some conventional wisdom by showing that in the context of the study sites, the relationship between SRR, soil moisture and temperature is not so clear-cut, suggesting that other factors (such as soil texture and organic matter) may also play an important role. This nuanced view extends

existing research and highlights the complex interactions in tropical ecosystems (Borken and Matzner, 2009; Anokye et al., 2021; Owusu et al., 2024).

The projected CO_2 emissions under future land-use scenarios confirm concerns raised in other studies about the impact of continued deforestation and agricultural expansion on carbon emissions in the tropics (Liu et al., 2018; Georgiadis and Wang, 2021). The model projections for 2050 underscore the need for proactive conservation strategies and highlight the potential consequences of a business-as-usual scenario in land-use. This reflects wider concerns about the impact of land-use change on carbon cycling in tropical regions (Lambin et al., 2018).

6.2 Novelty and Contribution of the Study

The novelty of this study lies in its mixed methods approach, combining detailed historical data analysis of LULC change in the study area using remote sensing and GIS techniques, with a comprehensive dataset covering 13 months of biweekly SRR measurements from four land-use types: forest, fallow, maize and rice. In addition, the study developed a predictive model using edaphic variables such as soil organic matter, pH, silt and soil moisture, which together explained 58% of the variability in SRR. Furthermore, the study projected future LULC changes under the BAU scenario and estimated the associated emissions based on the emission factors calculated in the study.

6.3 Implications of Findings

The implications of this study are significant, particularly in the context of climate change and land management. The evidence of increased soil CO_2 emissions due to deforestation and long-term fallow, which leaves the soil uncultivated with reduced tree cover, highlights the urgent need for sustainable land management practices. The results suggest that policies promoting emission reduction strategies such as agroforestry, afforestation and forest conservation should prioritise fallow land with sparse tree cover to mitigate the high carbon emissions observed in these areas.

CHAPTER 7 : CONCLUSIONS AND RECOMMENDATIONS

This chapter summarises the main findings related to the research questions, general conclusions, and recommendations obtained from the previous chapters.

7.1 Conclusions

This study was conducted in a moist semi-deciduous forest and its surrounding environs in Ghana and aimed to provide baseline data and project the evolution of soil respiration in the study region. Specifically, the study first analysed the intensity of land transformation from 1986 to 2022 using GIS and remote sensing (RS) techniques. Secondly, it assessed the variation in soil CO_2 emissions across three land categories; forest, fallow, and croplands (maize and rice). Finally, the study projected future LULC changes to 2050, using 2022 as the reference year, and estimated the associated *SRR*. The key findings are summarized as follows:

- The intensity analysis revealed significant changes in LULC, with substantial development observed over the study period. The croplands and mixed vegetation and non-vegetated classes experienced the largest gains, while the closed forest class consistently showed losses. Non-vegetated areas primarily expanded from croplands and mixed vegetation, and active transitions from both closed and open forests to croplands and mixed vegetation were observed. The analysis further showed an annual deforestation rate of 0.06% within the Bobiri forest reserve compared to 0.64% in the surrounding environs, suggesting potential deforestation leakage in the environs of the protected area.
- The assessment of *SRR* across the land-use types showed that the rates were highest in fallow, rice and maize, while forests recorded the lowest emissions, likely due to minimal soil disturbance and lower sunlight reaching the forest floor. Seasonal variability significantly influenced soil respiration, with higher emissions during the wet season. However, no consistent relationship was observed between soil respiration and soil moisture and temperature. Furthermore, a model was developed which explained approximately 58% of the observed variability in *SRR* using soil

physiochemical properties, i.e., organic matter (OM), acidity (pH), slit and soil moisture (SM).

- The projected future LULC changes in the study area were analysed under a BAU scenario using Dinamica EGO modelling software, with 2022 as the baseline for projections through 2050. The results indicated that closed forest cover is expected to decrease by over 36% by 2050, while cropland and mixed vegetation and non-vegetated areas are projected to increase significantly due to the growing demand for food and fibre. Additionally, the study found that the protected area of Bobiri Forest will experience some losses in vegetation cover. The forest-based regression model suggests that by 2050, open forests will emit approximately 55 kg CO_2 ha^{-1} d^{-1}, compared to 50 kg CO_2 ha^{-1} d^{-1} for closed forests and 52 kg CO_2 ha^{-1} d^{-1} for cropland and mixed vegetation. These findings underscore the impact of LUCs on *SRR* and highlight the importance of effective land management to mitigate environmental impacts.

7.2 Recommendations

7.2.1 Recommendations for Policy (Ghanaian Government NGOs)

- The government, through the Ghana Forestry Commission, should implement and enforce policies to protect the legal boundaries of the Bobiri Forest Reserve (BFR) and other protected areas. This will reduce deforestation leakage and prevent future encroachment, thus safeguarding the integrity of the forest and its ecosystem services.
- Emission reduction policies and programmes should focus on fallow lands with less tree cover and enforce policies to increase forest cover on these lands. This will ensure soil stability and significantly reduce soil respiration rates, contributing to carbon emissions reduction.
- The Ministry of Lands and Natural Resources should implement large-scale tree-planting initiatives to restore degraded forests and expand overall forest cover. Incentives should be provided to encourage private and community participation in these efforts, helping to mitigate the projected 35% forest cover loss by 2050.

7.2.2 Recommendations for Future Research

- Explore the impact of soil microbial biomass carbon and nitrogen on soil respiration rate, as these factors were not fully examined in this study. Understanding their role will provide deeper insights into soil respiration processes and improve emission prediction models.
- Estimate the CO_2 sequestration potential or uptake of the land-use under study by using transparent chambers to account for both photosynthesis and respiration. Additionally, further research should be conducted on the interaction between *SRR* and soil moisture and temperature, to assess the extent to which changes in these factors influence *SRR*, particularly in the context of tropical climate conditions.
- Expand the scope of GHG analysis by including methane (CH_4) and nitrous oxide (N_2O) emissions, using advanced tools like gas chromatographs. This will provide a more comprehensive understanding of GHG dynamics across different land-use types and help develop targeted strategies for mitigating overall emissions in tropical ecosystems.
- Integrate alternative land-use scenarios, such as integrated land management or reforestation programs, alongside the Business-as-Usual (BAU) scenario. This would help assess the impact of restoration activities on future land development and CO_2 emissions, offering more accurate predictions of land-use change and its environmental consequences.
- Compare different modelling approaches for predicting *SRR* by using IPCC Tier 1 default values for both soil and vegetation datasets alongside Tier 2 or Tier 3 measured datasets. This would help validate the accuracy of the model's emissions predictions, assess potential overestimations or underestimations of emissions using Tier 1 emission factors, and improve the reliability of emission projections for more robust policy development.

REFERENCES

Acheampong, E. O., Macgregor, C. J., Sloan, S., and Sayer, J., 2019. Deforestation is driven by agricultural expansion in Ghana's forest reserves. *Scientific African*, p. 5. https://doi.org/10.1016/j.sciaf.2019.e00146

Acheampong, E. O., Sayer, J., Macgregor, C. J., and Sloan, S., 2021. Factors Influencing the Adoption of Agricultural Practices in. *Journal of Land Economics*, 10(266), pp. 1–21. https://doi.org/2021, 10, 266. https://doi.org/10.3390/land10030266

Acheampong, R. A., Agyemang, F. S. K., and Abdul-Fatawu, M., 2016. Quantifying the spatio-temporal patterns of settlement growth in a metropolitan region of Ghana. *GeoJournal*, 82(4), pp. 823–840. https://doi.org/10.1007/s10708-016-9719-x

Adams, V. M., Chauvenet, A. L. M., Stoudmann, N., Gurney, G. G., Brockington, D., and Kuempel, C. D., 2023. Multiple-use protected areas are critical to equitable and effective conservation. *One Earth*, 6(9), pp. 1173–1189. https://doi.org/10.1016/j.oneear.2023.08.011

Addo-Danso, S. D., 2010. Survival and Growth in a Moist-semi Deciduous Forest in Ghana: comparison of monoculture and mixed-species plantations [University of Freiburg]. In Researchgate.Net. https://www.researchgate.net/profile/Shalom-Addo-Danso/publication/265453828_Survival_and_Growth_in_a_Moist-semi_Deciduous_Forest_in_Ghana_comparison_of_monoculture_and_mixed-species_plantations/links/5776b0f208ae1b18a7e1aff7/Survival-and-Growth-in-a-Mois

Addo-Fordjour, P., and Ankomah, F., 2017. Patterns and drivers of forest land cover changes in tropical semi-deciduous forests in Ghana. *Journal of Land-use Science*, 12(1), pp. 71–86. https://doi.org/10.1080/1747423X.2016.1241313

Afriyie, J., Asare, M., Danquah, E., and Pavla, H., 2021. Assessing the Management Effectiveness of Three Protected Areas in Ghana. *Conservation and Society*, 19(1), pp. 19–24. https://doi.org/10.4103/cs.cs_20_28

Agarwal, C., Green, G. M., Grove, J. M., Evan, T. P., and Schweik, C. M., 2002. A Review and Assessment of Land-Use Change Models: Dynamics of Space, Time, and Human

Choice. In USDA FOREST SERVICE 100(3). https://doi.org/10.1016/0006-8993(75)90162-6

Agterberg, F. P., 1992. Combining indicator patterns in weights of evidence modelling for resource evaluation. *Non-renewable Resources*, 1(1), pp. 39–50. https://doi.org/10.1007/BF01782111

Ajayi, E. O., Akin-Idowu, P. E., Aderibigbe, O. R., Ibitoye, D. O., Afolayan, G., Adewale, O. M., Adesegun, E. A., and Ubi, B. E., 2023. We are IntechOpen , the world's leading publisher of Open Access books Built by scientists , for scientists TOP 1 %. IntechOpen, 11(tourism), pp. 13. https://doi.org/DOI:10.5772/intechopen.109823

Al-doski, J., Mansor, S. B., Zulhaidi, H., and Shafri, M., 2013. Image Classification in Remote Sensing. *Journal of Environment and Earth Science*, 3(10), pp. 141–148.

Aldwaik, S. Z., and Pontius, R. G., 2012. Intensity analysis to unify measurements of size and stationarity of land changes by interval, category, and transition. *Landscape and Urban Planning*, 106(2012), pp. 103–114. https://doi.org/10.1016/j.landurbplan.2012.02.010

Almaraz, M., Bai, E., Wang, C., Trousdell, J., Conley, S., Faloona, I., and Houlton, B. Z., 2018. Agriculture is a major source of NOx pollution in California. *Science Advances*, 4(6), pp. 1–9. https://doi.org/10.1126/SCIADV.AAU2561

Almeida, C. M., Gleriani, J. M., Castejon, E. F., and Soares-Filho, B. S., 2008. Using neural networks and cellular automata for modelling intra-urban land-use dynamics. *International Journal of Geographical Information Science*, 22(9), pp. 943–963. https://doi.org/10.1080/13658810701731168

Almeida, C. M., Souza, R. C., and Fonseca, L. M., 2008. Assessing land-use/land cover change through multi-temporal satellite images using fuzzy similarity indices. *International Journal of Applied Earth Observation and Geoinformation*, 10(3), pp. 200–210.

Alo, C. A., and Pontius, R. G., 2008. Identifying systematic land-cover transitions using remote sensing and GIS: The fate of forests inside and outside protected areas of

Southwestern Ghana. *Environment and Planning B: Planning and Design*, 35(2), pp. 280–295. https://doi.org/10.1068/b32091

Ameyaw, A. O., 2015. Soil respiration studies in two sites of different post-logging ages in a moist-semi deciduous forest in Ghana, MPhil. thesis, Kwame Nkrumah University of Science and Technology, Kumasi.

Ampim, P. A. Y., Ogbe, M., Obeng, E., Akley, E. K., and Maccarthy, D. S., 2021. Land cover changes in Ghana over the past 24 years. *Sustainability* (Switzerland), 13(9). https://doi.org/10.3390/su13094951

Amponsah, O., Armando, B. L., Anani, A. P., and Boateng, R. S., 2018. The impact of deforestation on carbon storage in soil and tree biomass in Ghana. *Forest Ecology and Management*, 419, pp. 98–108.

Ankomah, F., Kyereh, B., Asante, W., and Ansong, M., 2019. Patterns of forest cover change and their association with forest management regimes of forest reserves in the high forest zone of Ghana. *Journal of Land-use Science*, 14(3), pp. 242–257. https://doi.org/10.1080/1747423X.2019.1665116

Anokye, J., Logah, V., and Opoku, A., 2021. Soil carbon stock and emission: estimates from three land-use systems in Ghana. *Ecological Processes*, 10(1). https://doi.org/10.1186/s13717-020-00279-w

Ansari, M. A., Choudhury, B. U., Mandal, S., Jat, S. L., and Meitei, C. B., 2022. Converting primary forests to cultivated lands: Long-term effects on the vertical distribution of soil carbon and biological activity in the foothills of Eastern Himalaya. *Journal of Environmental Management*, 301(September 2021), 113886. https://doi.org/10.1016/j.jenvman.2021.113886

Anwar, S. M., 2002. Land-use change dynamics: A dynamic spatial simulation Asian Institute of Technology, Thailand. MSc., School of Advanced Technologies. http://cormas.cirad.fr/pdf/Thesis_Morshed.pdf

Anyanwu, C. N., Ojike, O., Emodi, N. V., Ekwe, E. B., Okereke, C., Diemuodeke, E. O., Elochukwu, A. E., and Nnamani, U. A., 2023. Deep decarbonization options for the

Agriculture, Forestry, and Other Land-use (AFOLU) sector in Africa: A systematic literature review. *Environmental Monitoring and Assessment*, 195(565).https://doi.org/https://doi.org/10.1007/s10661-023-11184-y

Artaxo, P., Hansson, H. C., Machado, L. A. T., and Rizzo, L. V., 2022. Tropical forests are crucial in regulating the climate on Earth. *PLOS Climate*, 1(8), e0000054. https://doi.org/10.1371/journal.pclm.0000054

Asante, W., and Ayee, B. Y., 2019. Illegal Logging, Land-use Change and GHG Emissions in Ghana: A Critical Look at the Environmental and Social Costs. *Environmental Development*, 31, pp. 1–11. https://doi.org/DOI:10.1016/j.envdev.2019.06.001.

Asner, G. P., Knapp, D. E., Broadbent, E. N., Oliveira, P. J. C., Keller, M., and Silva, J. N., 2005. Ecology: Selective logging in the Brazilian Amazon. *Science*, 310(5747), pp. 480–482. https://doi.org/10.1126/science.1118051

Aspinall, R., 2004. Modelling land-use change with generalized linear models: A multimodel analysis of change between 1860 and 2000 in Gallatin Valley, Montana. *J. Environ. Manage.*, 72(1–2), pp. 91–103. https://doi.org/10.1016/j. jenvman.2004.02.009 .

Asubonteng, K., Pfeffer, K., Ros-Tonen, M., Verbesselt, J., and Baud, I., 2018. Effects of Tree-crop Farming on Land-cover Transitions in a Mosaic Landscape in the Eastern Region of Ghana. *Environmental Management*, 62(3), pp. 529–547. https://doi.org/10.1007/s00267-018-1060-3

Asubonteng, O. K., 2007. Identification of Land-use / Cover Transfer Hotspots in the Ejisu-Juabeng District, Ghana. [Kwame Nkrumah University of Science and Technology]. In Itc. https://webapps.itc.utwente.nl/librarywww/papers_2007/msc/nrm/asubonteng.pdf

Atedhor, G. O., 2023. Greenhouse gases emissions and their reduction strategies: Perspectives of Africa's largest economy. *Scientific African*, 20, pp. 1–17. https://doi.org/10.1016/j.sciaf.2023.e01705

Ayele, G. T., Tebeje, A. K., Demissie, S. S., Belete, M. A., Jemberrie, M. A., Teshome, W. M., Mengistu, D. T., and Teshale, E. Z., 2018. Time series land cover mapping and change

detection analysis using geographic information system and remote sensing, Northern Ethiopia. *Air, Soil and Water Research*, 11. https://doi.org/10.1177/1178622117751603

Aziz, A. A., Wan, K., Za'Aba, S. K., Shahriman, A. B., Adnan, N. H., Asyekin, H., and Zuradzman, M. R., 2013. Human classification based on gestural motions by using components of PCA. IOP Conference Series: Materials Science and Engineering, 53(1). https://doi.org/10.1088/1757-899X/53/1/012023

Baan, L., Alkemade, R., and Koellner, T., 2013. Land-use impacts on biodiversity in LCA: a global approach. *International Journal of Life Cycle Assessment*, 18(6), pp. 1216–1230. https://doi.org/10.1007/s11367-012-0412-0

Baffour-Ata, F., Antwi-Agyei, P., and Nkiaka, E., 2021. Climate variability, land cover changes and livelihoods of communities on the fringes of Bobiri forest reserve, Ghana. *Forests*, 12(3), pp. 1–24. https://doi.org/10.3390/f12030278

Baker, J. M., Ochsner, T. E., Venterea, R. T., and Griffis, T. J., 2007. Tillage and soil carbon sequestration-What do we really know? *Agriculture, Ecosystems and Environment*, 118(1–4), pp. 1–5. https://doi.org/10.1016/j.agee.2006.05.014

Baldocchi, D. D., 2003. Assessing the eddy covariance technique for evaluating carbon dioxide exchange rates of ecosystems: Past, present and future. *Global Change Biology*, 9(4), pp. 479–492. https://doi.org/10.1046/j.1365-2486.2003.00629.x

Barry, R. G., and Chorley, R. J., 2009. Atmosphere, Weather and Climate (1st ed.). *Taylor and Francis*. https://doi.org/10.4324/9780203871027

Benefoh, D. T., Oppong, S., Matthew, E., and Jnr, O., 2008. Spatial mapping of carbon stocks in different land-use / cover types : A case study of Ejisu-Juaben District, Ghana. October.

Bessah, E., Bala, A., Agodzo, S. K., Okhimamhe, A. A., Boakye, E. A., and Ibrahim, S. U., 2019. The impact of crop farmers' decisions on future land-use, land cover changes in Kintampo North Municipality of Ghana. *International Journal of Climate Change Strategies and Management*, 11(1), pp. 72–87. https://doi.org/10.1108/IJCCSM-05-2017-0114

Bi, X., Li, B., Nan, B., Fan, Y., Fu, Q., and Zhang, X., 2018. Characteristics of soil organic carbon and total nitrogen under various grassland types along a transect in a mountain-basin system in Xinjiang, China. *Journal of Arid Land*, 10(4), pp. 612–627. https://doi.org/10.1007/s40333-018-0006-1

Biasi, C., Rusalimova, O., Meyer, H., Kaiser, C., Wanek, W., Barsukov, P., Junger, H., and Richter, A., 2005. Temperature-dependent shift from labile to recalcitrant carbon sources of arctic heterotrophs. Rapid Communications in Mass Spectrometry : *RCM*, 19(11), pp. 1401–1408. https://doi.org/10.1002/rcm.1911

Boajie, L., Hehe, G., and Yazhou, J., 2018. Simulation of Land-use Change in Coal Mining Area under Different Scenarios based on the CLUE-S model: A Case Study of Jiawang Mining Area in Xuzhou City. *Tropical Geography*, 38(2): pp. 274-281 https://doi.org/10.13284/j.cnki.rddl.003029

Boateng, P., 2023. Climate change and climate-smart agricultural practices in fringe communities around Bobiri and Pra-Anum forest reserves, MSc thesis, CSIR - College of Science and Technology, Kumasi, Ghana.

Boateng, K., Obeng, G., and Mensah, E., 2017. Rice Cultivation and Greenhouse Gas Emissions: A Review and Conceptual Framework with Reference to Ghana. *Agriculture*, 7(1), 7. https://doi.org/10.3390/agriculture7010007

Bond-Lamberty, B., and Thomson, A., 2010. A global database of soil respiration data. *Biogeosciences*, 7(6), pp. 1915–1926. https://doi.org/10.5194/bg-7-1915-2010

Bonham-Carter, G. F., 1994. Geographic information systems for geoscientists: Modelling with GIS. *Computers and Geosciences*, 21(9), pp. 1110–1112. https://doi.org/10.1016/0098-3004(95)90019-5

Borken, W., and Matzner, E., 2009. Reappraisal of drying and wetting effects on C and N mineralization and fluxes in soils. *Global Change Biology*, 15(4), pp. 808–824. https://doi.org/10.1111/j.1365-2486.2008.01681.x

Bosu, P. P., 2010. Alternative mixed plantation systems and restoration strategies for conservation and sustainable production of native tropical species in Ghana (issue march).

http://www.itto.int/files/itto_project_db_input/2526/Technical/ITTO MIXED PLANTATION TechnicalREPORT.pdf

Boumans, R., Roman, J., Altman, I., and Kaufman, L., 2015. The multiscale integrated model of ecosystem services (MIMES): Simulating the interactions of coupled human and natural systems. *Ecosystem Services*, 12(2015), pp. 30–41. https://doi.org/10.1016/j.ecoser.2015.01.004

Breiman, L., 2001. Random Forests. Springer Climate, 45, 5–32. https://doi.org/Leo Breiman (2001). Random Forests. , 45(1), pp. 5–32. http://doi:10.1023/a:1010933404324

Brobbey, L. K., Agyei, F. K., and Osei-Tutu, P., 2020. Drivers of Cocoa Encroachment into Protected Forests: The Case of Three Forest Reserves in Ghana. *International Forestry Review*, 22(4), pp. 425–437. https://doi.org/10.1505/146554820831255533

Brümmer, C., Papen, H., Wassmann, R. and Brüggemann, N., 2009. Fluxes of CH_4 and CO_2 from soil and termite mounds in South Sudanian savanna of Burkina Faso (West Africa). *Global Biogeochemical Cycles*, *23*(1).

Bufebo, B., and Elias, E., 2021. Land-use/Land Cover Change and Its Driving Forces in Shenkolla Watershed, South Central Ethiopia. *Scientific World Journal*, 2021. https://doi.org/10.1155/2021/9470918

Campbell, J. B., 2002. Introduction to Remote Sensing (Third Edit). CRC Press, 2002 *Taylor and Francis*. https://books.google.com.gh/books?id=1KfQxsN0vp8C

CBD., 1992. Article 8 in-situ conservation, Text of the Convention on Biological Diversity.

CBD., 2010. X/2.Strategic Plan for Biodiversity 2011-2020. CBD. at: https://www.cbd.int/decision/cop/?id=12268

Chadid, M. A., Dávalos, L. M., Molina, J., and Armenteras, D., 2015. A Bayesian spatial model highlights distinct dynamics in deforestation from coca and pastures in an Andean biodiversity hotspot. *Forests*, 6(11), pp. 3828–3846. https://doi.org/10.3390/f6113828

Chae, N., Kim, J., Kim, D., Lee, D., Kim, R. H., Ban, J., and Son, Y., 2003. Measurement of Soil CO_2 Efflux Using a Closed Dynamic Chamber System. *Korean Journal of Agricultural and Forest Meteorology*, 5(2), pp. 94–100.

Cheng-Fang, L., Dan-Na, Z., Zhi-Kui, K., Zhi-Sheng, Z., Jin-Ping, W., Ming-Li, C., and Cou-Gui, C., 2012. Effects of tillage and nitrogen fertilisers on CH4 and CO2 emissions and soil organic carbon in paddy fields of central China. *PLoS ONE*, 7(5), pp. 1–9. https://doi.org/10.1371/journal.pone.0034642

Cheng, L. lin, Liu, M., and Zhan, J. qi., 2020. Land-use scenario simulation of mountainous districts based on Dinamica EGO model. *Journal of Mountain Science*, 17(2), pp. 289–303. https://doi.org/10.1007/s11629-019-5491-y

Chicco, D., Warrens, M.J. and Jurman, G., 2021. The coefficient of determination R-squared is more informative than SMAPE, MAE, MAPE, MSE and RMSE in regression analysis evaluation. *Peerj computer science*, *7*, p.e623.

Christensen, M., and Arsanjani, J. J., 2020. Stimulating implementation of sustainable development goals and conservation action: Predicting future land-use/cover change in Virunga National Park, Congo. *Sustainability* (Switzerland), 12(4). https://doi.org/10.3390/su12041570

Ciais, P., Wattenbach, M., Vuichard, N., Smith, P., Piao, S. L., Don, A., Luyssaert, S., Janssens, I. A., Bondeau, A., Dechow, R., Leip, A., Smith, P. C., Beer, C., Van der werf, G. R., Gervois, S., Van oost, K., Tomelleri, E., Freibauer, A., and Schulze, E. D., 2010. The European carbon balance. Part 2: Croplands. *Global Change Biology*, 16(5), pp. 1409–1428. https://doi.org/10.1111/j.1365-2486.2009.02055.x

CILSS, (Comite Inter-etats de Lutte contre la Secheresse dans le Sahel)., 2016. Landscapes of West Africa - A Window on a Changing World.

Congalton, R. G., 1991. A review of assessing the accuracy of classifications of remotely sensed data. *Remote Sensing of Environment*, 37(1), pp. 35–46. https://doi.org/10.1016/0034-4257(91)90048-B

Congalton, R. G., and Green, K., 2019. Assessing the Accuracy of Remotely Sensed Data: Principles and Practices (Third Edit, Vol. 19, Issue 5). CRC Press, 2002 *Taylor and Francis*. https://doi.org/10.1201/9780429052729

Crisci, C., Ghattas, B., and Perera, G., 2012. A review of supervised machine learning algorithms and their applications to ecological data. *Ecological Modelling*, 240(June 2018), pp. 113–122. https://doi.org/10.1016/j.ecolmodel.2012.03.001

Cui, B., Feng, G., Liao, G., Yu, R., Zhang, X., Liu, H., Yang, L. Y., Zhao, J., and Tan, Z. H., 2020. Controls of Temporal Variations on Soil Respiration in a Tropical Lowland Rainforest in Hainan Island, China. *Tropical Conservation Science*, 13. https://doi.org/10.1177/1940082920914902

Cutler, D. R., Edwards, T. C., Beard, K. H., Cutler, A., Hess, K. T., Gibson, J., and Lawler, J. J., 2007. Random forests for classification in ecology. *Ecology*, 88(11), pp. 2783–2792. https://doi.org/10.1890/07-0539.1

Damnyag, L., Saastamoinen, O., Blay, D., Dwomoh, F. K., Anglaaere, L. C., and Pappinen, A., 2013. Sustaining protected areas: Identifying and controlling deforestation and forest degradation drivers in the Ankasa Conservation Area, Ghana. *Biological Conservation*, 165, 86–94. https://doi.org/10.1016/j.biocon.2013.05.024

Davidson, E. A., and Janssens, I. A., 2006. Temperature sensitivity of soil carbon decomposition and feedback to climate change. *Nature*, 440(7081), pp. 165–173. https://doi.org/10.1038/nature04514

Davidson, E. A., Janssens, I. A., and Lou, Y., 2006. On the variability of respiration in terrestrial ecosystems: Moving beyond Q10. *Global Change Biology*, 12(2), pp. 154–164. https://doi.org/10.1111/j.1365-2486.2005.01065.x

Davidson, E. A., Samanta, S., Caramori, S. S., and Savage, K., 2012. The Dual Arrhenius and Michaelis-Menten kinetics model for decomposition of soil organic matter at hourly to seasonal time scales. *Global Change Biology*, 18(1), pp. 371–384. https://doi.org/10.1111/j.1365-2486.2011.02546.x

Deer, P., 1995. Digital change detection techniques. Civilian and Military Application Published in the UK. *Taylor and Francis* Ltd., London.

DeFries, R., Karanth, K. K., and Pareeth, S., 2010. Interactions between protected areas and their surroundings in human-dominated tropical landscapes. *Biological Conservation*, 143(12), pp. 2870–2880. https://doi.org/10.1016/j.biocon.2010.02.010

Deka, J., Tripathi, O. P., Khan, M. L., and Srivastava, V. K., 2019. Study on land-use and land-cover change dynamics in Eastern Arunachal Pradesh, N.E. India using remote sensing and GIS. *Tropical Ecology*, 60(2), pp. 199–208. https://doi.org/10.1007/s42965-019-00022-3

Dembélé, F., Guuroh, R. T., Ansah, P. B., Asare, D. C. B. M., Da, S. S., Aryee, J. N. A., and Adu-Bredu, S., 2024. Land-use land cover change and intensity analysis of land transformation in and around a moist semi-deciduous forest in Ghana. *Trees, Forests and People*, 15(January). https://doi.org/10.1016/j.tfp.2024.100507

Dicko, G., 2016. Soil carbon change and CO2 fluxes under different agricultural land-use in the Vea catchment, Upper East Region of Ghana. In KNUST (Issue May). Kwame Nkrumah University of Science And Technology Kumasi, Ghana.

Dinamica., 2024. Spatial Patterns of Changes. https://www.dinamicaego.com/dinamica/dokuwiki/doku.php?id=patterns_of_change

Djagbletey, G. D., Adu-Bredu, S., Duah-Gyamfi, A., Abeney, E. A., Asante, W. A., Akyeampong, E., Addo-Danso, S., Ametsitsi, G. K., Amponsah-Manu, E., and Dabo, J., 2018. Floristic composition and carbon stocks of tree species of different conservation status following selective logging in a moist semi-deciduous forest in Ghana. *Ghana Journal of Forestry*, 34(01), pp. 15–34.

Dogbe, W., Sogbedji, J., and Buah, S., 2015. Site-specific Nutrient Management for Lowland Rice in the Northern Savannah Zones of Ghana. *Current Agriculture Research Journal*, 3(2), pp. 109–117. https://doi.org/10.12944/carj.3.2.04

Don, A., Schumacher, J., and Freibauer, A., 2011. Impact of tropical land-use change on soil organic carbon stocks - a meta-analysis. *Global Change Biology*, 17(4), pp. 1658–1670. https://doi.org/10.1111/j.1365-2486.2010.02336.x

Dossa, G. G. O., Paudel, E., Wang, H., Cao, K., Schaefer, D., and Harrison, R. D., 2015. Correct calculation of CO_2 efflux using a closed-chamber linked to a non-dispersive infrared gas analyser. *Methods in Ecology and Evolution*, 6(12), pp. 1435–1442. https://doi.org/10.1111/2041-210X.12451

Eastman, J. R., and Toledano, J., 2018. A Short Presentation of the Land Change Modeler (LCM) BT - Geomatic Approaches for Modeling Land Change Scenarios. In M. T. Camacho Olmedo, M. Paegelow, J.-F. Mas, and F. Escobar (Eds.), Lecture Notes in Geoinformation and Cartography (pp. 499–505). Springer International Publishing. https://doi.org/10.1007/978-3-319-60801-3_36

EOS, 2019. NDVI FAQ: All You Need To Know About Index. https://eos.com/blog/ndvi-faq-all-you-need-to-know-about-ndvi/#:~:text=HowToMeasureDensityOf,possibledensityofgreenleaves .

EPA., 2019. Ghana ' s Fourth National Greenhouse Gas Inventory Report. In National Greenhouse Gas Inventory to the United Nations Framework Convention on Climate Change (Issue February). www.epa.gov.gh

EPA., 2022. Ghana's fifth national greenhouse gas inventory. In National Greenhouse Gas Inventory to the United Nations Framework Convention on Climate Change (Issue May). www.epa.gov.gh

EPA., 2024. Ghana's Fourth Biennial Update Report to the United Nations Framework Convention on Climate Change (Issue March). www.epa.gov.gh.

Esri, 2023. *ArcGIS Pro*, Version 3.0 [Computer software]. Environmental Systems Research Institute, Inc. Available at: https://www.esri.com [Accessed 31 July 2024].

Ewers, R. M., and Rodrigues, A. S. L., 2008. Estimates of reserve effectiveness are confounded by leakage. *Trends in Ecology and Evolution*, 23(3), pp. 113–116. https://doi.org/10.1016/j.tree.2007.11.008

Fan, L. C., Yang, M. Z., and Han, W. Y., 2015. Soil respiration under different land-uses in Eastern China. *PLoS ONE*, 10(4), pp. 1–18. https://doi.org/10.1371/journal.pone.0124198

FAO., 2016. The state of food and agriculture. In The Eugenics review (Vol. 59, Issue 2).

FAO., 2017. Soil Organic Carbon: The hidden potential. In Food and Agriculture Organization of the United Nations (Issue March).

FAO., 2020. Global Forest Resources Assessment 2020 – Key finding. In Food and Agriculture Organization of the United Nations. https://doi.org/https://doi.org/10.4060/ca8753enThe

FAO, and ITPS., 2015. Status of the World's Soil Resources – Technical Summary. In Status of the World's Soil Resources. http://www.fao.org/3/i5126e/i5126e.pdf link accessed on 28/04/2020

Federici, S., Tubiello, F. N., Salvatore, M., Jacobs, H., and Schmidhuber, J., 2015. New estimates of CO2 forest emissions and removals: 1990-2015. *Forest Ecology and Management*, 352, pp. 89–98. https://doi.org/10.1016/j.foreco.2015.04.022

Feng, Y., 2017. Modelling dynamic urban land-use change with geographical cellular automata and generalised pattern search-optimized rules. *International Journal of Geographical Information Science*, 31(6), pp. 1198–1219. https://doi.org/10.1080/13658816.2017.1287368

Firdaus, R., 2014. Assessing land-use and land cover change toward sustainability in humid tropical watersheds, Indonesia (Issue March) [Hiroshima University]. http://ir.lib.hiroshima-u.ac.jp/00036290

Foley, J. A., DeFries, R., Asner, G. P., Barford, C., Bonan, G., Carpenter, S. R., Chapin, F. S., Coe, M. T., Daily, G. C., Gibbs, H. K., Helkowski, J. H., Holloway, T., Howard, E. A., Kucharik, C. J., Monfreda, C., Patz, J. A., Prentice, I. C., Ramankutty, N., and Snyder, P. K., 2005. *Global consequences of land-use Science*, 309(5734), pp. 570–574. https://doi.org/10.1126/science.1111772

Foody, G. M., 2002. Land Cover Classification Accuracy Assessment. *Remote Sensing of Environment Environ*, 80, pp. 105–118. https://doi.org/10.1007/978-981-16-5149-6_6

Foody, G. M., and HILL, R. A., 1996. Classification of tropical forest classes from Landsat TM data. *International Journal of Remote Sensing*, 17(12), pp. 2353–2367. https://doi.org/10.1080/01431169608948777

Ford, S. A., Jepsen, M. R., Kingston, N., Lewis, E., Brooks, T. M., MacSharry, B., and Mertz, O., 2020. Deforestation leakage undermines conservation value of tropical and subtropical forest-protected areas. *Global Ecology and Biogeography*, 29(11), pp. 2014–2024. https://doi.org/10.1111/geb.13172

Franzluebbers, A. J., 2002. Soil organic matter stratification ratio as an indicator of soil quality. *Soil and Tillage Research*, 66(2), pp. 95–106. https://doi.org/10.1016/S0167-1987(02)00018-1

Frimpong, F. F., Koranteng, A., Atta-Darkwa, T., Junior, O. F., and Nied´zwiecki, Z., 2023. Land Cover Changes Utilising Landsat Satellite Imageries for the Kumasi Metropolis and Its Adjoining Municipalities in. *MDPI, Sensor*, 23(2644). https://doi.org/10.3390/s23052644

Fuchs, R., Herold, M., Verburg, P. H., and Clevers, J. G. P. W., 2013. A high-resolution and harmonized model approach for reconstructing and analysing historic land changes in Europe. *Biogeosciences*, 10(3), pp. 1543–1559. https://doi.org/10.5194/bg-10-1543-2013

Fuller, C., Ondei, S., Brook, B. W., and Buettel, J. C., 2019. First, do no harm: A systematic review of deforestation spillovers from protected areas. *Global Ecology and Conservation*, 18(2019), e00591. https://doi.org/10.1016/j.gecco.2019.e00591

Garcia, R. A., Soares-Filho, B. S., and Sawyer, D. O., 2007. Socioeconomic dimensions, migration, and deforestation: An integrated model of territorial organization for the Brazilian Amazon. *Ecological Indicators*, 7(3), pp. 719–730. https://doi.org/10.1016/j.ecolind.2006.08.003

Garnaut, R., 2008. The Garnaut climate change review: final report (Issue September). www.cambridge.org/9780521744447

Gary, N. G., Patrick, N. H., Brian, H., Erin, L. H., Andrew, S., Abrams, M. J., Aguirre, N., Blair, M., Botha, E., Colloff, M., Dawson, T., Franklin, J., Horning, N., Craig, J., Magnusson, W., Santos, M. J., Schill, S. R., and Kristen, W., 2017. Remote Sensing for Biodiversity. In M. Walters and R. J. Scholes (Eds.), The Geo Handbook Biodiversity Observation Networks (Vol. 34, Issue 4, pp. 227–228). Springer. https://doi.org/10.2989/10220119.2017.1387815

Gashu, K., and Gebre-Egziabher, T., 2018. Spatiotemporal trends of urban land-use/land-cover and green infrastructure change in two Ethiopian cities: Bahir Dar and Hawassa. *Environmental Systems Research*, 7(1). https://doi.org/10.1186/s40068-018-0111-3

GCF., 2010. A unique fund for humanity's greatest challenge. Green Climate Fund. www.greenclimate.fund

GCIC., 2016. Business Incubation Program. Ghana Climate Innovation Centre. https://ghanacic.org/

Gebrehiwet, K. B., 2004. Land-use and Land Cover Changes in the Central Highlands of Ethiopia: The Case of Yerer Mountain and its Surroundings. In 2004 (Issue June). Addis Ababa University, Ethiopia.

Georgiadis, T., and Wang, S., 2021. Predicting CO2 Emissions from Land-use/Land Cover Change in a Coastal Watershed Using Random Forest Regression. *Environmental Modelling and Assessment*, 26(3), pp. 451–465.

Ghana Government., 2015. Ghana's intended nationally determined contribution (INDC) and accompanying explanatory note. In Ministry of Environment, Science, Technology and Innovation, Ghana. https://www4.unfccc.int/sites/ndcstaging/PublishedDocuments/Ghana First/GH_INDC_2392015.pdf

Gibson, L., Lee, T. M., Koh, L. P., Brook, B. W., Gardner, T. A., Barlow, J., Peres, C. A., Bradshaw, C. J. A., Laurance, W. F., Lovejoy, T. E., and Sodhi, N. S., 2011. Primary forests are irreplaceable for sustaining tropical biodiversity. *Nature*, 478(7369), pp. 378–381. https://doi.org/10.1038/nature10425

Gislason, P. O., Benediktsson, J. A., and Sveinsson, J. R., 2006. Random Forests for land cover classification. *Pattern Recognition Letters*, 27(4), pp. 294–300. https://doi.org/10.1016/j.patrec.2005.08.011

Goodacre, A. K., Bonham-Carter, G. F., Agterberg, F. P., and Wright, D. F., 1993. A statistical analysis of the spatial association of seismicity with drainage patterns and magnetic anomalies in western Quebec. *Tectonophysics*, 217(3–4), pp. 285–305. https://doi.org/10.1016/0040-1951(93)90011-8

Goswami, M., Ravishankar, C., Nautiyal, S., and Schaldach, R., 2019. Integrated Landscape Modelling in India: Evaluating the Scope for Micro-Level Spatial Analysis over Temporal Scale. In S. C. Garkoti, J. S. Van Bloem, P. Z. Fule, and R. L. Semwal (Eds.), Tropical Ecosystems: Structure, Functions and Challenges in the Face of Global Change (pp. 289–315). *Springer*, Singapore. https://doi.org/10.1007/978-981-13-8249-9_5

Grace, J., José, J. S., Meir, P., Miranda, H. S., and Montes, R. A., 2006. Productivity and carbon fluxes of tropical savannas. *Journal of Biogeography*, 33(3), pp. 387–400. https://doi.org/10.1111/j.1365-2699.2005.01448.x

Grassi, G., House, J., Dentener, F., Federici, S., Den Elzen, M., and Penman, J., 2017. The key role of forests in meeting climate targets requires science for credible mitigation. *Nature Climate Change*, 7(3), pp. 220–226. https://doi.org/10.1038/nclimate3227

Green, K., Kempka, D., and Lackey, L., 1994. and Remote to Detect Using Sensing Ghange Monitor and Land-Use. *Photogrammetric Engineering and Remote Sensing*, 60(3), pp. 331–337.

GreenGaDe., 2024. Greenhouse Gas Determination in West Africa's Agricultural Landscapes. Consorcium. https://www.uni-potsdam.de/en/greengade/project/tier-2-assessment-based-on-field-measurements/wp-5

Griffiths, P., Kuemmerle, T., Baumann, M., Radeloff, V. C., Abrudan, I. V., Lieskovsky, J., Munteanu, C., Ostapowicz, K., and Hostert, P., 2014. Forest disturbances, forest recovery, and changes in forest types across the Carpathian ecoregion from 1985 to 2010

based on Landsat image composites. *Remote Sensing of Environment*, 151, pp. 72–88. https://doi.org/https://doi.org/10.1016/j.rse.2013.04.022

Grimm, V., and Railsback, S. F., 2005. Individual-based Modelling and Ecology. Princeton University Press. https://doi.org/doi:10.1515/9781400850624

GSS., 2005. Population Data Analysis Reports. Policy Implications of Population Trends Data, 2(August), pp. 1–495.

GSS., 2021. Ghana 2021 population and housing census. https://statsghana.gov.gh/gssmain/fileUpload/pressrelease/2021PHCGeneralReportVol3A_PopulationofRegionsandDistricts_181121.pdf

Hackman, K. O., Gong, P., and Wang, J., 2017. New land-cover maps of Ghana for 2015 using Landsat 8 and three popular classifiers for biodiversity assessment. *International Journal of Remote Sensing*, 38(14), pp. 4008–4021. https://doi.org/10.1080/01431161.2017.1312619

Hagen, A., 2003. Fuzzy set approach to assessing similarity of categorical maps. *International Journal of Geographical Information Science*, 17(April), pp. 37–41. http://dx.doi.org/10.1080/13658810210157822

Haile-Mariam, S., Collins, H. P., and Higgins, S. S., 2008. Greenhouse Gas Fluxes from an Irrigated Sweet Corn (Zea mays L.)–Potato (Solanum tuberosum L.) Rotation. *Journal of Environmental Quality*, 37(3), pp. 759–771. https://doi.org/10.2134/jeq2007.0400

Hall, J. B., and Swaime, M., 1981. Distribution and ecology of vascular plants in a tropical rain forest (W. Dr Junk (ed.); Forest Veg). The Hague, Netherlands.

Han, G., Xing, Q., Luo, Y., Rafique, R., Yu, J., and Mikle, N., 2014. Vegetation types alter soil respiration and its temperature sensitivity at the field scale in an estuary wetland. *PLoS ONE*, 9(3). https://doi.org/10.1371/journal.pone.0091182

Hansen, M. C., Potapov, P. V., Moore, R., Hancher, M., Turubanova, S. A., Tyukavina, A., Thau, D., Stehman, S. V., Goetz, S. J., Loveland, T. R., Kommareddy, A., Egorov, A., Chini, L., Justice, C. O., and Townshend, J. R. G., 2013. High-Resolution Global Maps of

21st-Century Forest Cover Change. *Science*, 342(November), pp. 850–853. https://doi.org/10.1126/science.1244693

Hansen, M. C., Stehman, S. V., Potapov, P. V., Arunarwati, B., Stolle, F., and Pittman, K., 2009. Quantifying changes in the rates of forest clearing in Indonesia from 1990 to 2005 using remotely sensed data sets. *Environmental Resource Letter*, 4 (2009), pp. 1–12. https://doi.org/10.1088/1748-9326/4/3/034001

Hashim, H., Abd Latif, Z., and Adnan, N. A., 2019. Urban vegetation classification with NDVI threshold value method with very high resolution (vhr) Pleiades imagery. The International Archives of the Photogrammetry, Remote Sensing and Spatial Information Sciences, XLII-4/W16, pp. 237–240. https://doi.org/10.5194/isprs-archives-XLII-4-W16-237-2019

Hassan, G. F., and Elhag, A. M. H., 2013. Assessment and Mapping of Land-use/Land Cover, Using Remote Sensing And GIS Techniques; Case Study: Ahable And Wad Grabou Area, Whaite Nile State, Sudan. *International Journal of Scientific and Technology Research*, 2(2), pp. 194–198. www.ijstr.org

Hawthorne, W., and Abu-Juam, M., 1995. Forest Protection in Ghana: With Particular Reference to Vegetation and Plant Species. IUCN, ODA/Forest Department Republic of Ghana.

Hidalgo, C. A., Klinger, B., Barabási, A. L., and Hausmann, R., 2007. Research Articles Research Articles. *Science*, 317(july), 4.

Houghton, R. A., and Goodale, C. L., 2004. Effects of land-use change on the carbon balance of terrestrial ecosystems. *Geophysical Monograph Series*, 153, pp. 85–98. https://doi.org/10.1029/153GM08

Houghton, R. A., House, J. I., Pongratz, J., Van Der Werf, G. R., Defries, R. S., Hansen, M. C., Le Quéré, C., and Ramankutty, N., 2012. Carbon emissions from land-use and land-cover change. *Biogeosciences*, 9(12), pp. 5125–5142. https://doi.org/10.5194/bg-9-5125-2012

Huang, H. H., Hsiao, C. K., and Huang, S. Y., 2009. Nonlinear Regression Analysis. International Encyclopedia of Education, Third Edition, January 2010, pp. 339–346. https://doi.org/10.1016/B978-0-08-044894-7.01352-X

Humanas, G. C., Paraense, M., Goeldi, E., Antunes, B., Filho, R., Adams, A., Sereni Murrieta, C., and Sergio, R., 2013. Boletim do Museu Paraense Emílio The impacts of shifting cultivation on tropical forest soil: a review Boletim do Museu Paraense Emílio Goeldi. *Ciências Humanas*, 8, pp. 693–727. http://www.redalyc.org/articulo.oa?id=394035001013

Iais, P. C., Bombelli, A., Williams, M., Piao, S. L., Chave, J., Ryan, C. M., Henry, M., Brender, P., and Valentini, R., 2011. The carbon balance of Africa: Synthesis of recent research studies. Philosophical Transactions of the Royal Society A: Mathematical, Physical and Engineering Sciences, 369(1943), pp. 2038–2057. https://doi.org/10.1098/rsta.2010.0328

Ibrahim, W., 2020. Greenhouse gas fluxes from land-use, land-use change from forests and smallholder based agricultural systems in East Africa, PhD thesis, International Livestock Research Institute (ILRI). November 2018. https://doi.org/10.13140/RG.2.2.29113.11369

Ingalls, M. L., and Dwyer, M. B., 2016. Missing the forest for the trees? Navigating the trade-offs between mitigation and adaptation under REDD. *Climatic Change*, 136(2), pp. 353–366. https://doi.org/10.1007/s10584-016-1612-6

IPCC., 2018. Global Warming of 1.5°C: An IPCC Special Report on the Impacts of Global Warming of 1.5°C Above Pre-industrial Levels and Related Global Greenhouse Gas Emission Pathways. https://www.ipcc.ch/sr15/

IPCC., I. P. On C. C., 2014. AR5 Climate Change 2014: Mitigation of Climate Change. In Managing the Risks of Extreme Events and Disasters to Advance Climate Change Adaptation: Special Report of the Intergovernmental Panel on Climate Change (Vol. 9781107025). https://doi.org/10.1017/CBO9781139177245.003

IPCC., 2006. Intergovernmental Panel on Climate Change 2006 IPCC Guidelines for National Greenhouse Gas inventories. In Institute for Global Environmental Strategies.

IPCC., 2007. Summary for Policymakers. In: Climate Change 2007: The Physical Science Basis. Contribution of Working Group I to the Fourth Assessment Report of the Intergovernmental Panel on Climate Change.

IPCC., 2019. Climate Change and Land: an IPCC special report on climate change, desertification, land degradation, sustainable land management, food security, and greenhouse gas fluxes in terrestrial ecosystems. In Intergovernmental Panel on Climate Change. https://doi.org/10.1002/9781118786352.wbieg0538

IPCC., 2021. Climate Change 2021 The Physical Science Basis Working. In Climate Change 2021 – The Physical Science Basis. https://doi.org/10.1017/9781009157896

Islam, S. M. M., Gaihre, Y. K., Islam, R., Akter, M., Al Mahmud, A., Singh, U., and Sander, B., 2020. Effects of water management on greenhouse gas emissions from farmers' rice fields in Bangladesh. *Science of the Total Environment*, 734. https://doi.org/10.1016/j.scitotenv.2020.139382

Issa, A. F. E., 2018. Assessment of the Vegetation Cover Change at Qala El-Nahal Locality - Gedaref State - Sudan [Sudan University of Science and Technology]. http://www.secheresse.info/spip.php?article97554

Jandl, R., Lindner, M., Vesterdal, L., Bauwens, B., Baritz, R., Hagedorn, F., Johnson, D. W., Minkkinen, K., and Byrne, K. A., 2007. How strongly can forest management influence soil carbon sequestration? *Geoderma*, 137(3), pp. 253–268. https://doi.org/10.1016/j.geoderma.2006.09.003

Jensen, J. R., 2015. Introductory Digital Image Processing A Remote Sensing Perspective. In J. R. Jensen (Ed.), News.Ge (4th Edition). Pearson Education Limited.

Kahmark, K., Millar, N., Robertson, G. P., and Kellogg, W. K., 2020. Static Chamber Method for Measuring Soil Greenhouse Gas Fluxes. *KBS LTER Special Publication*, pp. 1–15. http://doi.org/10.5281/zenodo.3629774

Kennedy, R. E., Yang, Z., and Cohen, W. B., 2010. Detecting trends in forest disturbance and recovery using yearly Landsat time series: 1. LandTrendr — Temporal segmentation

algorithms. *Remote Sensing of Environment*, 114(12), pp. 2897–2910. https://doi.org/10.1016/J.RSE.2010.07.008

Khan, S. A., Mulvaney, R. L., Ellsworth, T. R., and Boast, C. W., 2007. The Myth of Nitrogen Fertilization for Soil Carbon Sequestration. *Journal of Environmental Quality*, 36(6), pp. 1821–1832. https://doi.org/10.2134/jeq2007.0099

Kirschbaum, M. U., 2000. Will changes in soil organic carbon act as a positive or negative feedback on global warming? *Biogeochemistry*, 48, pp. 21–51. https://doi.org/10.1023/A:1006238902976

Kleemann, J., Baysal, G., Bulley, H. N. N., and Fürst, C., 2017. Assessing driving forces of land-use and land cover change by a mixed-method approach in north-eastern Ghana, West Africa. *Journal of Environmental Management*, 196, pp. 411–442. https://doi.org/10.1016/j.jenvman.2017.01.053

Kögel-Knabner, I., Amelung, W., Cao, Z., Fiedler, S., Frenzel, P., Jahn, R., Kalbitz, K., Kölbl, A., and Schloter, M., 2010. Biogeochemistry of paddy soils. *Geoderma*, 157(1–2), pp. 1–14. https://doi.org/10.1016/j.geoderma.2010.03.009

Kong, J., He, Z., Chen, L., Zhang, S., Yang, R., and Du, J., 2022. Elevational variability in and controls on the temperature sensitivity of soil organic matter decomposition in alpine forests. *Ecosphere*, 13(4), pp. 1–12. https://doi.org/10.1002/ecs2.4010

Koomson, E., 2013. Measurement of CO2 Emission from Bio-Char-Amended Rice Paddy Field in the Coastal Savannah Zone of Ghana. (Issue 10229856). University of Legon.

Koranteng, A., 2021. Multi-Temporal Study of Land-use Land Cover Changes. *International Journal of Environmental Sciences and Natural Resources*, 29(1). https://doi.org/10.19080/ijesnr.2021.29.556254

Koranteng, A., Adu-Poku, I., Donkor, E., and Zawiła-Niedźwiecki, T., 2020. Geospatial assessment of land-use and land cover dynamics in the mid-zone of Ghana. *Folia Forestalia Polonica, Series A*, 62(4), pp. 288–305. https://doi.org/10.2478/ffp-2020-0028

Koranteng, A., Adu-poku, I., and Zawila-niedzwiecki, T., 2017. Drivers of land-use change and carbon mapping in the Savannah area of Ghana Drivers of land-use change and carbon

mapping in the Savannah area of Ghana. *Folia Forestalia Polonica, Series A*, 59(4), pp. 287–311. https://doi.org/10.1515/ffp-2017-0031

Koranteng, A., Donkor, E., Zawila-Niedzwiecki, T., and Kombat, D., 2018. Synergies of Satellite Images for Forest Loss and Other Land-use Study in Ghana. International Conference on Applied Science and Technology Conference Proceedings, 4(1), pp. 211–228.

Koranteng, A., Zawiła-Niedźwiecki, T., and Kombat, D., 2015. Land-use dynamics in rural-urban environs : a study of the Kumasi metropolis and its adjoining districts – Ghana. *Teledetekcja Środowiska*, 52((2015/1)), pp. 67–85.

Kumar, Y. R., Kaushal, S., Kaur, G., and Gulati, D., 2020. Effect of soil organic matter on physical properties of soil. Applied Soil Mechanics, 1(October), pp. 1–20. https://doi.org/10.1002/9780470168097.ch1

Kutner, M. H., 2005. Applied Linear Statistical Models (5th Illust). McGraw-Hill Irwin. https://books.google.com.gh/books?id=0xqCAAAACAAJ

Kuzyakov, Y., 2006. Sources of CO_2 efflux from soil and review of partitioning methods. *Soil Biology and Biochemistry*, 38(3), pp. 425–448. https://doi.org/10.1016/j.soilbio.2005.08.020

Lal, R., 2004. Soil carbon sequestration impacts on global climate change and food security. *Science*, 304(5677), pp. 1623–1627. https://doi.org/10.1126/science.1097396

Lambers, H., and Oliveira, R. S., 2019. Photosynthesis, Respiration, and Long-Distance Transport: Respiration BT - Plant Physiological Ecology. In H. Lambers and R. S. Oliveira (Eds.), Plant Physiological Ecology (Third edit, pp. 115–172). Springer International Publishing. https://doi.org/10.1007/978-3-030-29639-1_3

Lambin, E. F., Geist, H. J., and Lepers, E., 2003. Dynamics of land-use and land-cover change in tropical regions. *Annual Review of Environment and Resources*, 28, pp. 205–241. https://doi.org/10.1146/annurev.energy.28.050302.105459

Lambin, E. F., Geist, H., McConnell, W., Moran, E., Alves, D., and Rudel, T., 2006. Causes and Trajectories of Land-Use/Cover Change. In Land-Use and Land-Cover Change. https://doi.org/10.1007/3-540-32202-7_3

Lambin, E. F., and Meyfroidt, P., 2011. Global land-use change, economic globalization, and the looming land scarcity. *Proceedings of the National Academy of Sciences of the United States of America*, 108(9), pp. 3465–3472. https://doi.org/10.1073/pnas.1100480108

Lambin, E., and Geist, H. J., 1997. Causes of land-use and land-cover change. Washington DC: Encyclopedia of Earth, Environmental Information Coalition, National Council for Science and the Environment, 61(2), pp. 181–200. https://doi.org/http://www.eoearth.org/article/Land-use_and_land-cover_change

Landis, J. R., and Koch, G. G., 1977. The Measurement of Observer Agreement for Categorical Data. *Biometrics*, 33(1), pp. 159–174. https://doi.org/10.2307/2529310

Landon, J. R., 1991. Booker tropical soil manual: A handbook for soil survey and agricultural land evaluation in the tropics and subtropics. (D. W. Hoffman (ed.)). Longman Scientific and Technical.

Laurance, W. F., 2013. Does research help to safeguard protected areas? *Trends in Ecology and Evolution*, 28(5), pp. 261–266. https://doi.org/10.1016/j.tree.2013.01.017

Laurance, W. F., Carolina Useche, D., Rendeiro, J., Kalka, M., Bradshaw, C. J. A., Sloan, S. P., Laurance, S. G., Campbell, M., Abernethy, K., Alvarez, P., Arroyo-Rodriguez, V., Ashton, P., Benítez-Malvido, J., Blom, A., Bobo, K. S., Cannon, C. H., Cao, M., Carroll, R., Chapman, C., Zamzani, F., 2012. Averting biodiversity collapse in tropical forest protected areas. *Nature*, 489(7415), pp. 290–294. https://doi.org/10.1038/nature11318

Lawrence, D., and Vandecar, K., 2015. Effects of tropical deforestation on climate and agriculture. *Nature Climate Change*, 5(1), pp. 27–36. https://doi.org/10.1038/nclimate2430

Le Quéré, C., Raupach, M. R., Canadell, J. G., Marland, G., Bopp, L., Ciais, P., Conway, T. J., Doney, S. C., Feely, R. A., Foster, P., Friedlingstein, P., Gurney, K., Houghton, R. A., House, J. I., Huntingford, C., Levy, P. E., Lomas, M. R., Majkut, J., Metzl, N.,

Woodward, F. I., 2009. Trends in the sources and sinks of carbon dioxide. *Nature Geoscience*, 2(12), pp. 831–836. https://doi.org/10.1038/ngeo689

Li, X., Zhou, W., and Ouyang, Z., 2013. Forty years of urban expansion in Beijing: What is the relative importance of physical, socioeconomic, and neighbourhood factors? *Appl. Geogr.*, 38, pp. 1–10. https://doi.org/10.1016/j.apgeog.2012.11.004.

Li, Y., Li, L., Dong, J., and Bai, J., 2021. Assessing MODIS carbon and water fluxes in grasslands and shrublands in semiarid regions using eddy covariance tower data. *International Journal of Remote Sensing*, 42(2), pp. 595–616. https://doi.org/10.1080/01431161.2020.1811915

Liaw, A., and Wiener, M., 2002. Classification and Regression by RandomForest. *R News*, 2(3), pp. 18–22.

Lillesand, T. M., Kiefer, R. W., and Chipman, J. W., 2015. Remote Sensing and Image Interpretation. 7th Edition. In T. M. Lillesand, R. W. Ralph, and J. W. Chipman (Eds.), Photogrammetric Engineering and Remote Sensing (7th ed., Vol. 81, Issue 8). John Wiley and Sons, Inc. https://doi.org/10.14358/pers.81.8.615

Lima, J. R. S., Souza, R. M. S., Santos, E. S., Souza, E. S., Oliveira, J. E. S., Medeiros, E. V., Pessoa, L. G. M., Antônio, A. C. D., and Hammecker, C., 2020. Impacts of land-use changes on soil respiration in the semi-arid region of Brazil. *Revista Brasileira de Ciência Do Solo*, 44, pp. 1–19. https://doi.org/10.36783/18069657rbcs20200092

Liping, C., Yujun, S., and Saeed, S., 2018. Monitoring and predicting land-use and land cover changes using remote sensing and GIS techniques: A case study of a hilly area, Jiangle, China. *PLOS ONE*, 13(7). https://doi.org/10.1371/journal.pone.0200493

Liu, W., Zhang, Z., and Wan, S., 2009. Predominant role of water in regulating soil and microbial respiration and their responses to climate change in a semiarid grassland. *Global Change Biology*, 15(1), pp. 184–195. https://doi.org/10.1111/j.1365-2486.2008.01728.x

Liu, X., Wang, S., Zhuang, Q., Jin, X., Bian, Z., Zhou, M., Meng, Z., Han, C., Guo, X., Jin, W., and Zhang, Y., 2022. A Review on Carbon Source and Sink in Arable Land Ecosystems. *Land*, 11(4), pp. 1–17. https://doi.org/10.3390/land11040580

Liu, X., Zhang, W., Zhang, B., Yang, Q., Chang, J., and Hou, K., 2016. Diurnal variation in soil respiration under different land-uses on Taihang Mountain, North China. *Atmospheric Environment*, 125, pp. 283–292. https://doi.org/10.1016/j.atmosenv.2015.11.034

Liu, Y., Wang, C., and Li, X., 2018. Using Random Forest Regression for CO2 Emission Estimation in Forest Ecosystems. *Science of the Total Environment*, 6(15), pp. 370–378.

Lloyd, J., and Taylor, J. A., 1994. On the Temperature Dependence of Soil Respiration Author (s): J. Lloyd and J. A. Taylor Published by: British Ecological Society Stable URL: http://www.jstor.org/stable/2389824 references linked references are available on jstor for this article : Functional Ecology, 8(3), pp. 315–323.

Lu, D., Mausel, P., Brondízio, E., and Moran, E., 2004. Change detection techniques. *International Journal of Remote Sensing*, 25(12), pp. 2365–2401. https://doi.org/10.1080/0143116031000139863

Lu, D., and Weng, Q., 2007. A survey of image classification methods and techniques for improving classification performance. *International Journal of Remote Sensing*, 28(5), pp. 823–870. https://doi.org/10.1080/01431160600746456

Luedeling, E., Girvetz, E. H., Semenov, M. A., and Brown, P. H., 2014. Climate change affects African agriculture through high temperatures. *Proceedings of the National Academy of Sciences*, 111(8), pp. 3223–3228.

Lui, G. V., and Coomes, D. A., 2016. Tropical nature reserves are losing their buffer zones , but leakage is not to blame. *Environmental Research*, 147, pp. 580–589. https://doi.org/10.1016/j.envres.2015.11.008

Luo, Y., and Zhou, X., 2006. CHAPTER 1 - Introduction and Overview. In Y. Luo and X. B. T.-S. R. and the E. Zhou (Eds.), Soil Respiration and the Environment (pp. 3–15). Academic Press. https://doi.org/10.1016/B978-012088782-8/50001-2

Ma, K., and Lu, Y., 2011. Regulation of microbial methane production and oxidation by intermittent drainage in rice field soil. *FEMS Microbiology Ecology*, 75(3), pp. 446–456. https://doi.org/10.1111/j.1574-6941.2010.01018.x

Maccarthy, D. S., Zougmoré, R. B., Akponikpè, P. B. I., Koomson, E., Savadogo, P., and Adiku, S. G. K., 2018. Assessment of Greenhouse Gas Emissions from Different Land-Use Systems: A Case Study of CO_2 in the Southern Zone of Ghana. *Applied and Environmental Soil Science*, 2018. https://doi.org/10.1155/2018/1057242

Maeda, E. E., Clark, B. J. F., Pellikka, P., and Siljander, M., 2010. Modelling agricultural expansion in Kenya's Eastern Arc Mountains biodiversity hotspot. *Agricultural Systems*, 103(9), pp. 609–620. https://doi.org/10.1016/j.agsy.2010.07.004

Maeda, E. E., Pellikka, P. K. E., Siljander, M., and Clark, B. J. F., 2010. Potential impacts of agricultural expansion and climate change on soil erosion in the Eastern Arc Mountains of Kenya. *Geomorphology*, 123(3–4), pp. 279–289. https://doi.org/10.1016/j.geomorph.2010.07.019

Manandhar, R., Odeh, I. O. A., and Pontius, R. G., 2010. Analysis of twenty years of categorical land transitions in the Lower Hunter of New South Wales, Australia. *Agriculture, Ecosystems and Environment*, 135(4), pp. 336–346. https://doi.org/10.1016/j.agee.2009.10.016

Manu, E. A., 2023. Soil respiration in a forest and adjoining cocoa agroforests in a moist semi-deciduous forest of Ghana, MPhil, College of Science and Technology. CSIR College of Science and Technology, Kumasi.

Manzoor, S. A., Griffiths, G. H., Robinson, E., Shoyama, K., and Lukac, M., 2022. Linking Pattern to Process : Intensity Analysis of Land-Change Dynamics in Ghana as Correlated to Past Socioeconomic and Policy Contexts. Land, 11(1070), pp. 1–16.

Mark, M., and Kudakwashe, M., 2010. Rate of land-use/cover changes in Shurugwi District, Zimbabwe: drivers for change. *Journal of Sustainable Development in Africa*, 12(3), pp. 107–121. https://www.researchgate.net/publication/268370671_Rate_of_land-useland-cover_changes_in_Shurugwi_district_Zimbabwe_drivers_for_change

Marshall, G. J., Dowdeswell, J. A., and Rees, W. G., 1994. The spatial and temporal effect of cloud cover on the acquisition of high quality Landsat imagery in the European Arctic

sector. *Remote Sensing of Environment*, 50(2), pp. 149–160. https://doi.org/10.1016/0034-4257(94)90041-8

Mas, J. F., Kolb, M., Paegelow, M., Camacho Olmedo, M. T., and Houet, T., 2014. Inductive pattern-based land-use/cover change models: A comparison of four software packages. *Environmental Modelling and Software*, 51, pp. 94–111. https://doi.org/10.1016/j.envsoft.2013.09.010

Mboyerwa, P. A., Kibret, K., Mtakwa, P., and Aschalew, A., 2022. Greenhouse gas emissions in irrigated paddy rice as influenced by crop management practices and nitrogen fertilization rates in eastern Tanzania. *Frontiers in Sustainable Food Systems*, 6. https://doi.org/10.3389/fsufs.2022.868479

Meyfroidt, P., Lambin, E. F., Erb, K. H., and Hertel, T. W., 2013. Globalization of land-use: Distant drivers of land change and geographic displacement of land-use. *Current Opinion in Environmental Sustainability*, 5(5), pp. 438–444. https://doi.org/10.1016/j.cosust.2013.04.003

Mishra, S., Sarkar, U., Taraphder, S., Datta, S., Swain, D. P., Saikhom, R., Pandan, S., and Laishram, M., 2017. Multivariate Statistical Data Analysis - Principal Component Analysis (PCA). *International Journal of Livestock Research*, 7(5), 19. https://doi.org/10.5455/ijlr.20170415115235

Mo, J., Zhang, W., Zhu, W., Fang, Y., Li, D., and Zhao, P., 2007. Response of soil respiration to simulated N deposition in a disturbed and rehabilitated tropical forest in southern China. *Plant and Soil*, 296(1–2), pp. 125–135. https://doi.org/10.1007/s11104-007-9303-8

Mohd Hasmadi, I., Pakhriazad, H. Z., and Shahrin, M. F., 2009. Evaluating supervised and unsupervised techniques for land cover mapping using remote sensing data. *Malaysian Journal of Society and Space*, 5(1), pp. 1–10.

Monserud, R. A., and Leemans, R., 1992. Comparing global vegetation maps with the Kappa statistic. *Ecological Modelling*, 62(4), 275–293. https://doi.org/10.1016/0304-3800(92)90003-W

Montzka, S. A., Dlugokencky, E. J., and Butler, J. H., 2011. Non-CO2 greenhouse gases and climate change. *Nature*, 476(7358), pp. 43–50. https://doi.org/10.1038/nature10322

Moriaque, A. T., Félix, K. A., Pascal, H., Hessou, A. A., Moncef, B., Naivo, R., Emil, F., and Lionel, M., 2020. Soil erosion risk mapping using Rusle, GIS and Remote Sensing: A case study of the watershed of Zou, centre of Benin. 1(6), pp. 281–290. https://doi.org/10.5897/JSSEMXXXXXXX

Moriasi, D.N., Gitau, M.W., Pai, N. and Daggupati, P., 2015. Hydrologic and water quality models: Performance measures and evaluation criteria. *Transactions of the ASABE*, *58*(6), pp.1763-1785.

Motsara, M. R., and Roy, R. N., 2008. Guide to laboratory establishment for plant nutrient analysis, Food and Agriculture Organization of United Nations Rome. In Fao Fertilizer and Plant Nutrition Bulletin 19. FAO, Rome.

Müller, K., Steinmeier, C., and Küchler, M., 2010. Urban growth along motorways in Switzerland. *Landscape Urban Planning*, 98(1), pp. 3–12. https://doi.org/10.1016/j.landurbplan.2010.07.004 .

Mwangi, H. M., Lariu, P., Julich, S., Patil, S. D., McDonald, M. A., and Feger, K. H., 2017. Characterizing the intensity and dynamics of land-use change in the Mara River Basin, East Africa. *Forests*, 9(1), pp. 1–17. https://doi.org/10.3390/f9010008

Nasser, F., Maguire-Rajpaul, V. A., Dumenu, W. K., and Wong, G. Y., 2020. Climate-Smart Cocoa in Ghana: How Ecological Modernisation Discourse Risks Side-Lining Cocoa Smallholders. *Frontiers in Sustainable Food Systems*, 4(May), pp. 1–17. https://doi.org/10.3389/fsufs.2020.00073

Nelson, D. W., and Sommers, L. W., 1982. Total carbon and organic matter. In A. L. Page, R. H. Miller, and D. R. Keeney (Eds.), Methods of soil analysis Part 2 (2nd ed., Vol. 84, Issue 0, pp. 456–462). No.9. American Society of Agronomy. Soil Science of America.

Neya, O., Neya, T., Abunyewa, A. A., Zoungrana, B. J. B., Tiendrebeogo, H., Dimobe, K., and Korahire, J. A., 2020. Land-use Land Cover Dynamics and Farmland Intensity

Analysis at Ouahigouya Municipality of Burkina Faso, West Africa. *American Journal of Climate Change*, 09(01), pp. 23–33. https://doi.org/10.4236/ajcc.2020.91003

Nguyen, A. T., and Hens, L., 2019. Human ecology of climate change hazards in Vietnam: Risks for nature and humans in lowland and upland areas. In J. D. Memai (Ed.), Springer Climate. Springer International Publishing AG.

Nieveen, J. P., Campell, D. I., Schipper, L. A., and Blair, I. J., 2005. Carbon exchange of grazed pasture on drained peat soil. *Global Change Biology*, 11(4), pp. 607–618. https://doi.org/10.1111/j.1365-2486.2005.00929.x

Nyamekye, C., Kwofie, S., Ghansah, B., Agyapong, E., and Boamah, L. A., 2020. Assessing urban growth in Ghana using machine learning and intensity analysis: A case study of the New Juaben Municipality. *Land-use Policy*, 99(2020). https://doi.org/10.1016/J.LANDUSEPOL.2020.105057

Oduro Appiah, J., Agyemang-Duah, W., Sobeng, A. K., and Kpienbaareh, D., 2021. Analysing patterns of forest cover change and related land-uses in the Tano-Offin forest reserve in Ghana: Implications for forest policy and land management. *Trees, Forests and People*, 5, 100105. https://doi.org/10.1016/j.tfp.2021.100105

Oduro, K. A., 2016. Ghana's high forests: trends, scenarios and pathways for future developments (K. A. Oduro (ed.)). https://doi.org/DOI 10.18174/378343

Oechel, W. C., Laskowski, C. A., Burba, G., Gioli, B., and Kalhori, A. A. M., 2014. Annual patterns and budget of CO_2 flux in an Arctic tussock tundra ecosystem. *Journal of Geophysical Research: Biogeosciences*, 119(3), pp. 323–339. https://doi.org/10.1002/2013JG002431

Offiong, R. A., and Iwara, A. I., 2012. Effects of Fallow Genealogical Cycles on the Build-up of Nutrients in Soils of the Cross River Rainforest, South-Southern Nigeria. *Ethiopian Journal of Environmental Studies and Management*, 4(4), pp. 84–95. https://doi.org/10.4314/ejesm.v4i4.10

Oorts, K., Merckx, R., Gréhan, E., Labreuche, J., and Nicolardot, B., 2007. Determinants of annual fluxes of CO_2 and N_2O in long-term no-tillage and conventional tillage systems

in northern France. *Soil and Tillage Research*, 95(1), pp. 133–148. https://doi.org/10.1016/j.still.2006.12.002

OpenGenus, I., 2022. Basics of Image Classification Techniques in Machine Learning. Computing Expertise and Legacy. https://iq.opengenus.org/basics-of-machine-learning-image-classification-techniques/

Owusu-Prempeh, N., Amekudzi, L.K. and Kyereh, B., 2024. Assessment of soil carbon dioxide efflux from contrasting land-uses in a semi-arid savannah ecosystem, northeastern Ghana (West Africa). *Scientific African*, 26, p.e02420. https://doi.org/10.1016/j.sciaf.2024.e02420

Owusu, P. A., and Asumadu-Sarkodie, S., 2017. Is there a causal effect between agricultural production and carbon dioxide emissions in Ghana? *Environmental Engineering Research*, 22(1), pp. 40–54. https://doi.org/10.4491/eer.2016.092

Pachauri, R. K., and Meyer, L. A., 2014. Climate Change 2014: Synthesis Report. Contribution of Working Groups I, II and III to the Fifth Assessment Report of the Intergovernmental Panel on Climate Change. IPCC New York, NY, USA.

Panwar, S., and Malik, D. S., 2017. Evaluating Land-use/Land Cover Change Dynamics in Bhimtal Lake Catchment Area, Using Remote Sensing and GIS Techniques. *Journal of Remote Sensing and GIS*, 06(02), pp. 4–7. https://doi.org/10.4172/2469-4134.1000199

Parkin, T. B., Doran, J. W., and Franco-Vizcaíno, E., 1997. Field and laboratory tests of soil respiration. *Methods for Assessing Soil Quality*, 49, pp. 231–245.

Parkin, T. B., and Kaspar, T. C., 2003. Temperature Controls on Diurnal Carbon Dioxide Flux. *Soil Science Society of America Journal*, 67(6), pp. 1763–1772. https://doi.org/10.2136/sssaj2003.1763

Paustian, K., Lehmann, J., Ogle, S., Reay, D., Robertson, G. P., and Smith, P., 2016. Climate-smart soils. *Nature*, 532(7597), pp. 49–57. https://doi.org/10.1038/nature17174

Perumal, K., and Bhaskaran, R., 2010. Supervised Classification Performance of Multispectral Images. *Journal of Computing*, 2(2). https://doi.org/10.48550/arXiv.1002.4046

Pervez, W., Uddin, V., Khan, S. A., and Khan, J. A., 2016. Satellite-based land-use mapping: comparative analysis of Landsat-8, Advanced Land Imager, and big data Hyperion imagery. *Appl. Remote Sens*, 10(2), 26004. https://doi.org/10.1117/1.JRS.10.026004

Peters, M. K., 2019. Assessing land-use and land cover change in the keta municipality of ghana using remote sensing, MSc thesis, University of Ghana. www.ugspace.ug.edu.gh

Pingintha-Durden, N., Chayawat, C., Hong, J., and LeClerc, M., 2007. Y. Luo and X. Zhou, Soil Respiration and the Environment, Academic Press, An Imprint of Elsevier Science, London (2006) ISBN 0-12-088782-7. Agricultural and Forest Meteorology, 144(March 2019), pp. 243–244. https://doi.org/10.1016/j.agrformet.2007.01.008

Pontius, G. R., and Malanson, J., 2005. Comparison of the structure and accuracy of two land change models. *International Journal of Geographical Information Science*, 19(2), pp. 243–265. https://doi.org/10.1080/13658810410001713434

Pontius Jr, R. G., and Millones, M., 2011. Death to Kappa: birth of quantity disagreement and allocation disagreement for accuracy assessment. *International Journal of Remote Sensing*, 32(15), pp. 4407–4429. https://doi.org/10.1080/01431161.2011.552923

Pontius, R. G., Shusas, E., and McEachern, M., 2004. Detecting important categorical land changes while accounting for persistence. *Agriculture, Ecosystems and Environment*, 101(2–3), pp. 251–268. https://doi.org/10.1016/j.agee.2003.09.008

Prabhu, S., and Kulkarni, N., 2012. Biodiversity and Conservation of Coastal and Marine Ecosystems of India. In IUCN. University of Mumbai.

Prasetyo, L. B., Setiawan, Y., and Nursal, W., 2009. The Analysis of the Landcover Change Effect to Soil Erosion Using Spatial Modeling and Analysis (As a Key for Land-use Planning in Telaga Warna Catchment Area). *Center For Environmental Research*, 13, 15. http://repository.ipb.ac.id/handle/123456789/21544

Pumpanen, J., Kolari, P., Ilvesniemi, H., Minkkinen, K., Vesala, T., Niinistö, S., Lohila, A., Larmola, T., Morero, M., Pihlatie, M., Janssens, I., Yuste, J. C., Grünzweig, J. M., Reth, S., Subke, J. A., Savage, K., Kutsch, W., Østreng, G., Ziegler, W., Hari, P., 2004.

Comparison of different chamber techniques for measuring soil CO_2 efflux. *Agricultural and Forest Meteorology*, 123(3–4), pp. 159–176. https://doi.org/10.1016/j.agrformet.2003.12.001

Qader, S. H., 2016. Monitoring decadal land cover and crop production in Iraq using time series remote sensing data (Issue September). University of Southampton.

Qian, Y., Zhou, W., Yan, J., Li, W., and Han, L., 2015. Comparing Machine Learning Classifiers for Object-Based Land Cover Classification Using Very High-Resolution Imagery. *Remote Sensing*, 7(1), pp. 153–168. https://doi.org/10.3390/rs70100153

Quansah, E., Mauder, M., Balogun, A. A., Amekudzi, L. K., Hingerl, L., Bliefernicht, J., and Kunstmann, H., 2015. Carbon dioxide fluxes from contrasting ecosystems in the Sudanian Savanna in West Africa. *Carbon Balance and Management*, 10(1), pp. 1–17. https://doi.org/10.1186/s13021-014-0011-4

Rai, R., Zhang, Y., Paudel, B., Li, S., and Raj Khanal, N., 2017. A Synthesis of Studies on Land-use and Land Cover Dynamics during 1930-2015 in Bangladesh. *Sustainability*, 9(1899). https://doi.org/10.3390/su9101866

Raich, J. W., and Schlesinger, W. H., 1992. The global carbon dioxide flux in soil respiration and its relationship to vegetation and climate. Tellus, Series B: Chemical and Physical Meteorology, 44(2), pp. 81–00. https://doi.org/10.3402/tellusb.v44i2.15428

Raich, J. W., and Tufekcioglu, A., 2000. Vegetation and soil respiration: Correlations and controls. *Biogeochemistry*, 48(1), pp. 71–90. https://doi.org/10.1023/A:1006112000616

Ramesh, T., Bolan, N. S., Kirkham, M. B., Wijesekara, H., Kanchikerimath, M., Cherukumalli, S. R., Sandeep, S., Rinklebe, J., Yong Sik Ok, C. B., U., Wang, H., Tang, C., Wang, X., Song, Z., and Freeman, O. W., 2019. Soil organic carbon dynamics: Impact of land-use changes and management practices: A review. *Advances in Agronomy*, 156, pp. 1–107. https://doi.org/10.1016/bs.agron.2019.02.001

Republic of Ghana., 2021. Ghana's Updated Nationally Determined Contribution (NDC) to the UNFCCC. https://www4.unfccc.int/sites/ndcstaging/PublishedDocuments/Ghana First/Ghana's UpdatedNDCtotheUNFCCC.pdf

Rodrigues, C. I. D., Brito, L. M., and Nunes, L. J. R., 2023. Soil Carbon Sequestration in the Context of Climate Change Mitigation: A Review. *Soil Systems*, 7(3), pp. 1–21. https://doi.org/10.3390/soilsystems7030064

Rodrigues, H., and Soares-Filho, B., 2018. A Short Presentation of Dinamica EGO. Lecture Notes in Geoinformation and Cartography, pp. 493–498. https://doi.org/10.1007/978-3-319-60801-3_35

Sanfilippo, M., Akampulira, E., Mohase, A., Okonkwo, H., Ouyoumb, P., Tumber, R., Walmsley, J., and Rayment, M., 2017. Reduced Impact Logging and Silvicultural Interventions in Ghana: The Case of Bobiri Forest Reserve. *International Forestry Review*, 19(3), 369–380. https://doi.org/10.1505/146554817821865090

Schaldach, R., Alcamo, J., Koch, J., Kölking, C., Lapola, D. M., Schüngel, J., and Priess, J. A., 2011. An integrated approach to modelling land-use change on continental and global scales. *Environmental Modelling and Software*, 26(8), pp. 1041–1051. https://doi.org/10.1016/j.envsoft.2011.02.013

Schimel, D. S., 2014. Terrestrial Ecosystems and the Carbon Cycle. *Global Change Biol.*, 1(December 1994), pp. 77–91. https://doi.org/doi:10.1111/j.1365-2486.1995.tb00008.x

Schlesinger, W. H., and Andrews, J. A., 2000. Soil respiration and the global carbon cycle. *Biogeochemistry*, 48(1), pp. 7–20. https://doi.org/10.1023/A:1006247623877

Shehzad, K., Qamer, F. M., Murthy, M. S. R., Abbas, S., and Bhatta, L. D., 2014. Deforestation trends and spatial modelling of its drivers in the dry temperate forests of northern Pakistan — A case study of Chitral. *Journal of Mountain Science*, 11(5), pp. 1192–1207. https://doi.org/10.1007/s11629-013-2932-x

Shoyama, K., Braimoh, A. K., Avtar, R., and Saito, O., 2018. Land Transition and Intensity Analysis of Cropland Expansion in Northern Ghana. *Environmental Management*, 62(5), pp. 892–905. https://doi.org/10.1007/s00267-018-1085-7

Sileshi, G. W., 2014. A critical review of forest biomass estimation models, common mistakes and corrective measures. *Forest Ecology and Management*, 329, pp. 237–254. https://doi.org/10.1016/j.foreco.2014.06.026

Silva, S. R., Silva, I. R., Barros, N. F., and Sá Mendonça, E., 2011. Effect of compaction on microbial activity and carbon and nitrogen transformations in two oxisols with different mineralogy. *Revista Brasileira de Ciência Do Solo*, 35(4), pp. 1141–1149. https://doi.org/10.1590/s0100-06832011000400007

Singh, P., Kikon, N., and Verma, P., 2017. Impact of land-use change and urbanization on urban heat island in Lucknow city, Central India. A remote sensing-based estimate. *Sustainable Cities and Society*, 32, pp. 100–114. https://doi.org/10.1016/J.SCS.2017.02.018

Singh, S. K., Mustak, S., Srivastava, P. K., Szabó, S., and Islam, T., 2015. Predicting Spatial and Decadal LULC Changes Through Cellular Automata Markov Chain Models Using Earth Observation Datasets and Geo-information. *Environ. Process*, 2(1), pp. 61–78. https://doi.org/10.1007/s40710-015-0062-x

Smith, P., Calvin, K., Nkem, J., Campbell, D., Cherubini, F., Grassi, G., Korotkov, V., Hoang, A. L., Lwasa, S., McElwee, P., Nkonya, E., Saigusa, N., Soussana, J. F., Taboada, M. A., Manning, F., Nampanzira, D., Arias-Navarro, C., Vizzarri, M., House, J., Arneth, A., 2020. Which practices co-deliver food security, climate change mitigation and adaptation, and combat land-degradation and desertification? *Global Change Biology*, 26(3), pp. 1532–1575. https://doi.org/https://doi.org/10.1111/gcb.14878

Smith, P., 2008. Soil Organic Carbon Dynamics and Land-Use Change BT - Land-use and Soil Resources. In A. K. Braimoh and P. L. G. Vlek (Eds.), Land-use and Soil Resources (pp. 9–22). Springer Netherlands. https://doi.org/10.1007/978-1-4020-6778-5_2

Smith, P., Bustamante, M., Ahammad, H., Clark, H., Dong, H., Elsiddig, E. A., Haberl, H., Harper, R., House, J., Jafari, M., Masera, O., Mbow, C., Ravindranath, N. H., Rice, C. W., Robledo Abad, C., Romanovskaya, A., Sperling, F., and Tubiello, F. N., 2014. Agriculture, forestry and other land-use (AFOLU). In O. Edenhofer, R. Pichs-Madruga, Y. Sokona, E. Farahani, S. Kadner, K. Seyboth, A. Adler, I. Baum, S. Brunner, P. Eickemeier, B. Kriemann, J. Savolainen, S. Schlömer, C. von Stechow, T. Zwickel, and J. C. Minx (Eds.), Climate Change 2014: Mitigation of Climate Change. Contribution of Working Group III

to the Fifth Assessment Report of the Intergovernmental Panel on Climate Change (pp. 433–456). Cambridge University Press. https://doi.org/10.4337/9781839101595.00025

Soares-Filho, B. S., Cerqueira, G. C., and Pennachin, C. L., 2002. DINAMICA - a stochastic cellular automata model designed to simulate the landscape dynamics in an Amazonian colonization frontier. Ecological Modelling, 154, pp. 217–235. d:%5CVEILLE~1%5CPDFBIB%5CSOARES-FILHOandAL2002EM.PDF

Soares-Filho, B. S., Coutinho Cerqueira, G., and Lopes Pennachin, C., 2002. DINAMICA - A stochastic cellular automata model designed to simulate the landscape dynamics in an Amazonian colonization frontier. *Ecological Modelling*, 154(3), pp. 217–235. https://doi.org/10.1016/S0304-3800(02)00059-5

Soares-Filho, B. S., Rodrigues, H. O., Costa, W. L., and Schlesinger, P., 2010. Dinamica_EGO_guidebook (W. L. S. C. Britaldo Silveira Soares-Filho, Hermann Oliveira Rodrigues (ed.); 2ed ed.). Belo Horizonte: Britaldo Silveira Soares-Filho. http://www.lapa.ufscar.br/geotecnologias-1/Dinamica_EGO_guidebook.pdf

Song, X., Peng, C., Zhao, Z., Zhang, Z., Guo, B., Wang, W., Jiang, H., and Zhu, Q., 2014. Quantification of soil respiration in forest ecosystems across China. *Atmospheric Environment*, 94, pp. 546–551. https://doi.org/10.1016/j.atmosenv.2014.05.071

Srivastava, P. K., Singh, S. K., Gupta, M., Thakur, J. K., and Mukherjee, S., 2013. Environmental Engineering and Management. *Environmental Engineering and Management Journal*, 12(12), pp. 2343–2355. https://doi.org/10.30638/eemj.2013.287

Stavi, I., and Lal, R., 2013. Agriculture and greenhouse gases, a common tragedy. A review. *Agronomy for Sustainable Development*, 33(2), pp. 275–289. https://doi.org/10.1007/s13593-012-0110-0

Sterman, J. D., 2002. Massachusetts institute of technology. *Journal of Chemical Education*, January 2000. https://doi.org/10.1021/ed025p187

Subke, J. A., Inglima, I., and Cotrufo, M. F., 2006. Trends and methodological impacts in soil CO2 efflux partitioning: A meta-analytical review. *Global Change Biology*, 12(6), pp. 921–943. https://doi.org/10.1111/j.1365-2486.2006.01117.x

Sutherland, C., Hare, D., Johnson, P.J., Linden, D.W., Montgomery, R.A. and Droge, E., 2023. Practical advice on variable selection and reporting using Akaike information criterion. *Proceedings of the Royal Society B*, *290*(2007), p.20231261.

Tekbox Digital Solutions., 2024. Air Humidity, Temperature and Barometric Pressure Sensor Manual.https://doi.org/chrome-extension://efaidnbmnnnibpcajpcglclefindmkaj/https://www.tekbox.com/product/TBSHTP05_manual.pdf

Tekle, K., and Hedlund, L., 2000. Land cover changes between 1958 and 1986 in Kalu District, Southern Wello, Ethiopia. *Mountain Research and Development*, 20(1), pp. 42–51. https://doi.org/10.1659/0276-4741(2000)020[0042:LCCBAI]2.0.CO;2

Tempfli, K., Kerle, N., Huurneman, G. C., Janssen, L. L. F., Bakker, W. H., Feringa, W., Gieske, A. S. M., Gorte, B. G. H., Grabmaier, K. A., Hecker, C. A., Horn, J. A., Huurneman, G. C., Janssen, L. L. F., Kerle, N., Meer, F. D., Parodi, G. N., Pohl, C., Reeves, C. V., Ruitenbeek, F. J., Woldai, T., 2009. Principles of Remote Sensing An introductory textbook. In K. Tempfli, N. Kerle, G. C. Huurneman, and L. L. F. Janssen (Eds.), The International Institute for Geo-Information Science and Earth Observation (ITC). The International Institute for Geo-Information Science and Earth Observation (ITC). https://webapps.itc.utwente.nl/librarywww/papers_2009/general/principlesremotesensing.pdf

Théau, J., 2008. Change Detection (S. Shekhar and H. Xiong (eds.)). Encyclopedia of GIS. Springer, Boston. https://doi.org/10.1007/978-0-387-35973-1_129

Tiao, G. C., Draper, N. R., and Smith, H., 1998. Applied Regression Analysis. Revue de l'Institut International de Statistique / Review of the International Statistical Institute, 36(1), 104. https://doi.org/10.2307/1401351

Todisco, F., Vergni, L., Vinci, A., and Torri, D., 2022. Infiltration and bulk density dynamics with simulated rainfall sequences. CATENA, 218, 106542. https://doi.org/10.1016/j.catena.2022.106542

Toku, A., Osumanu, I. K., Owusu-Sekyere, E., and Amoah, S. T., 2021. Conflicting urban land-uses at the fringes: issues and experiences of peri-urban farmers in an urbanising city in Ghana. *SN Social Sciences*, 1(7), pp. 1–23. https://doi.org/10.1007/s43545-021-00136-3

Tong, R., Ji, B., Wang, G. G., Lou, C., Ma, C., Zhu, N., Yuan, W., and Wu, T., 2024. Canopy gap impacts on soil organic carbon and nutrient dynamic: a meta-analysis. Annals of Forest Science, 81(1). https://doi.org/10.1186/s13595-024-01224-z

Turner, B. L., Lambin, E. F., and Reenberg, A., 2007. The Emergence of Land Change Science for Global Environmental Change and Sustainability. *Proceedings of the National Academy of Sciences of the United States of America*, 104(52), pp. 20666–20671. http://www.jstor.org/stable/25450958

Turner, B. L., Skole, D., Sanderson, S., Fischer, G., Fresco, L., and Leemans, R., 1995. Land-use and land-cover change: Science/research plan. Stockholm: International Geosphere-Biosphere Programme. International Geosphere-Biosphere Program "Global Changes."

UN-REDD., 2008. Halting deforestation can reduce CO_2 emissions by more than 4 gigatons a year. United Nations. www.un-redd.org

UN., 2022. World Population Prospects 2022. United Nation, 9, pp. 1–52. www.un.org/development/desa/pd/.

UNDP., 2022. Environment and Climate Change in Ghana: Policy Brief. United Nations. https://www.undp.org/ghana/publications/environment-and-climate-change-ghana-policy-brief

Vaisala., 2024. VAISALA: Industrial Measurements. https://www.vaisala.com/en/products/instruments-sensors-and-other-measurement-devices/instruments-industrial-measurements/gmp252#:~:text=Theoperatingtemperaturerangeis,dynamicallyoutdoorCO_2levels .

Veldkamp, E., Becker, A., Schwendenmann, L., Clark, D. J. A., and Schulte-Bisping, H., 2003. Substantial labile carbon stocks and microbial activity in deeply weathered soils

below a tropical wet forest. *Global Change Biology*, 9(8), pp. 1171–1184. https://doi.org/10.1046/j.1365-2486.2003.00656.x

Venkateswaran, C. J., Vijaya, R., and Saravanan, A. M., 2013. A fuzzy-based approach to classify remotely sensed images. International Journal of Engineering and Technology, 5(3), pp. 3051–3055.

Verburg, P. H., Erb, K. H., Mertz, O., and Espindola, G., 2013. Land System Science: between global challenges and local realities. *Current Opinion in Environmental Sustainability*, 5(5), pp. 433–437. https://doi.org/10.1016/j.cosust.2013.08.001

Verburg, P. H., Soepboer, W., Veldkamp, A., Limpiada, R., Espaldon, V., and Mastura, S. S. A., 2002. Modelling the spatial dynamics of regional land-use: The CLUE-S model. *Environmental Management*, 30(3), pp. 391–405. https://doi.org/10.1007/s00267-002-2630-x

Versace, V. L., Ierodiaconou, D., Stagnitti, F., and Hamilton, A. J., 2008. Appraisal of random and systematic land cover transitions for regional water balance and revegetation strategies. *Agriculture, Ecosystems and Environment*, 123(4), pp. 328–336. https://doi.org/10.1016/j.agee.2007.07.012

Vicca, S., Luyssaert, S., Peñuelas, J., Campioli, M., Chapin, F. S., Ciais, P., Heinemeyer, A., Högberg, P., Kutsch, W. L., Law, B. E., Malhi, Y., Papale, D., Piao, S. L., Reichstein, M., Schulze, E. D., and Janssens, I. A., 2012. Fertile forests produce biomass more efficiently. *Ecology Letters*, 15(6), pp. 520–526. https://doi.org/10.1111/j.1461-0248.2012.01775.x

Vitousek, P. M., Aber, J. D., Howarth, R. W., Likens, G. E., Matson, P. A., Schindler, D. W., Schlesinger, W. H., and Tilman, D. G., 1997. Human alteration of the global nitrogen cycle: Sources and consequences. *Ecological Applications*, 7(3), pp. 737–750. https://doi.org/10.1890/1051-0761(1997)007[0737:HAOTGN]2.0.CO;2

Wang, Y., Xie, Y., Rapson, G., Ma, H., Jing, L., Zhang, Y., Zhang, J., and Li, J., 2021. Increased precipitation enhances soil respiration in a semi-arid grassland on the Loess Plateau, China. PeerJ, 9, e10729. https://doi.org/10.7717/peerj.10729

Wanyama, I., Pelster, D. E., Butterbach-Bahl, K., Verchot, L. V., Martius, C., and Rufino, M. C., 2019. Soil carbon dioxide and methane fluxes from forests and other land-use types in an African tropical montane region. *Biogeochemistry*, 143(2), pp. 171–190. https://doi.org/10.1007/s10533-019-00555-8

Watts, J., and Lawrence, R., 2008. Merging random forest classification with an object-oriented approach for analysis of agricultural lands. The International Archives of the Photogrammetry, Remote Sensing and Spatial Information Sciences, 37.

West, G. B., Brown, J. H., and Enquist, B. J., 1997. A general model for the origin of allometric scaling laws in biology. *Science* (New York, N.Y.), 276(5309), pp. 122–126. https://doi.org/10.1126/science.276.5309.122

Wolff, S., Meijer, J., Schulp, C. J. E., and Verburg, P. H., 2020. Contextualizing local landscape initiatives in global change: a scenario study for the high forest zone, Ghana. *Regional Environmental Change*, 20(4). https://doi.org/10.1007/s10113-020-01701-x

WRI (World Resources Institute)., 2017. Historical GHG Emissions. Climate Analysis Indicators Tool. https://www.climatewatchdata.org/ghg-emissions?end_year=2019andstart_year=1990

Wright, S. J., 2010. The future of tropical forests. Annals of the New York Academy of Sciences, 1195, pp. 1–27. https://doi.org/10.1111/j.1749-6632.2010.05455.x

Xiaojun, N., Jianhui, Z., and Zhengan, S., 2013. Dynamics of Soil Organic Carbon and Microbial Biomass Carbon in Relation to Water Erosion and Tillage Erosion. *PLoS ONE*, 8(5), pp. 1–7. https://doi.org/10.1371/journal.pone.0064059

Xu, M., and Shang, H., 2016. Contribution of soil respiration to the global carbon equation. *Journal of Plant Physiology*, 203, pp. 16–28. https://doi.org/10.1016/j.jplph.2016.08.007

Díaz, Y.M. I., Cantú Silva, I., González Rodríguez, H., Marmolejo Monsiváis, J. G., Jurado, E., and Gómez Meza, M. V., 2017. Soil respiration in four land-use systems. *Revista Mexicana de Ciencias Forestales*, 8(42), pp. 123–149.

Yang, J., Lu, H., Ma, Z., Lu, Y., Wang, W., Zhu, J., Wu, C., Zhu, H., Chen, M., and Sun, Y., 2024. Predicting CO_2 emissions through partitioned land-use change simulations

considering urban hierarchy. *International Journal of Digital Earth*, 17(1), pp. 1–18. https://doi.org/10.1080/17538947.2024.2405541

Yang, Y., Luo, W., Xu, J., Guan, P., Chang, L., Wu, X., and Wu, D., 2022. Fallow Land Enhances Carbon Sequestration in Glomalin and Soil Aggregates Through Regulating Diversity and Network Complexity of Arbuscular Mycorrhizal Fungi Under Climate Change in Relatively High-Latitude Regions. *Frontiers in Microbiology*, 13(July), pp. 1–14. https://doi.org/10.3389/fmicb.2022.930622

Yiran, G. A. B., Kusimi, J. M., and Kufogbe, S. K., 2012. A synthesis of remote sensing and local knowledge approaches in land degradation assessment in the Bawku East District, Ghana. *International Journal of Applied Earth Observation and Geoinformation*, 14(1), pp. 204–213. https://doi.org/10.1016/j.jag.2011.09.016

Zaman, M., Kleineidam, K., Bakken, L., Berendt, J., Bracken, C., Butterbach-Bahl, K., Cai, Z., Chang, S. X., Clough, T., Dawar, K., Ding, W. X., Dörsch, P., dos Reis Martins, M., Eckhardt, C., Fiedler, S., Frosch, T., Goopy, J., Görres, C. M., Gupta, A., Müller, C., 2021. Measuring emission of agricultural greenhouse gases and developing mitigation options using nuclear and related techniques: Applications of nuclear techniques for GHGs. In Measuring Emission of Agricultural Greenhouse Gases and Developing Mitigation Options using Nuclear and Related Techniques: Applications of Nuclear Techniques for GHGs. Springer. https://doi.org/10.1007/978-3-030-55396-8

Żarczyński, P. J., Krzebietke, S. J., Sienkiewicz, S., and Wierzbowska, J., 2023. The Role of Fallows in Sustainable Development. Agriculture (Switzerland), 13(12). https://doi.org/10.3390/agriculture13122174

Zhang, Q., Wu, J., Yang, F., Lei, Y., Zhang, Q., and Cheng, X., 2016. Alterations in soil microbial community composition and biomass following agricultural land-use change. *Scientific Reports*, 6(October), pp. 1–10. https://doi.org/10.1038/srep36587

Zomer, R. J., Bossio, D. A., Sommer, R., and Verchot, L. V., 2017. Global Sequestration Potential of Increased Organic Carbon in Cropland Soils. *Scientific Reports*, 7(1), pp. 1–8. https://doi.org/10.1038/s41598-017-15794-8

Zomer, R. J., Trabucco, A., Bossio, D. A., and Verchot, L. V., 2008. Climate change mitigation: A spatial analysis of global land suitability for clean development mechanism afforestation and reforestation. *Agriculture, Ecosystems and Environment*, 126(1–2), pp. 67–80. https://doi.org/10.1016/j.agee.2008.01.014

Zou, J., Huang, Y., Zheng, X., and Wang, Y., 2007. Quantifying direct N2O emissions in paddy fields during rice growing season in mainland China: Dependence on water regime. *Atmospheric Environment*, 41(37), pp. 8030–8042. https://doi.org/10.1016/j.atmosenv.2007.06.049

APPENDICES

The appendices provide supplementary material to support the main discussion in this thesis. Appendix A presents additional results related to Objective 2. Appendix B includes further results for Objective 3. Appendix C contains field photographs and details of the experimental setup for the soil respiration measurements.

Appendix A: Present additional results from the factorial ANOVA, comparing the four land uses (forest, fallow, maize, and rice) across the 13-month period. It also includes an analysis of the effects of topography and habitat types on the four land uses. Furthermore, the impact of seasonality, specifically soil moisture and temperature, on soil respiration rate is analysed for each land use type.

Appendix 1: Significance difference between land-use types

Fallow	Rice	Maize	Forest
"a"	"b"	"c"	"d"

Appendix 2: Significance difference across months

May24	Jun24	Mar24	Jun23	Jan24	Apr24	Oct23	Nov23	Aug23	Sep23	Jul23	Dec23	Feb24
"a"	"ab"	"ab"	"abc"	"abc"	"abcd"	"bcde"	"cdef"	"defg"	"defg"	"efg"	"fg"	"g"

Appendix 3: Interaction between land-use types*months and their significance difference (letters)

Fallow:Jan24	Rice:May24	Fallow:Jun24	Fallow:Mar24	Fallow:May24	Fallow:Jul23	Fallow:Nov23
"a"	"ab"	"abc"	"abcd"	"abcd"	"abcdef"	"abcde"

Fallow:Feb24	Rice:Jun23	Rice:Jan24	Fallow:Dec23	Fallow:Jun23	Rice:Jun24	Fallow:Sep23
"abcdef"	"abcdefghijk"	"abcdefghi"	"abcdefg"	"abcdefghi"	"abcdefghij"	"bcdefg"

Fallow:Apr24	Fallow:Oct23	Maize:Oct23	Rice:Oct23	Forest:Mar24	Forest:Jun23	Rice:Apr24
"bcdefg"	"cdefg"	"cdefgh"	"bcdefghijk"	"cdefghi"	"bcdefghijk"	"cdefghijk"
Rice:Feb24	Maize:Jun23	Fallow:Aug23	Maize:Aug23	Rice:Mar24	Forest:Jun24	Maize:Jun24
"cdefghijk"	"cdefghijk"	"defghijk"	"cdefghijklm"	"cdefghijklm"	"efghijk"	"efghijk"
Maize:May24	Rice:Nov23	Rice:Dec23	Maize:Mar24	Maize:Jul23	Forest:Apr24	Maize:Apr24
"efghijk"	"defghijklm"	"cdefghijklm"	"efghijk"	"efghijklm"	"efghijkl"	"efghijk"
Rice:Aug23	Forest:Nov23	Forest:Jan24	Maize:Jan24	Forest:May24	Maize:Sep23	Forest:Sep23
"efghijklm"	"efghijklm"	"fghijk"	"efghijklm"	"fghijklm"	"ghijklm"	"ijklmn"
Rice:Sep23	Maize:Nov23	Forest:Aug23	Maize:Dec23	Forest:Oct23	Forest:Dec23	Rice:Jul23
"ghijklmno"	"hijklmno"	"hijklmno"	"jklmno"	"klmno"	"lmno"	"hijklmno"
Forest:Feb24	Maize:Feb24	Forest:Jul23				
"mno"	"no"	"o"				

Appendix 4: ANOVA results of soil respiration rate

Source	Df	Sum Sq	Mean Sq	F value	Pr(>F)
LULC	3	209,838	69,946	104.9	$2e^{-16}$*
Topography	1	1,916	1,916	2.999	0.08346.
Habitat type	3	48,005	16,002	25.054	$6.65e^{-16}$*
LULC × habitat type	1	1,907	1,907	2.986	0.08416
LULC × topography	2	1,248	624	0.977	0.37668
Residuals	1953	1,247,375	639		

Appendix 5: Seasonal variation of soil respiration rate and related soil moisture across land-use types

		Fallow			Forest			Maize			Rice		
Seasons	**Months**	**SRR kg ha^{-1} d^{-1}**	**SM (%)**	**ST (℃)**	**SRR kg ha^{-1} d^{-1}**	**SM (%)**	**ST (℃)**	**SRR kg ha^{-1} d^{-1}**	**SM (%)**	**ST (℃)**	**SRR kg ha^{-1} d^{-1}**	**SM (%)**	**ST (℃)**
Wet	Jun23	64.59	31.64	29.30	58.52	13.99	27.43	57.17	37.85	29.50	66.40	51.75	30.91
	Jul23	70.78	22.39	28.75	17.46	21.66	26.09	51.70	25.37	29.61	31.46	66.84	28.74
	Sep23	64.27	26.11	27.97	41.77	22.67	25.61	45.85	27.26	31.11	41.42	57.14	30.83
	Oct23	63.99	23.75	29.25	36.29	21.21	26.40	59.79	21.70	33.13	59.41	51.36	32.88
	Nov23	67.93	19.84	28.64	50.03	14.15	26.92	40.95	28.52	32.48	53.72	44.78	33.18
	Apr24	64.19	5.95	33.33	51.08	4.38	29.31	50.62	4.96	37.18	58.31	29.28	37.11
	May24	76.43	11.67	30.75	46.25	9.41	26.82	53.76	12.59	35.27	85.80	25.56	35.54
	Jun24	78.43	15.65	28.80	54.01	10.35	26.57	53.93	14.42	32.18	64.30	41.80	32.91
	Mean	**68.83^{a}**	**19.62^{a}**	**29.60^{a}**	**44.43^{a}**	**14.73^{a}**	**26.89^{a}**	**51.72^{a}**	**21.58^{a}**	**32.56^{a}**	**57.60^{a}**	**46.06^{a}**	**32.76^{a}**
Dry	Aug23	56.12	25.20	27.71	40.91	23.35	25.03	55.64	31.69	27.69	50.51	57.90	27.93
	Dec23	65.46	14.42	27.91	33.52	5.23	25.43	37.91	9.09	37.19	53.48	36.19	34.55
	Jan24	88.36	1.02	30.08	49.26	0.70	28.21	48.70	0.00	38.09	65.54	27.05	34.30
	Feb24	67.40	0.62	38.73	28.99	0.00	29.42	24.56	0.00	37.70	57.50	22.31	32.64
	Mar24	77.24	9.55	33.68	58.82	1.98	30.29	53.44	4.97	37.15	54.89	34.61	32.66
	Mean	**70.91^{a}**	**10.16^{b}**	**31.62^{a}**	**42.30^{a}**	**6.25^{b}**	**27.68^{a}**	**44.05^{a}**	**9.15^{b}**	**35.56^{a}**	**56.38^{a}**	**35.61^{b}**	**32.41^{a}**

Appendix B: present supplementary material from Objective 3, including a comparison of predicted and observed LULC for 2050, along with residuals and statistical metrics. Additionally, it includes the mean annual soil respiration rate dataset collected from June 2023 to June 2024 across three land use types: closed forest, open forest, and cropland and mixed vegetation.

Appendix 6: Comparison of predicted and observed LULC for 2050 with residual and statistical metrics

LULC 2050	**Predicted**	**Observed**	**Residuals**	**Residuals^2**	**Predicted^2**	**Observed^2**
Closed forest	49.69	43.14	-6.55	42.87	2469.20	1861.34
Open forest	55.69	69.17	13.48	181.72	3101.78	4785.01
Cropland and mixed vegetation	51.30	51.49	0.19	0.04	2631.99	2651.32
PA - BFR	51.24	43.14	-8.10	65.61	2625.89	1861.34
Sum Residuals^2	290.24					
Sum Observed^2	11159.01					
Sum Observed	206.95					
Number of polygons	4688.00					
R^2	**0.97**					
LULC 2022						
Closed forest	49.69	43.14	-6.55	42.87	2469.20	1861.34
Open forest	55.69	69.17	13.48	181.72	3101.78	4785.01
Cropland and mixed vegetation	51.30	51.49	0.19	0.04	2631.99	2651.32
PA - BFR	51.24	43.14	-8.10	65.61	2625.89	1861.34
Sum Residuals^2	290.24					
Sum Observed^2	11159.01					
Sum Observed	206.95					
Number of polygons	8571.00					
R^2	**0.97**					

Appendix 7: Mean annual soil respiration rate dataset collected from June 2023 to June 2024 on three land-use land cover types (Closed forest, Open forest and Cropland and mixed vegetation)

Land-use/cover classes	Longitude	Latitude	Soil CO_2 (kg CO_2-C $ha^{-1}d^{-1}$)
Closed forest	-1.34186	6.68722	43.14
Closed forest	-1.34939	6.68672	42.53
Closed forest	-1.34861	6.68481	50.32
Closed forest	-1.34667	6.68767	40.00
Open forest	-1.35889	6.66889	72.93
Open forest	-1.35454	6.66941	74.32
Open forest	-1.36412	6.66202	64.27
Open forest	-1.36551	6.66038	65.17
Cropland and mixed vegetation	-1.34950	6.65645	50.15
Cropland and mixed vegetation	-1.35254	6.67146	45.56
Cropland and mixed vegetation	-1.34763	6.65484	47.48
Cropland and mixed vegetation	-1.34784	6.65478	49.42
Cropland and mixed vegetation	-1.36151	6.66833	57.87
Cropland and mixed vegetation	-1.35256	6.67190	58.48
Protected area	-1.34186	6.68722	43.14
Protected area	-1.34939	6.68672	42.53
Protected area	-1.34861	6.68481	50.32
Protected area	-1.34667	6.68767	40.00

Appendix C

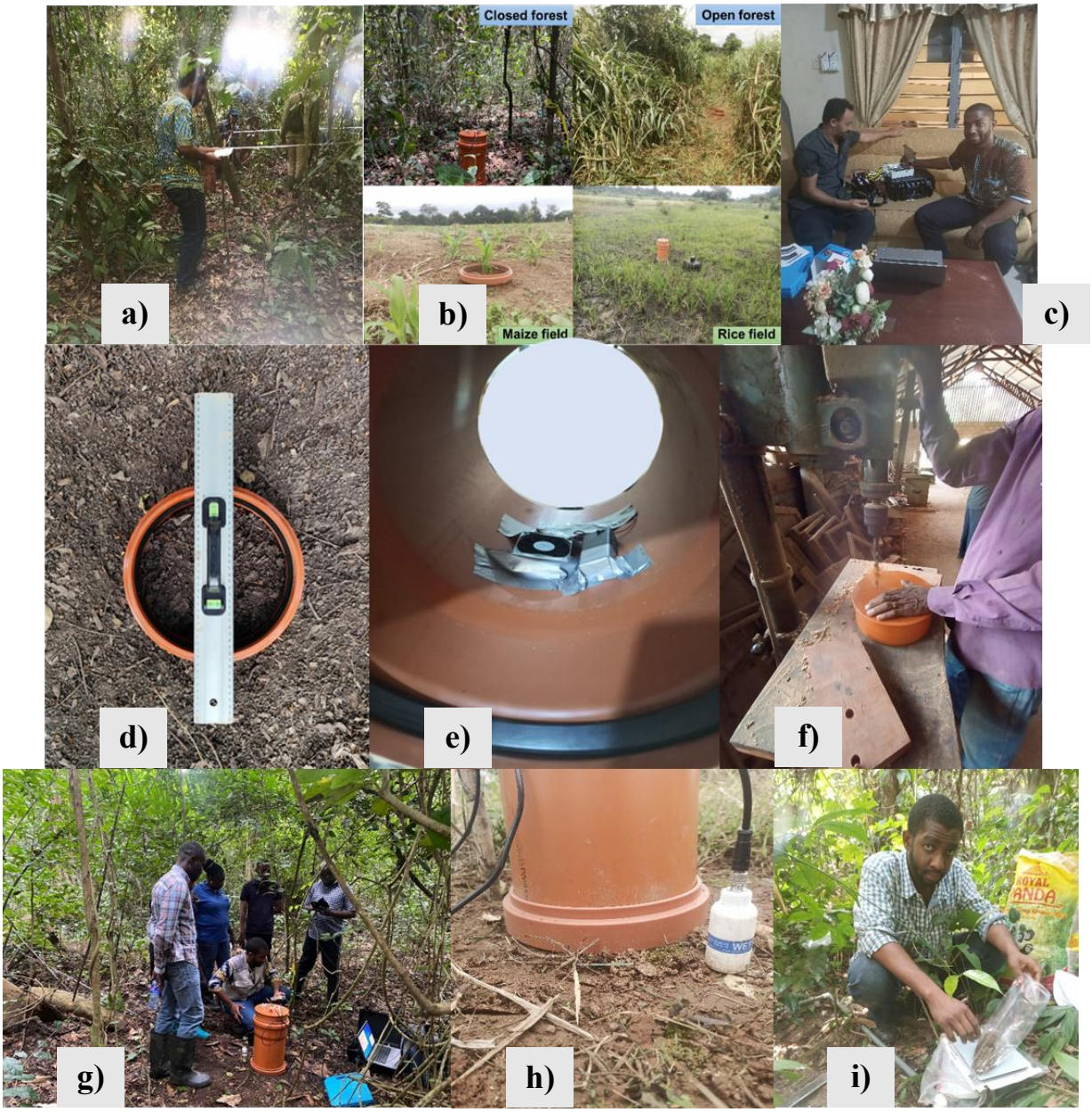

The plate illustrates the experimental setup for measuring soil respiration. Panel (a) shows the plot establishment for the land-use types, while panel (b) depicts the different land-use types. Panel (c) displays the configuration of the datalogger connected to the computer. Panel (d) shows the installation of the collar, levelled to the soil 72 hours before measurements were taken. Panel (e) shows the small fan fixed to the chamber for homogenising air inside. Panel (f) illustrates the creation of a small hole for inserting the two sensors (CO_2 and air temperature, RH, and air pressure). Panel (g) records the soil respiration for 7 minutes, and panel (h) shows the soil probe used to record soil moisture and temperature alongside soil respiration. Finally, panel (i) depicts the soil sample measurement.